

Chemical abundances in Galactic planetary nebulae with Spitzer spectra

D. A. García-Hernández^{1, 2} and S. K. Górný³

¹ Instituto de Astrofísica de Canarias, C/ Vía Láctea s/n, E-38205 La Laguna, Spain e-mail: agarcia@iac.es

² Departamento de Astrofísica, Universidad de La Laguna (ULL), E-38206 La Laguna, Spain

³ N. Copernicus Astronomical Center, Rabiańska 8, 87-100 Toruń, Poland e-mail: skg@ncac.torun.pl

Received February 19, 2014; accepted April 21, 2014

ABSTRACT

We present new low-resolution ($R \sim 800$) optical spectra of 22 Galactic planetary nebulae (PNe) with *Spitzer* spectra. These data are combined with recent optical spectroscopic data available in the literature to construct representative samples of compact (and presumably young) Galactic disc and bulge PNe with *Spitzer* spectra. Attending to the nature of the dust features - C-rich, O-rich, and both C- and O-rich dust features (or double chemistry) - seen in their *Spitzer* spectra, the Galactic disc and bulge PNe are classified according to four major dust types (oxygen chemistry or OC, carbon chemistry or CC, double chemistry or DC, featureless or F) and subtypes (amorphous and crystalline, and aliphatic and aromatic), and their Galactic distributions are presented. Nebular gas abundances of He, N, O, Ne, S, Cl, and Ar, as well as plasma parameters (e.g. N_e , T_e) are homogeneously derived by using the classical empirical method. We study the median chemical abundances and nebular properties in Galactic disc and bulge PNe depending on their *Spitzer* dust types and subtypes. The differences and similarities between PNe in the Galactic disc and bulge are reported. In particular, the median abundances for the major *Spitzer* dust types CC and OC are representative of the dominant dust subtype (which are different in both Galactic environments), while these values in DC PNe are representative of the two DC subtypes. A comparison of the derived median abundance patterns with AGB nucleosynthesis predictions mainly show that i) DC PNe, both with amorphous and crystalline silicates, display high-metallicity (solar/supra-solar) and the highest He abundances and N/O abundance ratios, suggesting relatively massive ($\sim 3-5 M_{\odot}$) hot bottom burning AGB stars as progenitors; ii) PNe with O-rich and C-rich unevolved dust (amorphous and aliphatic) seem to evolve from subsolar metallicity ($z \sim 0.008$) and lower mass ($< 3 M_{\odot}$) AGB stars; iii) a few O-rich PNe and a significant fraction of C-rich PNe with more evolved dust (crystalline and aromatic, respectively) display chemical abundances similar to DC PNe, suggesting that they are related objects. A comparison of the derived nebular properties with predictions from models combining the theoretical central star evolution with a simple nebular model is also presented. Finally, a possible link between the *Spitzer* dust properties, chemical abundances, and evolutionary status is discussed.

Key words. ISM: planetary nebulae: general – Stars: abundances – Stars: evolution – Galaxy: bulge – circumstellar matter – dust – Infrared: stars – stars: Wolf-Rayet

1. Introduction

Planetary nebulae (PNe) are a short evolutionary phase in the life of low- and intermediate-mass stars ($0.8 \leq M \leq 8 M_{\odot}$) occurring after they leave the asymptotic giant branch (AGB) and before ending their lives as white dwarfs (e.g. Iben 1995). However, many details of the physical processes leading to the creation of the nebula and its subsequent evolution remain unclear. Still, a better knowledge of the PN phase is necessary for understanding not only the final fate of stars like our Sun, but also the formation and the chemical evolution of the Milky Way and other galaxies.

At the tip of the AGB phase, stars experience a strong superwind that efficiently enriches the surrounding interstellar medium with huge amounts of gas and dust from the outer layers of the star (e.g. Herwig 2005). When the strong mass loss stops, they leave the AGB, and the future central star rapidly evolves towards hotter effective temperatures in the Hertzsprung–Russell diagram. Thus, when the ionization of the ejected gas takes place, a new PN emerges.

Owing to their emission-line nature, PNe can be easily observed at very large distances, and the chemical composition of the gas and other properties can be derived. Some of the abundances (e.g. the Ar/H and Cl/H ratios) may remain practically

unchanged in these objects, reflecting the primordial composition of the interstellar matter where their central stars were born. But there are other abundance ratios (e.g. N/O or C/O) that are strongly modified during the life of low- and intermediate-mass stars. The products of the hydrogen burning and shell helium burning are brought to the stars' outer layers in dredge-up episodes (the third dredge-up, TDU) taking place during the thermally pulsing phase on the AGB, converting originally O-rich stars into C-rich ones. In addition, the stellar surface can be enriched in products of the so-called hot bottom burning (HBB, e.g. Sackmann & Boothroyd 1992; Mazzitelli et al. 1999) process for the more massive ($M > 3-4 M_{\odot}$) AGB stars (e.g. García-Hernández et al. 2006b, 2007a, 2009), preventing formation of C-rich stars. At solar metallicity, low-mass ($\sim 1.5-3-4 M_{\odot}$) stars are expected to be C-rich ($C/O > 1$) at the end of the AGB phase, while more massive HBB stars may remain O-rich ($C/O < 1$) during the full AGB evolution.¹

It has been believed for a long time that post-AGB objects belong to only one of the two chemical branches mentioned above: either those characterized by an O-rich chemistry

¹ Very low-mass (e.g. $\leq 1.5 M_{\odot}$) and solar metallicity AGB stars are expected to be O-rich due to a rather inefficient TDU.

or those surrounded by C-rich material. PNe with rare Wolf–Rayet type central stars (e.g. Górny & Tyłenda 2000) were the first and the only ones in the Galactic disc to simultaneously show the presence of both carbon-based (e.g. polycyclic aromatic hydrocarbons; PAHs) and oxygen-based dust (e.g. crystalline silicates) - Waters et al. (1998a). However, a sample of Galactic bulge PNe (GBPNe) observed with *Spitzer/IRS* has been analysed, and a majority of them show such dual-dust chemistry (Gutenkunst et al. 2008; Perea-Calderón et al. 2009); the dual-dust chemistry phenomenon is clearly not restricted to objects with Wolf–Rayet (WR) central stars. More recently, Guzman-Ramirez et al. (2011) have proposed a scenario that may explain the simultaneous presence of PAHs and crystalline silicates in circumstellar disc-like structures around the central stars of GBPNe, but this scenario does not address the crucial question of why such a phenomenon is observed in Galactic disc PNe only in PNe with [WR] central stars. Apparently, in the Galactic bulge only a small fraction of PNe do not share that phenomenon and only have oxygen-based dust. The reason for the apparent difference between Galactic disc and bulge PNe remains unknown and is studied in this paper.

Various characteristics of GBPNe with peculiar *Spitzer* IR spectra were analysed by Górny et al. (2010), who found that PNe characterized by carbon-based dust (i.e. PAHs) and simultaneously oxygen-based dust (in the form of both crystalline and amorphous silicates) - the so-called DC_{a+cr}-type PNe in this paper - have unusual chemical compositions of the nebular gas. Oxygen seems to be under-abundant relative to hydrogen and nitrogen (see the location of DC_{a+cr}-type PNe in their figure 11) but not to other elements. This cannot be explained in the standard picture of the AGB chemical evolution for objects with the typical Milky Way metallicity. On the other hand, PNe surrounded by only oxygen-rich dust (both in amorphous and crystalline forms) - the so-called OC_{a+cr}-type PNe in this paper - have very low abundances of nitrogen (see their figure 11). The latter could be explained if these OC_{a+cr}-type PNe do not come from single stars but from binary systems because the presence of a companion may change the final abundances of the nebula (e.g. de Marco 2009).

Very recently, a large and complete sample (~150) of compact Galactic disc PNe have been analysed through *Spitzer/IRS* spectroscopy by Stanghellini et al. (2012). These authors find many PNe with peculiar dust characteristics (the DC_{a+cr}- and OC_{a+cr}-type PNe described above) similar to those previously found in the Galactic bulge (Górny et al. 2010). In particular, 28% (42 PNe) and 30% (45 PNe) of the sample turned out to be among the DC_{a+cr}- and OC_{a+cr}-type PNe, respectively. Owing to sensitivity limits of the *Infrared Space Observatory (ISO)*, most of the disc PNe with IR spectra have [WR] central stars probably because they are bright sources. It is a paradox of the high sensitivity of the *Spitzer* IRS instrument that, in contrast, only the optically fainter Galactic disc PNe could be observed (Stanghellini et al. 2012). As a result, proper optical spectra are not available yet for most of them. New optical spectroscopic observations are needed to form a proper reference sample of Galactic disc PNe and overcome selection effect problems. We want to alleviate this problem with the present paper by forming balanced samples of the Galactic disc and Galactic bulge PNe for a more extensive investigation.

In this paper, we present new low-resolution spectroscopy of 22 Galactic PNe with *Spitzer* spectra. These spectroscopic data are combined with recent data to construct representative samples of the Galactic disc and bulge PNe. Various nebular gas abundances of the Galactic disc and bulge PNe are

studied depending on their dust properties (i.e. *Spitzer* dust types/subtypes). PNe in environments with different metallicity and chemical history such, as the Galactic disc and bulge, are also compared. Our new low-resolution spectroscopic observations, the nebular chemical abundance analysis, and the optical data available in the literature are described in Section 2. We give an overview of the *Spitzer* dust types/subtypes and the Galactic distribution of our final samples of the Galactic disc and bulge PNe in Section 3, while in Section 4 we report the derived chemical abundances versus the *Spitzer* dust types and subtypes. Section 5 presents the nebular properties of the PNe with different *Spitzer* dust types and subtypes. Our results are discussed in Section 6, while a final summary of our work is given in Section 7.

2. Optical spectroscopy of Galactic PNe with *Spitzer* spectra

This section is devoted to the optical data available for PNe with *Spitzer* spectra. First, we present our own low-resolution spectroscopic observations. We determine their quality, present measured line intensities, and describe the way they were used to derive nebular plasma parameters and chemical abundances. At the end of the section we also describe the literature data collected for the same purpose. The six PNe with emission-line central stars discovered with our new spectroscopic observations and the three suspected symbiotic stars we observed are presented in Appendixes A and B, respectively.

2.1. New optical spectroscopic observations

We conducted low-resolution (R~800) optical spectroscopic observations of 19 PNe and three suspected symbiotic stars with the DOLORES spectrograph at the 3.6 m Telescopio Nazionale Galileo (TNG) located on the island of La Palma (Spain). The PNe were observed during two nights in August 2011 and two nights in July 2012. The detailed log of our TNG observations is presented in Table 1. By selecting the targets a strong preference was given to PNe not present in papers published after 1992 and that present large, homogeneous sets of spectroscopic observations. For this reason our data allow us to derive their chemical composition and plasma parameters for the first time for almost all of them.

During the observations, the DOLORES instrument was configured to the low-resolution long-slit spectroscopic mode. We used the volume phase holographic LR-B grism for science data and most of the instrument calibration frames (bias, dome flats, and arc lamps), plus the LR-R grism for some additional dome flats in the low sensitivity blue part. The effective useful range of the obtained spectra is ~3600–8050 Å.

The on-sky projected width of the slit was 0.7 arcsec for observations of the programme targets. This resulted in about 4 to 5 Å resolution of the secured spectra from the blue to the red part of the spectrum. Each night the spectrophotometric standard star Feige 110 was observed with at least one additional standard from the list of BD+25°3941, BD+28°4211, and G158-100. The standard stars were observed through 2 and 10 arcsec wide slits. The position angle of the slit was always aligned to the parallactic angle at the moment of the observations and positioned at the centre of the PN where its central star should be located. The combined light of Ar+Kr+Ne+Hg lamps were observed for wavelength calibration.

Table 1. Log of the TNG observations

PNG	name	dust type	date	exp. (s)	$-\log F(\text{H}\beta)$	diam. (")
107.4-02.6	K 3-87	CC _{al}	Aug 6, 2011	3600	13.4	6.
107.4-00.6	K 4-57	na / symb.	Aug 7, 2011	5400	13.6	stellar
097.6-02.4	M 2-50	OC _{am}	Aug 6, 2011	5400	12.48	4.5
095.2+00.7	Bl 2- 1	CC _{al}	Jul 26, 2012	2400	13.07	2.5
079.9+06.4	K 3-56	OC _{am}	Jul 25, 2012	2400	12.9	3.7
069.2+02.8	K 3-49	OC _{am}	Aug 7, 2011	3600	13.16	<0.5
068.7+01.9	K 4-41	OC _{cr}	Jul 26, 2012	2400	12.98	3.
060.5+01.8	He 2-440	OC _{cr}	Jul 25, 2012	2400	12.80	2.2
052.9+02.7	K 3-31	CC _{al}	Jul 26, 2012	2400	13.8	1.5
051.0+02.8	WhMe 1*	OC _{cr}	Jul 25, 2012	1800	13.52	stellar
044.1+05.8	CTSS 2	na / symb.	Aug 7, 2011	2400	13.5	stellar
042.9-06.9	NGC 6807	OC _{am+cr}	Aug 6, 2011	2400	11.48	0.8
041.8+04.4	K 3-15	CC _{ar+al}	Jul 26, 2012	2400	12.76	<0.5
038.7-03.3	M 1-69	F	Aug 6, 2011	3600	12.25	stellar
027.6-09.6	IC 4846	OC _{am}	Aug 6, 2011	2400	11.34	2.9
025.3-04.6	K 4- 8	OC _{am}	Aug 7, 2011	2400	12.35	stellar
011.1+07.0	Sa 2-237	OC _{am}	Aug 7, 2011	3600	13.3	stellar
008.6-02.6	MaC 1-11	OC _{am}	Jul 25, 2012	3600	13.45	3.1
007.5+04.3	Th 4- 1	OC _{cr} / symb.	Aug 7, 2011	1800	13.0	stellar
004.3-02.6	H 1-53	DC _{am+cr}	Jul 26, 2012	2400	12.56	stellar
000.6-02.3	H 2-32*	DC _{am+cr}	Jul 25, 2012	3600	13.20	stellar
354.9+03.5	Th 3- 6	DC _{cr}	Jul 26, 2012	2400	13.67	3.9

(*) - faint or unusual spectra, no chemical abundances could be derived.

The basic exposure times of PNe ranged from 30 to 90 minutes split into two or three sub-exposures. During such a long time, high S/N for the weak but important features could be achieved in most cases, but the strongest nebular emission lines ($\text{H}\alpha$, $[\text{O III}] \lambda 5007$, or $[\text{N II}] \lambda 6584$, rarely some other lines) were usually saturated. Therefore, additional snapshot spectra with exposures lasting from several seconds to a few minutes were also taken to allow the measurement of such prominent lines.

2.2. Data reduction and quality

We used the long-slit spectral package of MIDAS² to reduce and calibrate the optical spectra. That involved the standard procedures of bias subtraction, flat-field correction, atmospheric extinction correction, and wavelength calibration. After sky subtraction the one-dimensional spectra of standard stars and PNe were extracted by summing over the appropriate rows of the frames. In the case of PNe, however, since they were often located in crowded areas, we first had to remove contaminating continuum contributions of all stars in the field. Because this, a good fit to the sky emission could be found before it was subtracted from the nebular spectrum; see Górný et al. (2009) for a more detailed description of this method.

Two examples of PNe spectra obtained by us with the DOLORES spectrograph are presented in Fig. 1. This figure shows the reduced, integrated, and flux-calibrated one-dimensional spectra of the low ionization PN K 3-15 (top panel) and the higher ionization PN K 3-56.

The one-dimensional spectra were used to measure the intensities of the nebular emission lines with the REWIA package developed by J. Borkowski from the Copernicus Astronomical Centre (Torun, Poland). Gaussian profiles were used to fit the nebular lines and multi-Gaussian fits were performed when nec-

² MIDAS was developed and maintained by the European Southern Observatory.

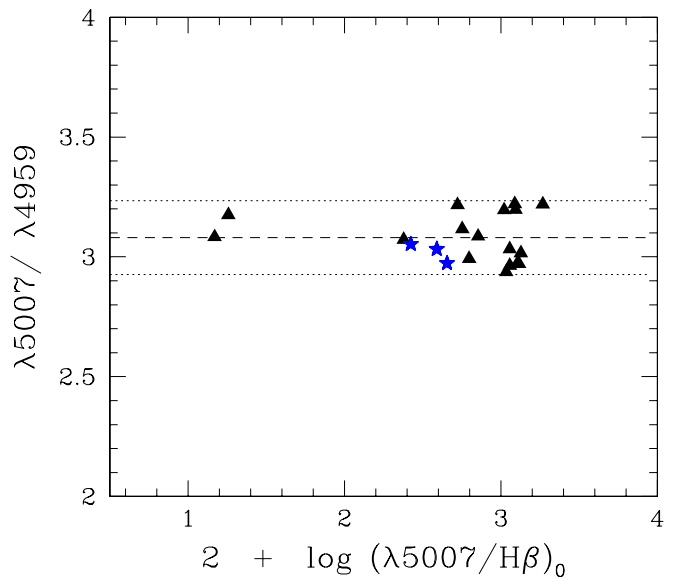


Fig. 2. Intensity ratio of the $[\text{O III}] \lambda 5007\text{\AA}$ to $\lambda 4959\text{\AA}$ lines as a function of the flux of $[\text{O III}] \lambda 5007\text{\AA}$ (in units of $\text{H}\beta$). The dashed line represents the mean value for the present TNG observations of PNe, and the dotted lines are 5% deviations from it. The observed PNe are marked by triangles, and the star symbols mark values for the suspected symbiotic stars observed.

essary. Table 2 presents the measured intensities of all important nebular lines on the scale $\text{H}(\beta)=100$ for the PNe observed in our TNG programme.

In Fig. 2 we present the intensity ratios of the $[\text{O III}] \lambda 5007\text{\AA}$ to $\lambda 4959\text{\AA}$ lines as derived from our optical spectra. The mean derived value is marked, along with 5% deviations from it.

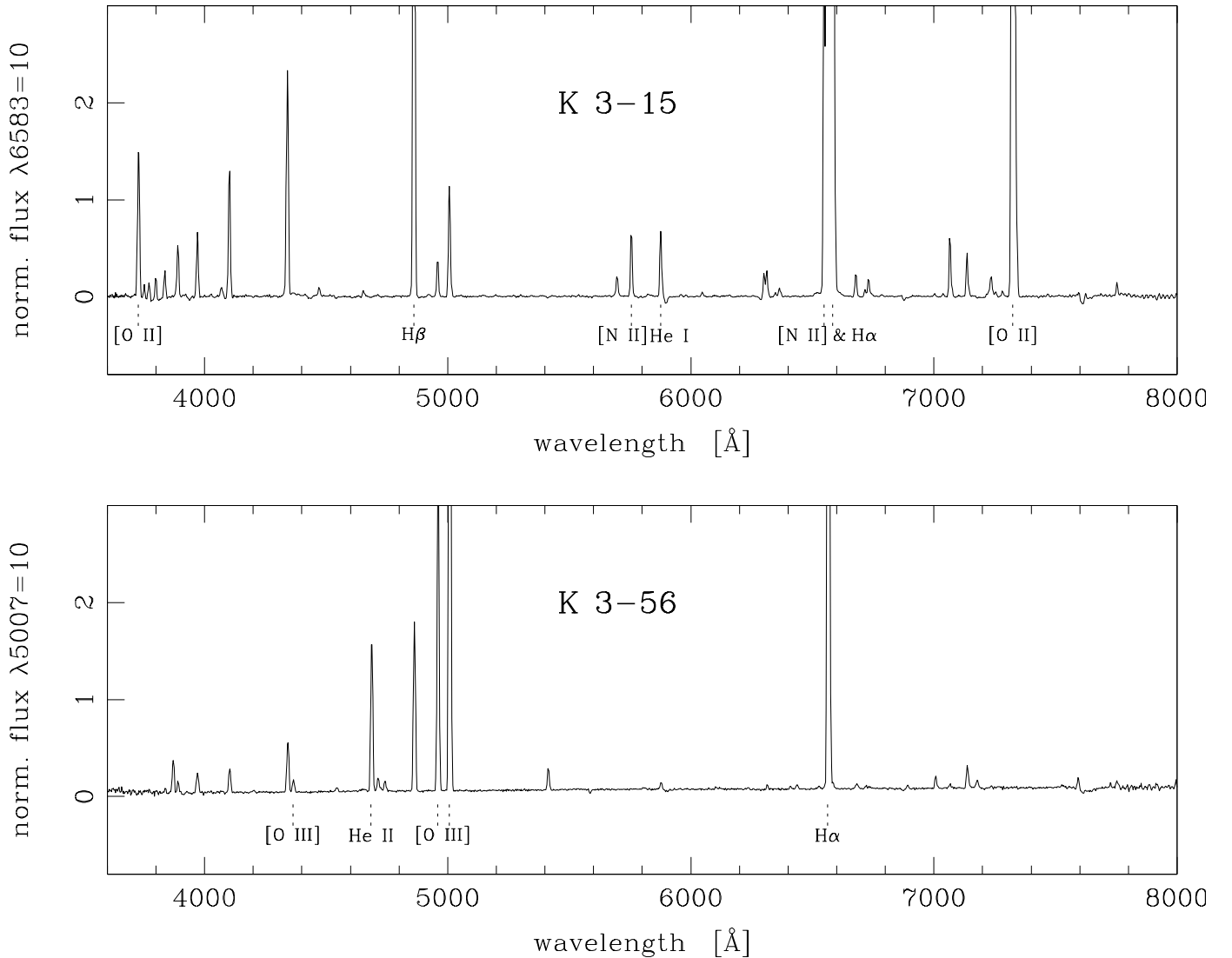


Fig. 1. Illustrative examples of the acquired low-resolution optical TNG/DOLORES spectra of a low ionization PN (K 3-15, top panel) and a high ionization PN (K 3-56, bottom panel) in our observing programme. Some spectral features are indicated.

From atomic physics the $\lambda 5007\text{\AA}/\lambda 4959\text{\AA}$ line ratio should have practically a constant value for all PNe and can therefore be used to assess the quality of our spectra. The error of this line ratio is mostly influenced by the error of the weakest spectral line that can be measured from our spectra, and this error is typically found to be less than 5%. It is to be noted here that, although the [O III] $\lambda 4959\text{\AA}$ is often one of the strongest spectral features in the PNe spectra, the $\lambda 5007\text{\AA}/\lambda 4959\text{\AA}$ line ratio has to be established using the additional snapshot spectra. This is due to the frequent saturation of [O III] $\lambda 5007\text{\AA}$ line in our long exposures. We therefore assume that 5% is a good error estimate also for the fainter lines measured from our basic spectra. In the case of some weaker lines or lines contaminated with sky features, the flux uncertainty is estimated to be around 20% (marked with a colon in Table 2) or rarely to be as high as 40% (marked with a semicolon in Table 2). In addition, in the case of some strongly blended nebular lines the uncertainty is assumed to be at the 10% level.

As mentioned above, the PNe observed in our TNG programme were deliberately selected among those PNe with

Spitzer spectra and without existing high-quality optical spectra. The only available large set of data for them are the survey spectra collected during the preparation of the Strasbourg–ESO Catalogue of Planetary Nebulae by A. Acker and co-workers. However, their spectra were of considerably lower quality where many important nebular lines were not detected. In Fig. 3 we compare our derived $H\alpha/H\beta$ ratios with those from Acker et al. (1992). A considerable spread can be observed in Fig. 3 that we naturally attribute to the lower quality of the latter data. Nevertheless, for half of the observed PNe an agreement with Acker et al. (1992) is better than 10%, and no systematic trend can be noticed.

As a final reduction step, we corrected the line intensities measured from our observations for the interstellar reddening by adopting the extinction law of Seaton (1979). An iterative procedure as described in Górný et al. (2004) was used to reproduce the theoretical case B Balmer $H\alpha/H\beta$ line ratios at the electron temperature and density derived for each object. However, with such a procedure, the reddening-corrected $H\gamma/H\beta$ and $H\delta/H\beta$ ratios were usually different than theoretically predicted. Those

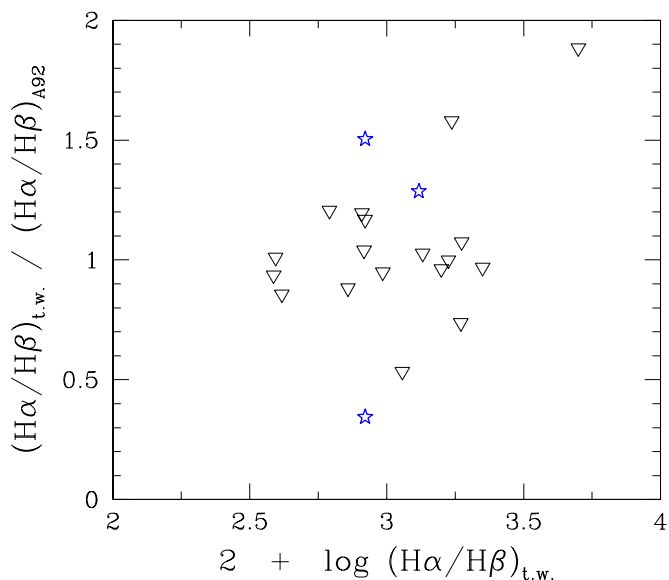


Fig. 3. Comparison of the derived $H\alpha/H\beta$ flux ratios in this work (t.w.) and the survey spectra of the Strasbourg–ESO Catalogue by Acker et al. (1992) (A92). The reversed triangles mark our observed PNe and stars the suspected symbiotic stars.

deviations had no systematic direction for our sample of PNe but were larger than could be expected from individual random errors of measurements of these lines. We attribute them rather to a generally lower accuracy of the flux calibration by the decreasing sensitivity in the blue part of the spectra. For the chemical abundance calculations, it is very important to determine the intensities of lines like $[O\text{ III}]\ \lambda 4363$ or $[O\text{ II}]\ \lambda 3727$ as reliably as possible. Thus, we used the method described in Górný et al. (2009) to calculate additional corrections that would bring the $H\gamma/H\beta$ ratio (and if still necessary the $H\delta/H\beta$ ratio) to the theoretical recombination values. These corrections were then linearly propagated to the observed fluxes at all wavelengths shorter than $4681\ \text{\AA}$.

The final extinction-corrected line intensities are listed in Table 2 and the lines additionally corrected in the way described above are marked with ‘c’ in this table.

2.3. Plasma parameters and chemical abundances

We used the ABELION code developed by G. Stasińska to derive plasma parameters and chemical abundances exactly as in Górný et al. (2009). This code is based on the classical empirical method. The electron densities (N_e) are obtained from the $[S\text{ II}]\ \lambda 6731/6717$ ratio and the electron temperatures (T_e) from the $[O\text{ III}]\ \lambda 4363/5007$ and $[N\text{ II}]\ \lambda 5755/6584$ ratios. These were first used to refine the inferred reddening correction as described above.

The chemical abundances of PNe were derived using the electron temperature derived from $[N\text{ II}]$ for ions of low ionization potential and that from $[O\text{ III}]$ for ions of high ionization potential. Objects for which the electron temperature could not be determined from either line ratio were discarded for abundance determinations. This concerned two PNe, H 2-32 and WhMe 1, both with $[O\text{ III}]\ \lambda 4363$ below the detection limit and with $[N\text{ II}]\ \lambda 5755$ too weak and uncertain to be used for electron temperature estimation. On the other hand, if the electron density (N_e) could not be precisely derived because the $[S\text{ II}]\ \lambda 6731/6717$

ratio was estimated to be outside of the useful range, then the chemical composition was nevertheless derived by assuming the N_e upper limit as 10^5 electrons per cm^3 . This was the case in nine of our targets and seems to be an unusually high proportion among our PN sample (see below).

We have attempted to investigate the unusually high electron densities derived from our observations in more detail. First, we established that the high ratios of $[S\text{ II}]\ \lambda 6731/6717$ are not caused by any defect in the CCD and is not an artefact of our reduction procedure. The two close lines of the $[S\text{ II}]$ doublet are resolved well in our spectra, and inspection of the raw frames already indicate that the $\lambda 6731$ line is usually much stronger than the $\lambda 6717$ line. A comparison with other observers is difficult because our observations are usually the first ones to have the high quality needed for plasma analysis. Out of the nine unusually high electron density cases mentioned above we have found literature entries with an $[S\text{ II}]\ \lambda 6731/6717$ ratio for only three PNe. In two cases (Th 3-6 and NGC 6807), Acker et al. (1992) give N_e values of 1.25 and 1.50 (in units of 10^5 electrons per cm^3), which are lower than our estimated N_e values of 3.10 and 2.33, respectively. In the case of NGC 6807, however, our N_e estimate is supported by the much closer value of 2.16 found by Aller & Keyes (1987).

In the third case (H 1-53), Acker et al. (1992) found an approximate N_e value of 3.0 that is comparable to our value of 2.74 but against the estimate by Exter et al. (2004), who derived $N_e=1.87$. It is worth mentioning that in another peculiar case (IC 4846), although not concerning extremely dense PNe, we derived an $[S\text{ II}]\ \lambda 6731/6717$ ratio of 2.13 that is comparable to the N_e value of 2.35 by Acker et al. (1992) but in disagreement with the N_e values of 1.70 and 1.67 by Aller & Czyzak (1979) and Barker (1978), respectively. However, the latter N_e measurements were derived from pre-CCD observations, and it is also doubtful that the $6731/17$ doublet was properly resolved. Finally, for PN H 2-32 we found an $[S\text{ II}]\ \lambda 6731/6717$ ratio of 1.47 in raw agreement with the N_e values of 1.79 and 1.27 by Ratag et al. (1997) and Exter et al. (2004), respectively. Thus, there is no indication that our electron density estimates is less reliable than those in earlier studies. We therefore conclude that the very high electron densities we derive for a considerable number of PNe in our sample are real and probably reflect the fact that these objects are extremely young PNe that are characterized by very high densities. This is not surprising if we consider that most of our observed objects are compact (with a size of $\leq 4''$) Galactic disc sources that are expected to be young, unevolved PNe (see Stanghellini et al. 2012).

In the applied empirical method, the derived elemental abundances are the sum of the ionic abundances derived from the measured intensities of the various lines available in the optical domain. Wherever information on ionic abundances is missing, this was corrected by the appropriate ionization correction factors (ICFs) using the same ICFs scheme as in Górný et al. (2009). The only noteworthy point is that similar to Górný et al. (2009), we compute the O^+ ionic abundance for all PNe as an average of the values derived by using the $[O\text{ II}]\ \lambda 3727$ and $[O\text{ II}]\ \lambda 7325$ lines. However, no additional correction factors have to be applied to the latter set of lines since both estimates from our TNG/DOLORES observations are, on average, in satisfactory agreement.

We also note that for the analysis presented in this work and discussed in the following sections, we have refrained from using the infrared atomic lines from the *Spitzer* spectra (beyond the scope of this paper) to preserve direct comparability with the results of the earlier studies conducted when such data were

not available for a representative sample of the Galactic PN population. The use of the *Spitzer* IR data in the nebular chemical analysis could provide some insight into additional ions, mainly O IV. However, ICFs for optical studies work well, as was shown by Shaw et al. (2010), who derived elemental abundances in Small Magellanic Cloud PNe both from optical and *Spitzer* spectra.

2.4. Nebular abundances from literature data

Apart from the new optical data presented in this work (Sect. 2.1), we also search optical spectroscopic literature data for all Galactic (bulge and disc) PNe with *Spitzer* spectra listed in Stanghellini et al. (2012), Perea-Calderón et al. (2009), and Gutenkunst et al. (2008). It is to be noted here that the Stanghellini et al. (2012) PNe sample was selected in a more uniform way (see below) than the Perea-Calderón et al. (2009) and Gutenkunst et al. (2008) PNe samples. The Stanghellini et al. (2012) PNe sample (157 PNe) is more complete, including PNe in both the Galactic disc and bulge, while the Perea-Calderón et al. (2009) (40 PNe) and Gutenkunst et al. (2008) PNe (11 PNe) samples mainly contain PNe in the Galactic bulge.³ In addition, all Galactic PNe in Stanghellini et al. (2012) are compact (size < 4") sources. This means that, in principle, the Stanghellini et al. (2012) PN sample is expected to be mainly composed of relatively young PNe, where we are sampling the early dust stages of the PN evolution (see Stanghellini et al. 2012, for more details). However, the Perea-Calderón et al. (2009) and Gutenkunst et al. (2008) Galactic bulge PN samples also contain some more extended (size > 4") sources.

In selecting literature data we have limited applicable entries to papers based on modern observations published after 1992 and making use of CCD-equipped spectrographs. They also had to contain enough objects to allow us to assess their quality and internal integrity in a way that is similar to our own data presented here. These requirements were met by the following papers: de Freitas Pacheco et al. (1992), Kingsburgh & Barlow (1994), Cuisinier et al. (1996), Ratag et al. (1997), Cuisinier et al. (2000), Escudero & Costa (2001), Kwitter & Henry (2001), Peña et al. (2001), Milingo et al. (2002), Escudero et al. (2004), Exter et al. (2004), Górny et al. (2004), Girard et al. (2007), Wang & Liu (2007), Górny et al. (2009), Cavichia et al. (2010), Henry et al. (2010), and Górny (2014). In short, we found useful optical spectroscopic literature data for 76, 30, and nine Galactic PNe in the lists by Stanghellini et al. (2012), Perea-Calderón et al. (2009), and Gutenkunst et al. (2008), respectively.

The same ABELION code with identical assumptions (see Sect. 2.3) was applied to these literature data. However, for obvious reasons the dereddening procedure and additional corrections to the blue nebular lines described above were calculated and applied only if the original still-reddened data were available. The corrections to match the O⁺ abundances derived from

³ We have excluded the three suspected symbiotic stars and five objects without *Spitzer* spectral classification in Stanghellini et al. (2012) from further consideration, as well as another five objects from Perea-Calderón et al. (2009) because their classification is uncertain (H 1-12, M 3-13, GLMP 698, NGC 6644, and 19W32). In addition, we excluded Wray 16-423 since it is located in the Sagittarius dwarf galaxy. Also, M2-10 was observed both by Stanghellini et al. (2012) and Gutenkunst et al. (2008), and we adopt its double-chemistry dust classification from the latter authors.

[O II] $\lambda 7325$ with those from [O II] $\lambda 3727$ were estimated individually for each set of data. If more than one reference to optical spectroscopic data was available for a given object, then we gave preference to papers with data of higher internal integrity, e.g. those containing complete measurements ranging from the blue to red spectral regions and thus also both [O II] doublets. However, if several literature sources had similar quality for a given PN, then N_e , T_e and the abundances were derived separately, and the averaged values were calculated for such objects.

By joining the useful optical spectroscopic literature data mentioned above with our new DOLORES optical data (17 PNe, by excluding two faint objects and the three suspected symbiotic stars; see Sect. 2.1), we end up with a final sample of 131 Galactic (bulge and disc) PNe with available *Spitzer* spectra and nebular abundances. The derived plasma diagnostics and elemental abundances are listed in Table 3 for the objects observed in our TNG programme and for all other PNe with optical data in the literature (see above). In Table 3 there are three rows for each object, and a fourth row used to separate them. The first row gives the values of parameters computed from the nominal values of the observational data or averages of estimates calculated from nominal values. The second and third rows give the upper and lower limits of these parameters, respectively. If there was only one source of data, these errors were calculated with Monte Carlo simulations (see Chiappini et al. 2009, for more details). Also, if there was more than one entry for a given object, these values are again averages of individually determined errors. However, if nominal values of individual entries were outside such estimated errors, then we replaced them with actual deviations of these values from the adopted mean value given in the first row.

Entries in Table 3 are ordered by PNG numbers that are given in column (1); col. (2) gives the usual name of the PN; col. (3) indicates whether the object belongs to the Galactic disc or bulge population of PNe (see Sect. 3 for more details); col. (4) informs whether the object was included in the sample of PNe with *Spitzer* spectra analysed by Stanghellini et al. (2012), Perea-Calderón et al. (2009), or Gutenkunst et al. (2008); col. (5) presents the dust classification of the object (see Sect. 3 for more details); col. (6) gives the references to data used in the calculations; col. (7) gives the electron density (N_e); cols (8) and (9) give the electron temperature (T_e) deduced from [O III] $\lambda 5007$ and [N II] $\lambda 6584$ line ratios, respectively; cols (10) to (16) list the He/H, N/H, O/H, Ne/H, S/H, Ar/H, Cl/H abundance ratios, respectively. Finally, col. (17) gives the logarithmic extinction C at $H\beta$.

We do not expect the results of our work to be affected by the so-called abundance discrepancy between collisionally excited lines (CELs) and optical recombination lines (ORLs) in PNe (see e.g. Liu et al. 2006, and references therein). If these discrepancies are produced by temperature fluctuations (Peimbert 1967) and they are moderate, then they would affect most of the elements in a similar way (see e.g. García-Rojas et al. 2009, 2013). On the other hand, if the discrepancy is due to the presence of chemical inhomogeneities, our analysis would not be affected, since the bulk of the emission of the PN is coming from CELs (Liu et al. 2006).

3. *Spitzer* dust types/subtypes and Galactic distribution

Galactic (disc and bulge) PNe in our final sample (131 PNe) can be classified into four major dust types that indicate the

Table 4. Correspondence of our major *Spitzer* dust types/subtypes with the dust classes defined by Stanghellini et al. (2012).

this work	Stanghellini et al. (2012)
CC _{ar}	1 (CRD)
CC _{al}	2 (CRD)
CC _{ar+al}	3 (CRD)
OC _{cr}	4 (ORD)
OC _{am}	5 (ORD)
OC _{am+cr}	6 (ORD)
DC _{cr}	7 = MCD *
DC _{am+cr}	7 = MCD *
F	0 = F

(*) - no dust subclasses were assigned for the MCD PNe by Stanghellini et al. (2012).

nature of the dust features in their *Spitzer* infrared spectra (Stanghellini et al. 2012). PNe with C-rich and O-rich dust features belong to the carbon chemistry (CC) and oxygen chemistry (OC) dust types, respectively, while those PNe with both C-rich and O-rich dust features belong to the double chemistry (DC) dust type. Finally, PNe with no dust emission features (and generally a very low dust continuum emission) are within the featureless (F) dust type. These major PN dust types can be subclassified into several dust subtypes depending on the specific nature of the C-rich (aromatic and/or aliphatic) and O-rich (crystalline and/or amorphous) dust features present in the *Spitzer* spectra. Thus, we define the following dust subtypes among the major dust CC, OC, and DC types: i) carbon chemistry (CC): CC_{ar} (aromatic), CC_{al} (aliphatic), and CC_{ar+al} (aromatic and aliphatic); ii) oxygen chemistry (OC): OC_{am} (amorphous), OC_{cr} (crystalline), and OC_{am+cr} (amorphous and crystalline); iii) double chemistry (DC): DC_{cr} (crystalline) and DC_{am+cr} (amorphous and crystalline)⁴.

For the sample of the compact Galactic disc and bulge PNe, we adopt the dust types and subtypes reported in Stanghellini et al. (2012). We note that no dust subclasses were defined for the DC (or mixed chemistry dust, MCD) PNe by Stanghellini et al. (2012), and we give the DC subtypes for the first time. For the Perea-Calderón et al. (2009) and Gutenkunst et al. (2008) PNe, we double-checked the major dust types, and we classified them among our defined dust subtypes by inspecting the *Spitzer* spectra published by these authors. Table 4 shows the correspondence of our major *Spitzer* dust types and subtypes with the equivalent dust classes defined by Stanghellini et al. (2012). All *Spitzer* dust types/subtypes are listed in Table 3.

To study the Galactic distribution of the Galactic PNe with *Spitzer* spectra, we use the sample of Stanghellini et al. (2012), which is the largest sample so was selected in a more uniform way. We divide them into PNe pertaining to the Galactic disc and those pertaining to the Galactic bulge. To select the latter PNe we use the following standard criteria: i) they have to be located within ten degrees of the centre of the Milky Way; ii) their diameters are smaller than 20'', and iii) known radio fluxes at 5 GHz are smaller than 100 mJy. It has been established from simulations by Stasińska et al. (1991) for a general population

⁴ DC PNe display C-rich aromatic (e.g. PAH) features only (see e.g. Perea-Calderón et al. 2009).

Table 5. Statistics of the major *Spitzer* dust types among the compact Galactic bulge and disc PNe found in this work. The number of PNe is given in parentheses.

dust type	bulge	disc
F	14% (7)	19% (18)
CC	8% (4)	33% (32)
OC	26% (13)	31% (31)
DC	52% (26)	18% (17)

of PNe that the contamination of the bulge PN sample defined in this way by disc PNe is most probably at the 5% level.

The sample of Stanghellini et al. (2012) that we use here, however, is different from the general population of PNe in the sense that it has been preselected, giving preference to small and presumably young objects. For this reason the second criterion concerning the nebular diameters is in fact fulfilled by all these PNe. Concerning the third requirement, radio fluxes at 5 GHz are available for 26 out of 52 PNe located in the direction of the bulge. Only those 26 PNe were considered by Stanghellini et al. (2012) as true bulge members, whereas the remainder have been adopted as disc members. In our opinion this may be rather unlikely, and we prefer to use the 5 GHz condition in the classical way to eliminate clear disc members. The 5 GHz flux has not been measured in existing radio surveys and can in general be regarded as smaller than the assumed 100 mJy limit. It seems that the 5 GHz flux is a rather poor discriminative parameter for the specific sample of Stanghellini et al. (2012). Indeed, only for six of them undoubtedly located in the Galactic disc, i.e. far away from the Galactic centre, is the 5 GHz flux larger than 100 mJy. We therefore prefer to adopt that all the 52 PNe in Stanghellini et al. (2012) sample pertain physically to the Galactic bulge and that the percentage of disc contaminants in this sample (52 compact Galactic PNe) is low.

We present in Table 5 the distribution of the compact PNe according to their main *Spitzer* dust types among the Galactic bulge and disc populations. By comparing with Table 6 in Stanghellini et al. (2012), one can see that with our criteria for bulge membership, there is little change ($\leq 10\%$) in the distribution into dust types in the Galactic bulge. We found almost identical percentages of CC and slightly increased ones of DC bulge PNe. The most prominent differences are a decrease and an increase (both of about 10%) in OC and F bulge PNe, respectively. We indeed found that both OC and F PNe seem to populate the Galactic disc and bulge with a very similar percentage (differences $\leq 6\%$). Taking into account that F-type PNe can be more evolved objects, hence radio-dimmed, selection criteria based on available 5 GHz flux measurements could discriminate artificially against them pertaining to the bulge population.

Regarding the dust distribution among disc PNe presented in Table 5, we also found percentages of CC, OC, DC, and F disc PNe similar (differences $\leq 6\%$) to those found by Stanghellini et al. (2012). The DC disc PNe seem to be slightly less common (although only by about 6%) than established by these authors. Stanghellini et al. (2012) have already noted that the DC PNe are apparently concentrated towards the inner regions (i.e. the Galactic centre) of the Milky Way. This fact is also reflected in our statistics (see also Fig. 4), and DC PNe are less common in the Galactic disc than CC and OC PNe, but they clearly dominate the Galactic bulge region.

More interesting is the distribution of the compact Galactic disc and bulge PNe depending on their *Spitzer* dust subtypes.

Table 6. Statistics of the *Spitzer* dust subtypes among the compact Galactic bulge and disc PNe found in this work. The number of PNe is given in parentheses.

subtype	bulge	disc
CC_{ar}	(2)	31% (10)
CC_{al}	(1)	66% (21)
CC_{ar+al}	(1)	3% (1)
OC_{cr}	46% (6)	29% (9)
OC_{am}	39% (5)	61% (19)
OC_{am+cr}	15% (2)	10% (3)
DC_{cr}	69% (18)	53% (9)
DC_{am+cr}	31% (8)	47% (8)

This is shown in Table 6 where we list the corresponding percentages of the *Spitzer* dust subtypes among the compact PNe in the Galactic disc and bulge. Table 6 immediately suggests that the several *Spitzer* dust subtypes are distributed differently between the Galactic disc and bulge. CC bulge PNe are very rare, as expected from the known lack of C-rich AGB stars in the Galactic bulge (see e.g. Uttenthaler et al. 2007, and references therein). In addition, CC PNe with aliphatic dust (CC_{al} and CC_{ar+al}) are extremely rare (only two sources!) in the Galactic bulge, while they completely dominate in the Galactic disc. The apparent lack of CC_{ar} disc PNe (i.e. with aromatic PAH-like dust features) may be understood in terms of the dominant dust evolutionary stage around these compact (and presumably young) Galactic disc PNe. There is no time for efficient dust processing (e.g. by the UV irradiation from the central star; Kwok et al. 2001) to transform aliphatic groups to aromatic ones. Thus, we generally see the early stages of the circumstellar dust grains (in the form of broad aliphatic dust features) or the precursors of the aromatic groups that are typically seen in much more evolved C-rich PNe (in the form of narrower and aromatic PAH-like features). Alternatively, CC_{al} PNe in the Galactic disc may have somewhat low metallicity, favouring the presence of unprocessed dust grains in their circumstellar envelopes (see Stanghellini et al. 2007).

On the other hand, the distributions of the OC and DC *Spitzer* dust subtypes in the Galactic disc and bulge also show remarkable differences. Both OC and DC PNe with O-rich amorphous dust features are more common in the Galactic disc than in the bulge. One expects the evolution of the O-rich dust features to proceed from amorphous silicates (in the AGB/post-AGB stage) to crystalline silicates (in the PN phase) (García-Lario & Perea Calderón 2003, see also Garcia-Hernandez 2012 and references therein). Similarly to the CC PNe, the higher detection rate of amorphous silicates in the compact Galactic disc PNe may be related to the early dust evolutionary stage around these presumably young objects and/or with a low metallicity. In particular, Stanghellini et al. (2012) have already pointed out that the OC_{cr} disc PNe occur at lower Galactic latitudes (b) than the OC_{am} disc PNe (see below; Fig. 4). This would be consistent with the OC_{cr} PNe being more massive (and/or more metal rich) than the OC_{am} ones. Curiously, similar fractions of OC_{am+cr} (with amorphous and crystalline silicate features) are found in both the Galactic disc and bulge, although they are very rare and uncommon in both environments. Finally, the OC and DC PNe with O-rich crystalline silicate features seem to be more frequent in the Galactic bulge. A higher detection rate of crystalline silicates in the Galactic bulge may

again be related to a more advanced evolutionary stage or with higher metallicity. For example, higher metallicity in the Galactic bulge may favour higher mass loss rates at the end of the previous AGB phase and a more efficient crystallization of silicates (e.g. Waters et al. 1996; see also Section 6).

In Fig. 4 we present the locations (in Galactic coordinates) of the compact Galactic disc (left panel) and bulge (right panel) PNe divided into the various dust subtypes. As mentioned above, DC PNe in the Galactic disc are mainly located towards the Galactic centre (Fig. 4, left panel), and there is no obvious difference between the DC_{cr} and DC_{am+cr} dust subtypes. CC and OC Galactic disc PNe are rather uniformly distributed in the Galaxy, although CC PNe seems to be more concentrated in the Galactic plane than (at least) the OC PNe with amorphous silicates (see below). In Fig. 4 (left panel) there is no significant difference for the Galactic coordinates exhibited by the several CC dust subtypes (CC_{am} , CC_{al} and CC_{ar+al}). However, the OC PNe in Fig. 4 (left panel) display, on average, different Galactic latitudes depending on the OC dust subtypes (mainly OC_{am} and OC_{cr}), as previously pointed out by Stanghellini et al. (2012). The OC_{cr} PNe in the Galactic disc are more concentrated at lower latitudes than the OC_{am} PNe, since they are consistent with the former objects being more massive (and/or more metal-rich) than the latter (see above). In fact, judging only by their median $b=6^\circ5$, OC_{am} PNe seem to be located two to three times further away from the Galactic plane than almost any other dust subtype in the disc. Surprisingly, the other PN group with high Galactic latitudes (with a median of $b=4^\circ0$) are the F PNe with featureless *Spitzer* spectra. The situation is very similar in the Galactic bulge (Fig. 4, right panel), and there is no clear distinction between the different *Spitzer* dust subtypes, although it has to be noted that the samples are considerably smaller, and the number of objects in the central region is naturally depleted due to strong obscuration by dust. As in the disc, the OC_{cr} bulge PNe seem to show lower Galactic latitudes (and longitudes) than their amorphous dust counterparts (OC_{am}); this difference, however, is marginal. Finally, PNe with amorphous and crystalline O-rich dust (OC_{am+cr} ; see e.g. Górny et al. 2010) are rather peculiar objects in both Galactic populations (disc and bulge) of PNe.

4. PNe nebular abundances versus *Spitzer* dust types/subtypes

In this section we compare nebular gas abundances (He, N, O, Ne, S, Cl, and Ar) of PNe in our sample with the several major dust types and subtypes as defined above. We also discuss the differences and similarities between PNe in the Galactic disc and bulge and compare our results with theoretical nucleosynthesis predictions for AGB stars. In the previous section, we only considered the Galactic bulge and disc PNe from the more uniform Stanghellini et al. (2012) sample of compact PNe. This is because we wanted to check the rate of occurrence of the different *Spitzer* dust types/subtypes in both environments when using different criteria (more appropriate in our opinion) for selecting bulge objects. In the following, however, we merge the bulge PNe from Stanghellini et al. (2012) - according to our criteria for selecting bulge objects as defined above - with those from Perea-Calderón et al. (2009) and Gutenkunst et al. (2008) in order to construct a unique sample of Galactic bulge PNe with a higher statistical significance. By comparing the derived abundances among these different bulge PNe samples, we find that the only apparent difference is that OC PNe from Perea-Calderón et al. (2009) have slightly lower N/O so we can

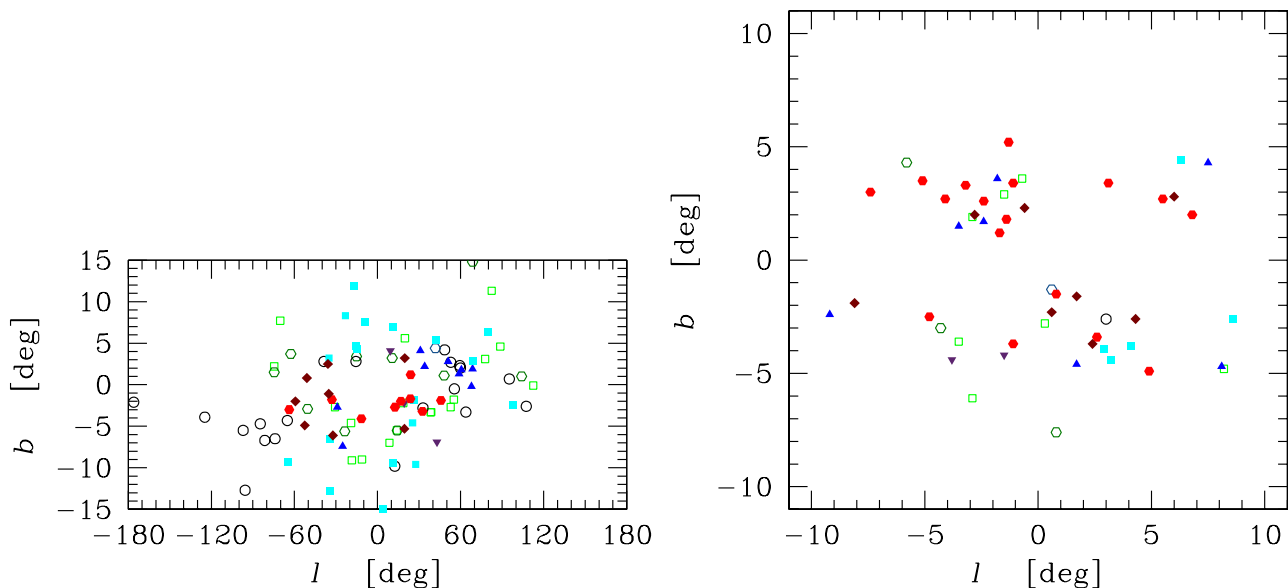


Fig. 4. The distribution of compact Galactic PNe of various subtypes in the Galactic coordinates (Galactic disc and bulge PNe in the left and right panels, respectively): CC_{ar-} open hexagons; CC_{al-} open circles; CC_{ar+al-} open diamonds; OC_{cr-} triangles; OC_{am-} filled squares; OC_{am+cr-} reversed triangles; DC_{cr-} filled hexagons; DC_{am+cr-} filled diamonds; F - open squares.

safely merge the latter bulge PNe samples. Finally, we do not include the derived abundances (X/H and X/Y) for low ionization PNe in the abundance diagrams and statistical tests presented in this section. This concerns the elements He, Ar, and S if the $O^{++}/(O^{+} + O^{++})$ ionization ratio is below 0.4 and Cl if this ratio is less than 0.8. In principle, also Ne cannot be derived if O^{++} ions are not observed (e.g. they are needed for ICF), but we checked that this is not the case for our objects. By inspecting high ionization PNe and assuming similar spectral energy distributions (SEDs) of the central stars it is clear that the differences in abundances through the several *Spitzer* dust types/subtypes discussed here are probably real and not due to ICFs.

4.1. PNe nebular abundances vs. major *Spitzer* dust types

In studying the derived nebular gas abundances vs. the major *Spitzer* dust types, we found several abundance diagrams (e.g. N/H vs. He/H , N/O vs. O/H) to be the most useful ones. Figures 5 and 6 display some of these useful abundance diagrams for the compact Galactic disc PNe by Stanghellini et al. (2012) and the bulge PNe by Stanghellini et al. (2012), Perea-Calderón et al. (2009), and Gutenkunst et al. (2008). The several major *Spitzer* dust types CC, OC, DC, and F (and their subtypes) are marked with different colours or symbols in these plots. We also carried out Kolmogorov–Smirnov (K-S) and Wilcoxon (W) statistical tests to confirm or discard possible differences in the chemical abundances among the major *Spitzer* dust types. This is shown in Table 7 where we present the results of both statistical tests for bulge PNe (OC vs. DC) and disc PNe (OC vs. DC, OC vs. CC, and DC vs. CC). In addition, Table 8 lists the results of our K-S and W statistical tests for OC and DC PNe (disc vs. bulge). It is to be noted here that we consider the differences in abundances to be real when the probability that the two compared samples stem from the same parent distribution is $\leq 1\%$ from both K-S and W statistical tests. Thus, if both probabilities are low (0.01 or less), then the difference is regarded as real,

and they are marked with boldface characters in Tables 7 and 8. The median plasma parameters and abundance values for the Galactic disc and bulge PNe are presented in Tables 9 and 10, respectively. The median values (and in particular the percentiles) in Tables 9 and 10 make no sense when we only have five or six objects. This is the case for the Galactic disc and bulge F PNe, and their values in these tables should be taken with some caution. In addition, as we see in Section 4.3, the median abundance patterns amongst the several major *Spitzer* dust types are dominated by the specific dust subtype, which are more numerous in each major dust group. Finally, we note that in the following we adopt the most recent Asplund et al. (2009) solar abundances of He (10.93), N (7.83), O (8.69), Ne (7.93), S (7.12), Cl (5.50), and Ar (6.40).⁵

Interestingly (although there are some clear outliers), Galactic disc DC PNe are, on average, mainly located towards higher N and He abundances and N/O abundance ratios, while just the opposite is seen for the OC objects (see Fig. 5). The DC disc PNe show median N and He abundances of $\log \epsilon(N)=8.38$ and $\log \epsilon(He)=11.10$, while OC disc PNe display lower median values of $\log \epsilon(N)=7.82$ and $\log \epsilon(He)=11.02$; however, CC and F disc PNe may populate the N/H vs. He/H and N/O vs. O/H diagrams more uniformly, although most CC disc PNe display N and He abundances (with median values of $\log \epsilon(N)=7.76$ and $\log \epsilon(He)=11.03$), similar to those of the OC disc PNe. Similar behaviour is seen for the Galactic bulge PNe shown in Fig. 6, with the exception that CC PNe are lacking towards this direction. The OC bulge PNe display median values of $\log \epsilon(N)=7.74$ and $\log \epsilon(He)=11.04$, while DC bulge PNe display higher median abundances of $\log \epsilon(N)=8.30$ and $\log \epsilon(He)=11.09$. Our K-S and W statistical tests shown in Table 7 confirm the differences in N/H , He/H , and N/O (also for Ar/H , Ar/O , and S/O , see below) between the DC and OC PNe in both Galactic environments. In addition, OC and DC PNe located in the Galactic disc and com-

⁵ The solar abundances between brackets are given on the usual scale $\log \epsilon(X) = \log(X/H) + 12$.

Table 7. Kolmogorov–Smirnov (K-S) and Wilcoxon (W) statistical tests for bulge PNe (OC vs. DC) and disc PNe (OC vs. DC, OC vs. CC, and DC vs. CC) (see text for more details).

Parameter/element	<i>bulge</i>	<i>disc</i>	<i>disc</i>	<i>disc</i>
	OC vs. DC K-S / W	OC vs. DC K-S / W	OC vs. CC K-S / W	DC vs. CC K-S / W
C	0.01 / 0.01			
log N_e	0.11 / 0.10	0.01 / 0.05	0.21 / 0.12	0.70 / 0.87
log T_e (O III)	0.22 / 0.30	0.01 / 0.01	0.98 / 0.88	0.01 / 0.00
log T_e (N II)	0.00 / 0.00	0.60 / 0.43	0.83 / 0.60	0.80 / 0.49
$O^{++}/(O^++O^{++})$	0.01 / 0.00	0.38 / 0.31	0.40 / 0.59	0.77 / 0.67
$He^{++}/(He^++He^{++})^*$	0.32 / 0.00	1.00 / 0.00	0.90 / 0.01	0.96 / 0.00
log ϵ (He)	0.01 / 0.01	0.00 / 0.00	0.45 / 0.49	0.82 / 0.02
log ϵ (O)	0.66 / 0.86	0.17 / 0.31	0.50 / 0.72	0.00 / 0.00
log ϵ (Ar)	0.00 / 0.00	0.00 / 0.00	0.43 / 0.52	0.00 / 0.00
log ϵ (Ne)	0.04 / 0.02	0.67 / 0.65	0.43 / 0.24	0.04 / 0.03
log ϵ (S)	0.03 / 0.01	0.00 / 0.00	0.17 / 0.08	0.00 / 0.00
log ϵ (N)	0.00 / 0.00	0.00 / 0.00	0.92 / 0.87	0.00 / 0.00
log ϵ (Cl)	0.38 / 0.11	0.21 / 0.13	0.54 / 0.39	0.01 / 0.02
log(S/O)	0.00 / 0.00	0.01 / 0.01	0.01 / 0.00	0.00 / 0.00
log(Ne/O)	0.00 / 0.00	0.55 / 0.53	0.00 / 0.00	0.00 / 0.00
log(Ar/O)	0.01 / 0.00	0.00 / 0.00	0.33 / 0.28	0.00 / 0.00
log(Cl/O)	0.81 / 0.39	0.72 / 0.41	0.98 / 0.87	0.51 / 0.24
log(N/O)	0.00 / 0.00	0.00 / 0.00	0.24 / 0.53	0.00 / 0.00
log(N/Ar)	0.00 / 0.00	0.18 / 0.28	0.70 / 0.38	0.16 / 0.04
log(N/Ne)	0.04 / 0.04	0.02 / 0.01	0.03 / 0.11	0.20 / 0.09
log(N/S)	0.62 / 0.37	0.00 / 0.00	0.00 / 0.01	0.43 / 0.74
log(N/Cl)	0.00 / 0.00	0.01 / 0.08	0.13 / 0.27	0.21 / 0.21
log(Ne/Ar)	0.96 / 0.87	0.00 / 0.00	0.00 / 0.01	0.85 / 0.50
log(S/Ne)	0.81 / 0.59	0.02 / 0.01	0.95 / 0.71	0.05 / 0.01
log(S/Ar)	0.76 / 0.65	0.09 / 0.02	0.00 / 0.00	0.04 / 0.00

* Results of Wilcoxon test are not reliable in this case.

Table 8. Kolmogorov–Smirnov (K-S) and Wilcoxon (W) statistical tests for OC and DC PNe (disc vs. bulge) (see text for more details).

Parameter/element	OC	DC
	<i>disc vs. bulge</i> K-S / W	<i>disc vs. bulge</i> K-S / W
log N_e	0.02 / 0.03	0.69 / 0.74
log T_e (O III)	0.43 / 0.29	0.91 / 0.88
log T_e (N II)	0.30 / 0.14	0.10 / 0.15
$O^{++}/(O^++O^{++})$	0.23 / 0.89	0.32 / 0.03
$He^{++}/(He^++He^{++})$	0.96 / 0.00	0.29 / 0.00
log ϵ (He)	0.14 / 0.10	0.98 / 0.87
log ϵ (O)	0.74 / 0.84	0.16 / 0.49
log ϵ (Ar)	0.03 / 0.05	0.54 / 0.36
log ϵ (Ne)	0.71 / 0.44	0.95 / 0.63
log ϵ (S)	0.95 / 0.75	0.03 / 0.04
log ϵ (N)	0.39 / 0.49	0.86 / 0.32
log ϵ (Cl)	0.21 / 0.32	0.90 / 0.93
log(S/O)	0.19 / 0.08	0.13 / 0.05
log(Ne/O)	0.01 / 0.03	0.88 / 0.47
log(Ar/O)	0.33 / 0.18	0.73 / 0.68
log(Cl/O)	0.70 / 0.66	0.38 / 0.72
log(N/O)	0.39 / 0.57	0.68 / 0.97
log(N/Ar)	0.21 / 0.04	0.63 / 0.34
log(N/Ne)	0.58 / 0.64	0.56 / 0.27
log(N/S)	0.42 / 0.44	0.21 / 0.21
log(N/Cl)	0.16 / 0.28	0.90 / 1.00
log(Ne/Ar)	0.15 / 0.04	0.05 / 0.08
log(S/Ne)	0.68 / 0.66	0.23 / 0.12
log(S/Ar)	0.01 / 0.00	0.25 / 0.11

pared to those pertaining to the Galactic bulge share the same abundance pattern (see Tables 8–10). The only difference seems to be in the S/Ar abundance ratio (see below).

Our preliminary interpretation is that Galactic disc DC PNe (with higher N and He contents) probably have, on average, more massive and more metal-rich central stars than the OC sources. At constant metallicity, high He/H and N/O ratios are characteristic of proton-capture nucleosynthesis (Stanghellini et al. 2006); for example, bipolar Type I PNe display high He/H and N/O ratios, indicating that their progeni-

tors are probably HBB AGB stars with initial masses $\sim 3\text{--}8 M_{\odot}$ (Peimbert 1978; Kingsburgh & Barlow 1994; Stanghellini et al. 2006; Karakas et al. 2009). On the other hand, we also expect different metallicities through our samples of Galactic PNe. Abundances of S, Cl, and Ar in PNe are usually assumed to be unaltered by AGB nucleosynthesis, while the Ne content can be slightly altered during the AGB (Karakas et al. 2009, and references therein). Under the assumption that S, Cl, and Ar are not altered by AGB evolution, we find Ar to be most useful and reliable metallicity indicator. This is because S may be depleted

Table 9. Median plasma parameters and abundance values for disc PNe. The 25 and 75 percentiles are given in brackets and the number of objects in parentheses.

Parameter/element	OC	DC	CC	F
$\log N_e$	4.09 [3.70, 5.00] (16)	3.76 [3.60, 3.89] (21)	3.83 [3.47, 4.00] (25)	3.32 [3.03, 3.44] (6)
$\log T_e$ (O III)	4.05 [4.01, 4.10] (16)	3.98 [3.96, 4.01] (16)	4.05 [4.00, 4.08] (22)	4.05 [3.93, 4.08] (6)
$\log T_e$ (N II)	4.07 [3.95, 4.13] (12)	4.00 [3.91, 4.07] (21)	4.05 [3.93, 4.09] (21)	- [- , -] (2)
$O^{++}/(O^+ + O^{++})$	0.92 [0.43, 0.96] (18)	0.84 [0.19, 0.94] (21)	0.83 [0.51, 0.93] (27)	0.95 [0.88, 0.96] (6)
$He^{++}/(He^+ + He^{++})$	0.00 [0.00, 0.02] (18)	0.00 [0.00, 0.10] (20)	0.00 [0.00, 0.07] (27)	0.33 [0.03, 0.38] (5)
$\log \epsilon$ (He)	11.02 [10.99, 11.03] (15)	11.10 [11.05, 11.13] (16)	11.03 [10.99, 11.07] (21)	11.07 [11.01, 11.09] (5)
$\log \epsilon$ (O)	8.57 [8.17, 8.72] (17)	8.66 [8.54, 8.71] (21)	8.52 [8.35, 8.59] (27)	8.52 [7.94, 8.67] (6)
$\log \epsilon$ (Ar)	6.04 [5.91, 6.12] (14)	6.56 [6.48, 6.71] (16)	6.07 [5.92, 6.42] (21)	6.21 [5.84, 6.40] (6)
$\log \epsilon$ (Ne)	8.00 [7.61, 8.19] (10)	8.10 [7.95, 8.22] (16)	7.75 [7.55, 7.96] (15)	7.83 [7.33, 7.98] (5)
$\log \epsilon$ (S)	6.66 [6.44, 6.83] (13)	7.02 [6.94, 7.17] (16)	6.47 [6.23, 6.71] (20)	6.43 [6.14, 6.52] (5)
$\log \epsilon$ (N)	7.82 [7.44, 8.02] (17)	8.38 [8.14, 8.56] (21)	7.76 [7.61, 8.07] (25)	7.71 [7.15, 7.74] (5)
$\log \epsilon$ (Cl)	6.08 [5.92, 6.13] (6)	6.21 [6.04, 6.57] (10)	5.99 [5.83, 6.01] (7)	- [- , -] (2)
$\log(S/O)$	-1.84 [-1.95, -1.68] (13)	-1.62 [-1.69, -1.52] (16)	-1.99 [-2.14, -1.94] (19)	-1.86 [-2.14, -1.71] (5)
$\log(Ne/O)$	-0.60 [-0.64, -0.58] (10)	-0.57 [-0.66, -0.52] (15)	-0.69 [-0.82, -0.66] (15)	-0.57 [-0.70, -0.52] (5)
$\log(Ar/O)$	-2.40 [-2.53, -2.27] (14)	-2.09 [-2.16, -1.99] (16)	-2.39 [-2.49, -2.17] (21)	-2.26 [-2.38, -2.38] (6)
$\log(Cl/O)$	-2.53 [-2.83, -2.33] (6)	-2.45 [-2.66, -2.10] (10)	-2.63 [-2.75, -2.49] (7)	- [- , -] (2)
$\log(N/O)$	-0.81 [-0.95, -0.53] (17)	-0.27 [-0.40, -.10] (21)	-0.70 [-0.81, -0.55] (25)	-0.65 [-1.35, -0.40] (5)

Table 10. Median plasma parameters and abundance values for bulge PNe.

Parameter/element	OC	DC
C	1.33 [1.15, 1.55] (15)	1.99 [1.44, 2.36] (30)
$\log N_e$	3.57 [3.32, 3.80] (17)	3.73 [3.61, 3.96] (38)
$\log T_e$ (O III)	4.01 [3.97, 4.05] (15)	3.98 [3.96, 4.03] (16)
$\log T_e$ (N II)	4.14 [4.03, 4.16] (13)	3.94 [3.83, 4.07] (37)
$O^{++}/(O^+ + O^{++})$	0.90 [0.71, 0.94] (17)	0.55 [0.00, 0.88] (38)
$He^{++}/(He^+ + He^{++})$	0.00 [0.00, 0.04] (16)	0.00 [0.00, 0.04] (38)
$\log \epsilon$ (He)	11.04 [11.01, 11.06] (17)	11.09 [11.05, 11.14] (22)
$\log \epsilon$ (O)	8.61 [8.38, 8.70] (17)	8.61 [8.21, 8.71] (38)
$\log \epsilon$ (Ar)	6.29 [6.05, 6.40] (17)	6.51 [6.38, 6.63] (22)
$\log \epsilon$ (Ne)	7.77 [7.67, 8.05] (14)	8.12 [7.86, 8.23] (17)
$\log \epsilon$ (S)	6.64 [6.41, 6.79] (17)	6.87 [6.66, 7.03] (22)
$\log \epsilon$ (N)	7.74 [7.38, 7.98] (17)	8.30 [8.03, 8.49] (38)
$\log \epsilon$ (Cl)	6.17 [5.84, 6.28] (10)	6.32 [6.14, 6.57] (8)
$\log(S/O)$	-1.98 [-2.03, -1.80] (17)	-1.71 [-1.78, -1.61] (22)
$\log(Ne/O)$	-0.66 [-0.69, -0.64] (14)	-0.55 [-0.60, -0.44] (17)
$\log(Ar/O)$	-2.31 [-2.39, -2.19] (17)	-2.03 [-2.27, -1.96] (22)
$\log(Cl/O)$	-2.44 [-2.63, -2.24] (10)	-2.37 [-2.47, -2.20] (8)
$\log(N/O)$	-0.80 [-1.04, -0.53] (17)	-0.23 [-0.48, -0.11] (38)

into dust (especially in CC PNe; Pottasch & Bernard-Salas 2006, see also below) and because we have fewer objects with Cl abundance determinations. The median Ar abundances are $\log \epsilon(Ar)=6.56$, 6.04, and 6.07 for the DC, OC, and CC disc PNe, respectively. In Fig. 7 we display Ar/H vs. O/H for the Galactic disc and bulge PNe depending on the major *Spitzer* dust types. Ar/H and O/H seem to be rather well correlated (although with some scatter) in CC, OC, and F Galactic disc PNe (Fig. 7, left panel), while most of the DC Galactic disc PNe display the highest Ar abundances (mostly supra-solar). The observed Ar-O correlation in CC and OC disc PNe may be interpreted as due to the different metallicity (Ar it is expected to evolve in lockstep with O) in disc PNe of rather low-mass central stars; O is expected to be almost unaltered in low mass non-HBB stars (e.g. Karakas et al. 2009). The F disc PNe with very little dust in their circumstellar shells are simply more evolved objects, as suggested by their lower electron densities and higher ionization (Table 9; see Section 5).

Thus, DC disc PNe (mostly with supra-solar metallicities) could be the descendants of more massive HBB stars where N production takes place. Another possibility could be that they evolve from supra-solar metallicity and less massive stars (say $\sim 1.5-2.5 M_{\odot}$) with some kind of extra mixing where the central star may or may not be converted to C-rich depending on the TDU episodes experienced. However, the detailed AGB evo-

lution and nucleosynthesis of such supra-solar metallicity stars remain to be theoretically investigated. At present, we favour the high-mass interpretation because DC PNe are mainly located towards the Galactic centre, as expected if they pertain to a more massive and younger population. There are a few DC sources in Fig. 7 (left panel) with supra-solar Ar abundances, together with slightly low O abundances. Strong HBB also may produce some O destruction. Alternatively, some O depletion could be possible if this element is being trapped in dust grains.

Another interesting feature in Fig. 7 (left panel) is that most OC disc PNe display subsolar Ar abundances (also an important fraction of CC disc PNe). This implies that the Stanghellini et al. (2012) sample is dominated by relatively low-mass and low-metallicity OC (and CC) PNe. This is consistent with the high rate (>60%) of OC and CC PNe with unevolved/unprocessed circumstellar dust - that is, OC_{am} and CC_{al} PNe (see Table 6) - found in the Galactic disc; for instance, CC_{al} PNe are very frequent in low-metallicity environments dominated by low-mass stars, such as those of the Magellanic Clouds (Stanghellini et al. 2007). Higher central star mass OC PNe in the Galactic disc, with their precursors being massive HBB AGB stars (see e.g. García-Hernández et al. 2006b, 2007a), evolve too fast to be detected in the optical (see García-Hernández et al. 2007b). The only exception is the OC outlier (PNG 011.1+07.0) in the N/H vs. He/H diagram (Fig. 5), which is the PN with the highest

Table 11. Nucleosynthesis predictions for AGB stars from Karakas (2010).

Mass	Z	PMZ	log $\epsilon(\text{He})$	log(N/O)	log(Ne/O)	log(S/O)
1.0	0.02	no	11.065	-0.742	-0.839	-1.685
1.5	0.02	no	11.056	-0.604	-0.839	-1.685
1.9	0.02	no	11.045	-0.579	-0.840	-1.684
2.5	0.02	no	11.056	-0.545	-0.774	-1.676
3.0	0.02	no	11.078	-0.515	-0.668	-1.663
3.0	0.02	yes	11.078	-0.519	-0.570	-1.668
4.0	0.02	no	11.062	-0.470	-0.742	-1.661
5.0	0.02	no	11.113	-0.282	-0.751	-1.644
6.0	0.02	no	11.160	0.070	-0.723	-1.609
1.0	0.008	no	10.982	-0.717	-0.838	-1.683
1.5	0.008	no	10.982	-0.573	-0.834	-1.683
1.9	0.008	no	10.984	-0.555	-0.766	-1.691
2.5	0.008	no	11.032	-0.496	-0.479	-1.673
3.0	0.008	no	11.065	-0.467	-0.273	-1.659
3.0	0.008	yes	11.064	-0.489	-0.103	-1.682
4.0	0.008	no	10.990	-0.469	-0.684	-1.671
5.0	0.008	no	11.086	0.724	-0.488	-1.572
6.0	0.008	no	11.111	0.691	-0.516	-1.467
1.0	0.004	no	10.964	-0.682	-0.837	-1.683
1.5	0.004	no	10.970	-0.574	-0.803	-1.692
1.9	0.004	no	10.992	-0.544	-0.644	-1.708
2.5	0.004	no	11.064	-0.504	-0.065	-1.700
3.0	0.004	no	11.044	-0.496	-0.133	-1.692
3.0	0.008	yes	11.042	-0.539	0.079	-1.736
4.0	0.004	no	11.016	0.649	-0.580	-1.693
5.0	0.004	no	11.114	1.165	-0.254	-1.509
6.0	0.004	no	11.135	1.209	-0.268	-1.290

The abundances listed here (on the usual scale $\log \epsilon(X) = \log(X/H) + 12$) have been calculated by us from the average abundances (mass fraction) given by Karakas (2010). We only consider the most abundant isotopes (i.e. ^4He , ^{14}N , ^{16}O , $^{20,22}\text{Ne}$, and ^{32}S).

Table 12. Kolmogorov–Smirnov (K-S) and Wilcoxon (W) statistical tests for the *Spitzer* dust subtypes DC (DC_{cr} vs. DC_{am+cr}), CC (CC_{ar} vs. CC_{al}), and OC (OC_{cr} vs. OC_{am}, OC_{cr} vs. OC_{am+cr}, and OC_{am} vs. OC_{am+cr}) in disc and bulge PNe.

Parameter/element	<i>disc + bulge</i>		<i>disc + bulge</i>		<i>disc + bulge</i>	
	DC subtypes		CC subtypes		OC subtypes	
	DC _{cr} vs. DC _{am+cr}	CC _{ar} vs. CC _{al}	OC _{cr} vs. OC _{am}	OC _{cr} vs. OC _{am+cr}	OC _{am} vs. OC _{am+cr}	
	K-S / W	K-S / W	K-S / W	K-S / W	K-S / W	
log N _e	0.05 / 0.03	0.05 / 0.07	0.56 / 0.65	0.08 / 0.12	0.25 / 0.40	
log T _e (O III)	0.22 / 0.46		0.21 / 0.56	0.19 / 0.83	0.05 / 0.03	
log T _e (N II)	0.22 / 0.09	0.97 / 0.76	0.23 / 0.11	0.08 / 0.05	0.33 / 0.32	
O ⁺⁺ /(O ⁺ +O ⁺⁺)	0.31 / 0.07	0.33 / 0.22	0.10 / 0.14	0.95 / 0.93	0.24 / 0.21	
He ⁺⁺ /(He ⁺ +He ⁺⁺)	0.00 / 0.00	0.71 / 0.10	0.63 / 0.02	0.09 / -	0.14 / 0.00	
log $\epsilon(\text{He})$	0.46 / 0.18	0.04 / 0.08	0.02 / 0.24	0.09 / 0.29	0.06 / 0.05	
log $\epsilon(\text{O})$	0.96 / 0.97	0.08 / 0.06	0.36 / 0.46	0.70 / 0.93	0.24 / 0.19	
log $\epsilon(\text{Ar})$	0.03 / 0.05	0.05 / 0.06	0.00 / 0.01	0.01 / 0.02	0.15 / 0.08	
log $\epsilon(\text{Ne})$	0.30 / 0.20		0.19 / 0.30	0.32 / 0.26	1.00 / 0.93	
log $\epsilon(\text{S})$	0.38 / 0.29	0.02 / 0.03	0.07 / 0.10	0.52 / 0.40	0.19 / 0.14	
log $\epsilon(\text{N})$	0.05 / 0.16	0.07 / 0.02	0.22 / 0.42	0.34 / 0.35	0.96 / 0.83	
log $\epsilon(\text{Cl})$	0.38 / 0.78					
log(S/O)	0.33 / 0.52	0.07 / 0.03	0.86 / 1.00	0.52 / 0.56	0.44 / 1.00	
log(Ne/O)	0.49 / 0.24		1.00 / 0.85	0.32 / 0.26	0.19 / 0.11	
log(Ar/O)	0.71 / 0.57	0.05 / 0.10	0.04 / 0.01	0.01 / 0.00	0.48 / 0.52	
log(Cl/O)	0.19 / 0.57					
log(N/O)	0.25 / 0.12	0.05 / 0.02	0.72 / 0.62	0.34 / 0.25	0.75 / 0.27	
log(N/Ar)	0.94 / 0.49	0.23 / 0.11	0.83 / 0.42	0.96 / 0.89	0.56 / 0.57	
log(N/Ne)	0.26 / 0.17		0.97 / 1.00	0.81 / 0.75	0.47 / 0.48	
log(N/S)	0.99 / 0.95	0.94 / 0.75	0.09 / 0.09	0.08 / 0.02	0.47 / 0.31	
log(N/Cl)	0.93 / 0.71					
log(Ne/Ar)	0.19 / 0.19		0.19 / 0.16	1.00 / 0.75	0.67 / 0.40	
log(S/Ne)	0.30 / 0.13		0.74 / 0.88	0.32 / 0.15	0.11 / 0.06	
log(S/Ar)	0.95 / 0.77	0.35 / 0.14	0.07 / 0.03	0.01 / 0.02	0.91 / 0.76	

N and He abundances in the disc sample. PNG 011.1+07.0 is very probably the unique very high-mass HBB PN in the Stanghellini et al. (2012) sample⁶.

⁶ PNG 011.1+07.0 is the only OC_{am} PN with the amorphous silicate features in absorption, indicating an extremely thick circumstellar envelope, and that the central star has just reappeared in the optical (e.g. Garcia-Hernandez et al. 2007b).

The situation is less clear for the bulge PNe shown in Figure 7 (right panel). Again, OC bulge PNe seem to follow an Ar-O correlation (this time with an even higher dispersion), and most DC bulge PNe are concentrated at solar and supra-solar Ar abundances. DC PNe in the bulge show a very similar median Ar abundance (log $\epsilon(\text{Ar})=6.51$) to the DC disc ones, while OC PNe show a higher median Ar abundance (log $\epsilon(\text{Ar})=6.29$) than their

Table 13. Median plasma parameters and abundance values for bulge + disc OC subtypes PNe.

Parameter/element	OC _{cr}	OC _{am}	OC _{am+cr}
log N _e	3.47 [3.15, 3.79] (9)	3.87 [3.23, 4.15] (15)	3.92 [3.65, 4.20] (9)
log T _e (O III)	4.00 [3.92, 4.28] (8)	4.04 [4.01, 4.10] (15)	4.00 [4.00, 4.04] (8)
log T _e (N II)	3.99 [3.87, 4.06] (6)	4.10 [4.04, 4.15] (11)	4.17 [4.04, 4.15] (8)
O ⁺⁺ /(O ⁺ +O ⁺⁺)	0.84 [0.59, 0.92] (10)	0.94 [0.67, 0.98] (16)	0.87 [0.57, 0.91] (9)
He ⁺⁺ /(He ⁺ +He ⁺⁺)	0.01 [0.00, 0.03] (9)	0.01 [0.00, 0.17] (16)	0.00 [0.00, 0.00] (9)
log ε(He)	11.06 [10.86, 11.09] (9)	11.02 [11.00, 11.03] (15)	11.03 [11.03, 11.05] (8)
log ε(O)	8.63 [7.60, 8.75] (9)	8.42 [8.29, 8.64] (16)	8.61 [8.43, 8.73] (9)
log ε(Ar)	6.44 [6.32, 6.58] (8)	6.03 [5.90, 6.11] (15)	6.13 [6.05, 6.25] (8)
log ε(Ne)	8.18 [7.26, 8.28] (6)	7.78 [7.67, 8.00] (12)	7.87 [7.63, 8.05] (6)
log ε(S)	6.82 [6.57, 6.96] (8)	6.50 [6.40, 6.66] (14)	6.68 [6.60, 6.83] (8)
log ε(N)	8.01 [7.10, 8.43] (10)	7.78 [7.34, 7.91] (15)	7.75 [7.47, 7.81] (9)
log ε(Cl)	- [- , -] ()	6.15 [6.00, 6.22] (8)	5.84 [5.61, 6.11] (5)
log(S/O)	-1.96 [-2.01, -1.65] (8)	-1.87 [-2.01, -1.70] (14)	-1.87 [-1.94, -1.81] (8)
log(Ne/O)	-0.63 [-0.78, -0.60] (6)	-0.62 [-0.73, -0.58] (12)	-0.61 [-0.83, -0.64] (6)
log(Ar/O)	-2.12 [-2.28, -2.03] (8)	-2.38 [-2.50, -2.28] (15)	-2.38 [-2.52, -2.35] (8)
log(Cl/O)	- [- , -] ()	-2.23 [-2.52, -2.17] (8)	-2.49 [-2.87, -2.42] (5)
log(N/O)	-0.65 [-1.05, -0.22] (10)	-0.80 [-0.96, -0.52] (15)	-0.88 [-1.04, -0.82] (9)

Table 14. Median plasma parameters and abundance values for bulge + disc DC and CC subtypes PNe.

Parameter/element	DC _{cr}	DC _{am+cr}	CC _{ar}	CC _{at}
log N _e	3.71 [3.85, 3.84] (42)	3.89 [3.65, 4.05] (17)	3.48 [3.31, 3.74] (8)	3.90 [3.50, 4.11] (15)
log T _e (O III)	3.99 [3.95, 4.03] (23)	3.97 [3.96, 3.98] (9)	4.07 [3.95, 4.08] (5)	4.05 [4.01, 4.08] (17)
log T _e (N II)	3.96 [3.84, 4.06] (40)	4.05 [3.90, 4.11] (17)	4.05 [3.92, 4.09] (8)	4.06 [3.97, 4.11] (12)
O ⁺⁺ /(O ⁺ +O ⁺⁺)	0.58 [0.04, 0.89] (42)	0.86 [0.10, 0.93] (17)	0.82 [0.45, 0.89] (8)	0.91 [0.62, 0.98] (18)
He ⁺⁺ /(He ⁺ +He ⁺⁺)	0.00 [0.00, 0.03] (41)	0.00 [0.00, 0.00] (17)	0.01 [0.00, 0.06] (8)	0.01 [0.00, 0.10] (18)
log ε(He)	11.10 [11.06, 11.14] (26)	11.08 [11.04, 11.13] (12)	11.12 [11.02, 11.12] (6)	11.03 [10.99, 11.06] (15)
log ε(O)	8.64 [8.49, 8.72] (42)	8.63 [8.38, 8.74] (17)	8.59 [8.54, 8.64] (8)	8.44 [8.32, 8.58] (18)
log ε(Ar)	6.56 [6.48, 6.69] (26)	6.44 [6.31, 6.60] (12)	6.44 [6.14, 6.46] (6)	5.97 [5.88, 6.18] (14)
log ε(Ne)	8.09 [7.94, 8.16] (21)	8.19 [7.94, 8.24] (12)	- [- , -] ()	7.66 [7.35, 7.84] (11)
log ε(S)	6.99 [6.84, 7.11] (26)	6.89 [6.66, 7.06] (12)	6.71 [6.45, 6.87] (6)	6.35 [6.06, 6.50] (13)
log ε(N)	8.39 [8.12, 8.52] (42)	8.24 [7.98, 8.35] (17)	8.20 [7.82, 8.46] (8)	7.66 [7.53, 8.02] (15)
log ε(Cl)	6.26 [6.11, 6.49] (12)	6.37 [5.95, 6.67] (6)	- [- , -] ()	6.00 [5.94, 6.12] (4)
log(S/O)	-1.65 [-1.75, -1.60] (26)	-1.72 [-1.81, -1.54] (12)	-1.88 [-2.06, -1.72] (6)	-2.07 [-2.28, -1.98] (13)
log(Ne/O)	-0.57 [-0.63, -0.48] (21)	-0.53 [-0.59, -0.37] (12)	- [- , -] ()	-0.73 [-0.84, -0.67] (11)
log(Ar/O)	-2.06 [-2.22, -1.96] (26)	-2.11 [-2.24, -1.97] (12)	-2.17 [-2.42, -2.15] (6)	-2.40 [-2.49, -2.32] (14)
log(Cl/O)	-2.43 [-2.51, -2.24] (12)	-2.24 [-2.65, -1.98] (6)	- [- , -] ()	-2.47 [-2.70, -2.20] (4)
log(N/O)	-0.21 [-0.41, -0.07] (42)	-0.36 [-0.62, -0.17] (17)	-0.38 [-0.71, -0.18] (8)	-0.71 [-0.96, -0.68] (15)

Galactic disc counterparts.⁷ This time, however, there are more DC bulge sources (and a few OC_{cr} ones) with somewhat low O content. Curiously, these DC bulge PNe with low O display even higher N abundances than their disc counterparts; similar objects seem to be absent in the Galactic disc sample (see Fig. 5). A higher N production at the expense of O could be an indication of strong HBB (i.e., the activation of the O-N cycle) but this is preferentially expected in lower metallicity environments, such as the Magellanic Clouds (e.g. Chiappini et al. 2009). The few (3–4) DC bulge PNe with reliable Ar abundances, however, display high Ar abundances (nearly solar), and the apparent N overproduction (and higher N/O ratios) could be due to stronger HBB in higher mass stars.

Figures 8 and 9 display S/H vs. O/H and Ne/H vs. O/H in our Galactic PNe samples, respectively. As for Fig. 7, we plot the Galactic disc and bulge PNe in the left-hand and right-hand panels, respectively, and the major *Spitzer* dust types (and their subtypes) are marked with different symbols and colours. Figure 8 (left panel) shows that there seems to be some correlation between S and O for disc PNe, as expected. The scatter for each major *Spitzer* dust type is similar to what is found for Ar, but there seems to be a different S-O relation among each dust type. In general, we find subsolar S abundances for all major *Spitzer*

dust types, with the CC disc PNe being the most S-depleted objects. The median S abundances are log ε(S)=7.02, 6.66 and 6.47 for the DC, OC, and CC disc PNe, respectively. PNe are known to display subsolar S abundances (e.g. Pottasch & Bernard-Salas 2006) although the importance of this finding is still unclear (see below). The most interesting facts from Fig. 8 (left panel) are that i) DC disc PNe are again clearly located towards the highest S abundances; and ii) CC disc PNe are, on average, more depleted in S than the OC and DC disc PNe. As mentioned above, the highest degree of S depletion in CC disc PNe may be understood if S is depleted into dust in these objects (e.g. Pottasch & Bernard-Salas 2006). We note, however, that the S anomaly in PNe is still an open question. For example, Henry et al. (2012) claim that a link with dust depletion of S can be ruled out and suggest that the S anomaly in PNe is merely a problem with the S abundances are determined directly from IR measurements. Our S results would tend to support the depletion hypothesis, but this should be evaluated more carefully in the future (e.g. by using the S lines in the *Spitzer* spectra). As in the case of Ar, the S/H vs. O/H diagram for bulge PNe is more complex, but again we find evidence of a different S-O relation among each major *Spitzer* dust type (Fig. 8, right panel). Both OC and DC bulge PNe populate this abundance diagram uniformly, although subsolar S abundances are also generally found. The median S abundances are log ε(S)=6.87 and 6.64 for the DC and OC bulge PNe, respectively. A few (3–4) DC PNe in the bulge are located

⁷ The higher median Ar content in OC bulge PNe is related to the fact that OC_{cr} PNe (with higher Ar abundances) are more numerous in the bulge (see Section 4.3 for more details).

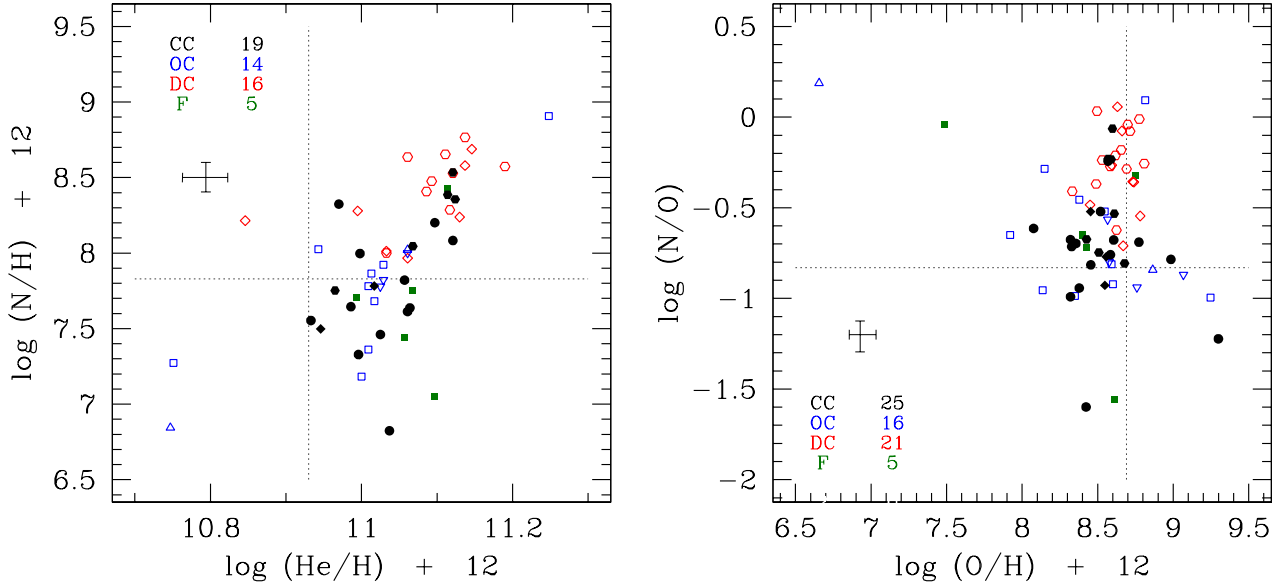


Fig. 5. Diagrams of nebular abundance ratios He/H vs. N/H (left panel) and O/H vs. N/O (right panel) for Galactic disc PNe. Blue symbols mark OC PNe (OC_{cr} - open triangles; OC_{am} - open squares; OC_{am+cr} - open reversed triangles). Red symbols mark CD PNe (DC_{cr} - open hexagons; DC_{am+cr} - open diamonds); Black symbols mark CC PNe (CC_{ar} - filled hexagon; CC_{al} - filled circles; CC_{ar+al} - filled diamonds); Green filled squares mark F type PNe. The horizontal/vertical lines mark the solar abundance values.

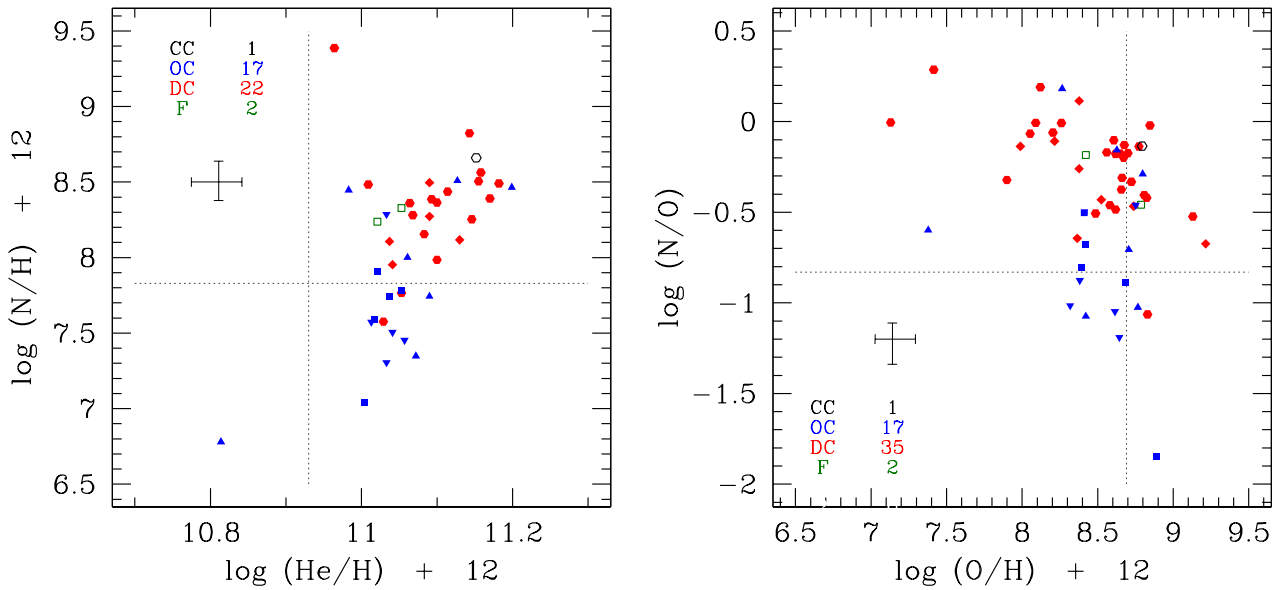


Fig. 6. Diagrams of nebular abundance ratios He/H vs. N/H (left panel) and O/H vs. N/O (right panel) for Galactic bulge PNe. Blue symbols mark OC PNe (OC_{cr} - filled triangles; OC_{am} - filled squares; OC_{am+cr} - filled reversed triangles). Red symbols mark CD PNe (DC_{cr} - filled hexagons; DC_{am+cr} - filled diamonds); Black symbols mark CC PNe (CC_{ar} - open hexagon); Green open squares mark F type PNe. The horizontal/vertical lines mark the solar abundance values.

at low S and O abundances. It is intriguing that these sources pertain to the group of DC bulge PNe with relatively high Ar abundances and showing the apparent signature of the O-N cycle.

Taking the abundance errors (typically ± 0.1 - 0.15 dex) and our previous results on Ar and S into account, we find a surprisingly tight correlation between Ne and O for Galactic PNe in both the disc and bulge (Figure 9). Ne could be slightly mod-

ified by AGB nucleosynthesis when ^{22}Ne is overproduced. An increase in ^{22}Ne is theoretically predicted to occur in a rather narrow mass range of ~ 2.5 - $3.5 M_{\odot}$ or in higher mass stars as a consequence of some O destruction by strong HBB and slight Ne enrichments via dredge-up; although the latter effect seems to be more important at low metallicity (Karakas & Lattanzio 2003; Karakas et al. 2009). In addition, in very low mass AGB models, the partial mixed zone (PMZ) can produce ^{22}Ne , further increas-

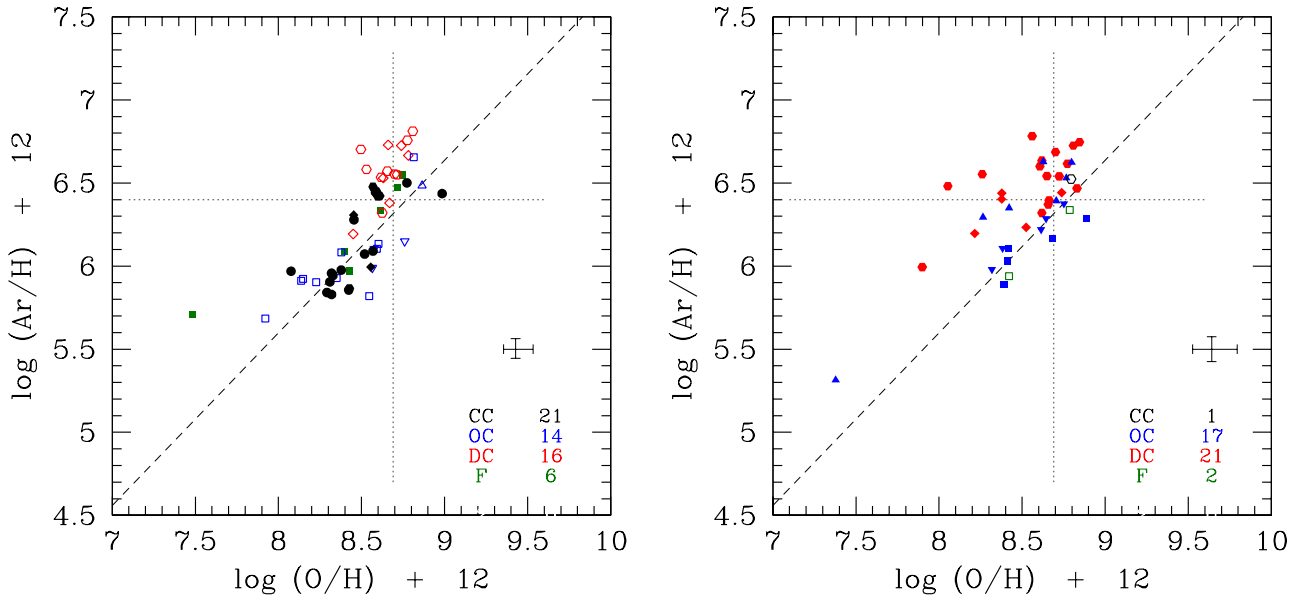


Fig. 7. Diagrams of nebular abundance ratio O/H vs. Ar/H for Galactic disc PNe (left panel) and Galactic bulge PNe (right panel). The same meaning of symbols as in Figs. 5 and 6. The horizontal/vertical lines mark the solar abundance values, while the dashed line marks the relation derived by Izotov et al. (2006).

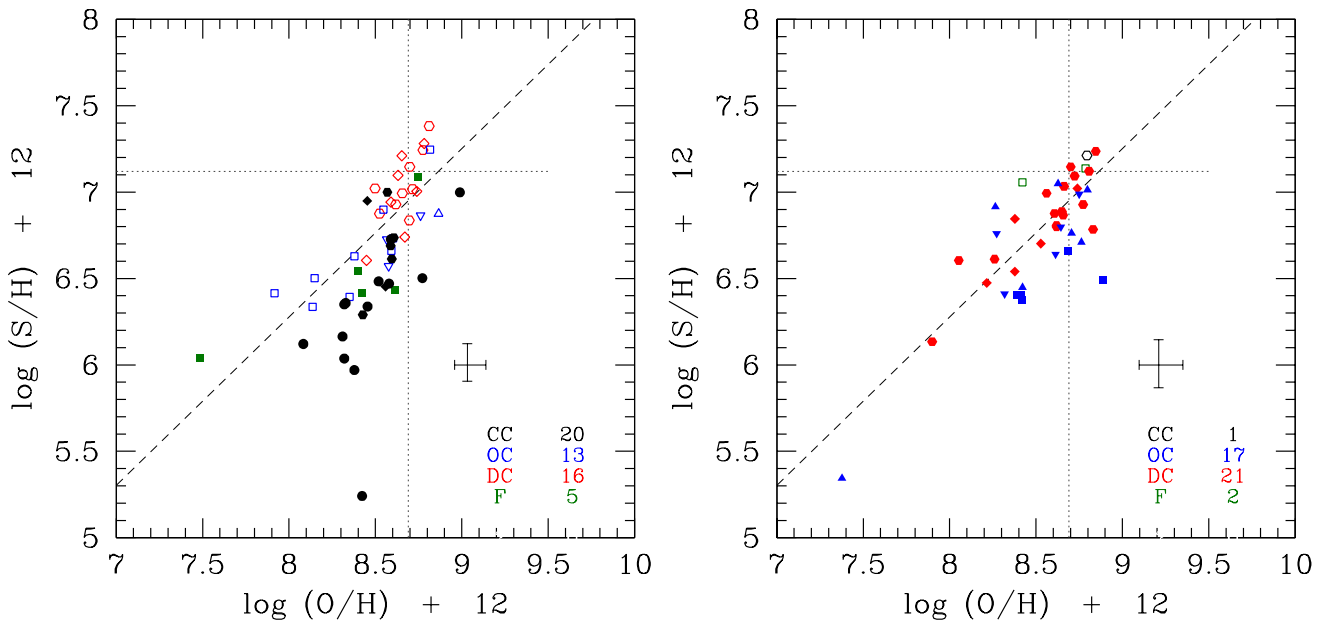


Fig. 8. Diagrams of nebular abundance ratio O/H vs. S/H for Galactic disc PNe (left panel) and Galactic bulge PNe (right panel). The same meaning of symbols as in Figs. 5 and 6. The horizontal/vertical lines mark the solar abundance values, while the dashed line marks the relation derived by Izotov et al. (2006).

ing the Ne/O ratio (e.g. Karakas et al. 2009, see also next section for more details). The tight Ne-O correlations displayed in Fig. 9 seem to suggest that, in most cases, Ne is not strongly altered by AGB evolution and that it closely follows the O content. Indeed, this would agree with the remarkably constant Ne/O ratio observed in PNe with very different chemical compositions (see e.g. Stasińska et al. 1998). As we see in the next section, however, the median Ne/O values observed in our Galactic PNe are slightly higher than the AGB nucleosynthesis predictions with no PMZ, and they seem to require including the PMZ in the theoretical models.

Also, some outliers may be identified in the Ne/H vs. O/H diagram for Galactic disc PNe shown in Figure 9 (left panel). For example, a clear outlier in Fig. 9 (left panel) is again PNG 011.1+07.0 (probably a high-mass HBB PN), which shows a huge Ne overabundance (or Ne/O ratio) and which clearly deviates from the observed Ne-O trend. Also, some DC disc PNe display some Ne enhancements, although more modest than that in PNG 011.1+07.0. The Ne abundances in the latter DC disc PNe are higher than those in other objects at similar O/H and than those observed in other types of PNe (e.g. most of the OC and CC disc PNe). The median Ne abundances are $\log \epsilon(\text{Ne})=8.10$,

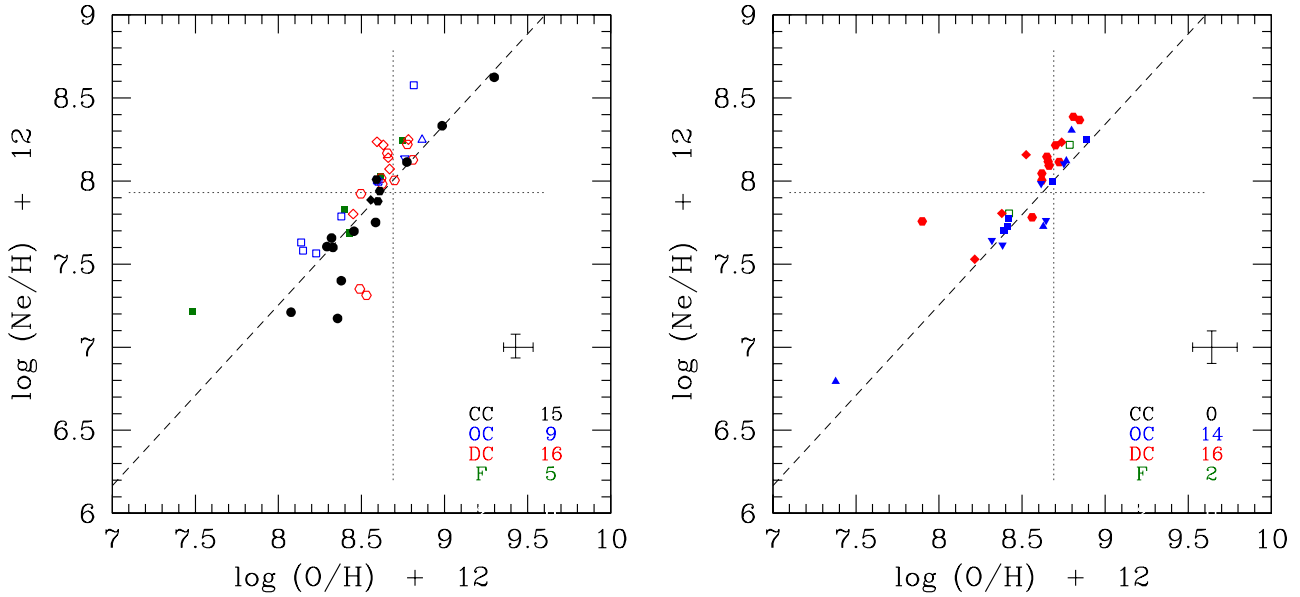


Fig. 9. Diagrams of nebular abundance ratio O/H vs. Ne/H for Galactic disc PNe (left panel) and Galactic bulge PNe (right panel). The same meaning of symbols as in Figs. 5 and 6. The horizontal/vertical lines mark the solar abundance values, while the dashed line marks the relation derived by Izotov et al. (2006).

8.00, and 7.75 for the DC, OC, and CC disc PNe, respectively. The apparent Ne enhancements in some DC disc PNe could indicate that their central stars are more massive than most OC and CC disc PNe but less massive than the high-mass HBB PN PNG 011.1+07.0. We note also that there are a few DC and CC disc PNe outliers that show unusually low Ne contents. On the other hand, the Ne/H vs. O/H diagram for bulge PNe (Fig. 9, right panel) shows an even tighter Ne-O correlation, where less clear outliers are identified. A clear outlier is PNG 358.6+01.8, which shows a strong Ne overabundance that deviates from the Ne-O relation. Remarkably, PNG 358.6+01.8 is the lowest metallicity ($\log \epsilon(\text{Ar})=6.0$) object among the small group of DC bulge PNe showing the apparent signature of the O-N cycle and with all abundances available. Its abundance pattern suggests the activation of the O-N cycle by strong HBB in a low metallicity and relatively massive progenitor. DC PNe in the bulge display similar median Ne abundances ($\log \epsilon(\text{Ne})=8.12$), while OC PNe show a median Ne abundance ($\log \epsilon(\text{Ne})=7.7$) that is lower than their counterparts in the Galactic disc.

In summary, we conclude that, on average, DC disc PNe probably evolve from AGB progenitors that are more massive and metal rich than most of the OC and CC disc PNe, as already suggested by their higher N and He abundances. The same conclusion seems to be applicable to the sample of PNe in the bulge, with the important peculiarity of the complete lack of CC PNe in this Galactic environment (see Section 6).

4.2. Major *Spitzer* dust types vs. AGB nucleosynthesis predictions

For comparison with the chemical abundances observed in our sample of PNe with *Spitzer* spectra, in Table 11 we present the nucleosynthesis theoretical predictions for He, N/O, Ne/O, and S/O in AGB stars of different progenitor masses (from 1 to 6 M_{\odot})

and metallicities ($z=0.02, 0.008, \text{ and } 0.004$) by Karakas (2010).⁸ These models assume the Vassiliadis & Wood (1993) mass loss on the AGB and do not include either convective overshooting or a partially mixed zone (PMZ), which is required for including a ^{13}C pocket that produces neutron capture elements (see e.g. Lugaro et al. 2012; Kamath et al. 2012). The only exception are the 3 M_{\odot} models, for which Karakas (2010) also give the nucleosynthesis predictions with PMZ. The predictions of the latter 3 M_{\odot} models with PMZ are also given in Table 11. We note that the Karakas (2010) AGB nucleosynthesis predictions are calculated with Anders & Grevesse (1989) solar abundances, while here we assume the most recent solar abundances by Asplund et al. (2009) (see below). The He abundance and the abundance ratios given in Table 11 (Karakas 2010) are consistent with similar models calculated with Asplund et al. (2009) solar abundances (A. Karakas 2013, private communication). The comparison of the median chemical abundances observed in our sample of Galactic disc PNe (Table 9) with the theoretical predictions for AGB stars listed in Table 11 seems to support our preliminary interpretation above.

The DC disc PNe display median O (8.66), Ar (6.56), Ne (8.10), and S (7.02) abundances that compare reasonably well (within the errors) with the corresponding O, Ar, Ne, and S solar abundances of 8.69, 6.40, 7.93, and 7.12, respectively (Asplund et al. 2009). The median He abundance (11.10) and N/O (-0.27) abundance ratios observed in DC disc PNe agree very well (especially the N/O ratio, which is much more sensitive to AGB nucleosynthesis) with the theoretical predictions for a solar metallicity ($z \sim 0.02$) $\sim 5 M_{\odot}$ AGB star (see Table 11). According to Karakas (2010) models, such a star is within the limit for HBB occurrence. A relatively weak HBB activation would be consistent with the nearly solar O abundances observed in DC disc PNe (there is no important O destruction by too strong an

⁸ Karakas (2010) does not give predictions for Ar and Cl but these elements are expected to be unaltered by AGB evolution (e.g. Karakas et al. 2009, and references therein).

HBB). The S/O and Ne/O ratios are less sensitive to AGB evolution (see Table 11), as expected. The median S/O (-1.62) in DC disc PNe is consistent with the AGB predictions (Table 11), suggesting a low degree of S depletion in these objects. The median Ne/O (-0.57), however, is somewhat higher than AGB predictions in Table 11.

This apparent Ne overproduction in DC disc PNe seems to be real and the median Ne/O in DC disc PNe is further increased by the few sources with some Ne enhancements mentioned above (see Figure 9). A higher mass limit for the DC disc PNe is put by the chemical abundances observed in PNG 011.1+07.0, the only very high-mass HBB PN in the disc sample. The high He (11.25) and N/O (0.09) in this source are consistent with a progenitor mass of $6 M_{\odot}$ (see Table 11). The S/O (-1.57) ratio also agrees with the $6 M_{\odot}$ model predictions, but the observed Ne/O (-0.24) is about 0.5 dex higher than these predictions (Table 11). Higher mass (7–8 M_{\odot}) nucleosynthesis models predict slightly higher He and N/O (and S/O) (A. Karakas 2013; private communication) but still consistent (within the errors) with the abundances observed in PNG 011.1+07.0. The extremely high Ne/O in PNG 011.1+07.0 is intriguing. At $z=0.02$, Ne/O increases only slightly with increasing stellar mass. Interestingly, the Ne/O ratio can increase significantly (e.g. up to 0.2–0.3 dex in a $5 M_{\odot}$ star) in massive AGB models with delayed superwinds (which also includes a small PMZ of $1 \times 10^{-4} M_{\odot}$; Karakas et al. 2012) when compared to the Karakas (2010) models. The study of the Ne/O ratio in massive HBB AGB stars with delayed superwinds should be extended to higher masses, PMZ sizes, and supra-solar metallicities in the future. Apart from the unusually high Ne/O ratio, we conclude that PNG 011.1+07.0 should have evolved from an AGB star of at least $6 M_{\odot}$.

The OC disc PNe show median O (8.57), Ar (6.04), Ne (8.00), and S (6.66) abundances that correspond to a subsolar metallicity of $[M/H] \sim -0.4$ (or $z \sim 0.008$). The median O (8.57) abundance seems to only be a little depleted only, but the median Ne (8.00) content is nearly solar. The median N/O (-0.81) (and He within the errors) in OC disc PNe is consistent with the theoretical predictions for a $z=0.008 \sim 1 M_{\odot}$ AGB star (see Table 11). However, the median Ne/O (-0.60) is similar to that in DC disc PNe, being 0.24 dex higher than the $1 M_{\odot}$ model predictions in Table 11. In very low-mass AGB models, the PMZ can produce ^{22}Ne , further increasing the Ne/O ratio (e.g. Karakas et al. 2009). The PMZ effect on the Ne/O ratio can be seen in Table 11, where the $3 M_{\odot}$ model predictions with and without PMZ are compared.⁹ It can be seen that Ne/O can be further enhanced by ~ 0.2 dex (with He, N/O, and S/O less altered) in the low-metallicity models with PMZ. The Ne/O ratio increases with increasing size of the PMZ; e.g. metal-poor ($z=0.01$) $1.25 M_{\odot}$ models with PMZ show that Ne/O can vary from ~ -0.7 to -0.4 dex for PMZ sizes between 1×10^{-3} and $8 \times 10^{-3} M_{\odot}$ (A. I. Karakas 2013, private communication). Thus, the relatively high Ne/O abundances in OC disc PNe may be reflecting the effect of PMZ during the previous AGB phase. Indeed, our chemical abundances in OC disc PNe could perhaps be used to put observational constraints on the size of the PMZ in the very low-mass AGB models.

Furthermore, CC disc PNe show median O (8.52) and Ar (6.07) abundances similar to those in OC disc PNe. The median Ar abundance also indicates a subsolar metallicity ($[M/H] \sim -0.3$ – -0.4 or $z \sim 0.008$) in CC disc PNe. However, both median abundances of Ne (7.75) and S (6.47) in CC disc PNe are lower

than those in the OC ones by about 0.2–0.3 dex. The median N/O (-0.70) is higher than the corresponding value in OC sources, which could suggest higher progenitor masses in CC disc PNe (the predicted N/O ratios increase with increasing stellar mass; see Table 11), but this possible difference is not confirmed by our statistical tests (Table 7). At $z=0.008$, only models with progenitor masses $1.9 \leq M < 3 M_{\odot}$ become C-rich. This simple fact already suggests that CC disc PNe should, on average, have higher central star masses than the OC disc PNe. The best fit to the observed median N/O and Ne/O ratios in CC PNe is given by the $1.9 M_{\odot}$ model.

Comparison of AGB theoretical predictions with the median chemical abundances observed in our sample of Galactic bulge PNe (where CC PNe are absent) turns out to be very simple. The DC PNe in the bulge and disc share the same median abundance pattern, which is consistent with the theoretical predictions for a solar-metallicity ($z \sim 0.02$) $\sim 5 M_{\odot}$ AGB star (see above). The OC PNe in the bulge display median chemical abundances that are almost identical to their Galactic disc counterparts. The only difference (although not confirmed by our statistical tests) is that OC bulge PNe seem to show a higher median Ar abundance. We will see in the following sections that this apparently higher Ar abundance is due to the fact that OC PNe with crystalline silicate dust features (OC_{cr}), being more numerous in the bulge, are more metal rich than the other types of OC PNe with amorphous silicates (OC_{am} and OC_{am+cr}). We anticipate that the median abundances of OC bulge PNe with amorphous silicates are identical to those of the bulk of OC PNe in the Galactic disc,¹⁰ in agreement with the model predictions for a $z=0.008 \sim 1 M_{\odot}$ AGB star. The median abundances of the OC_{cr} subtype are more consistent with higher metallicity (nearly solar) and slightly more massive AGB progenitors (see Section 4.4).

Finally, it is to be noted here that the lower mass limits to produce C-rich ($\text{C/O} > 1$) AGB stars is a longstanding issue. This problem is related with how convection is theoretically treated in stellar interiors. Including convective overshooting (see e.g. Herwig 2000) is a way to increase the efficiency of the third dredge-up (TDU) and to reduce the lower mass limit for C-star formation. The mass limit for the HBB occurrence is also another parameter that strongly depends on the theoretical details (convection treatment, mass loss prescription, etc.; see e.g. García-Hernández et al. 2013, and references therein). Thus, we would like to point out that the exact progenitor masses of Galactic PNe with *Spitzer* spectra that we infer from our comparison with the Karakas (2010) AGB nucleosynthesis models may be rather uncertain. However, our main finding of different average progenitor masses and metallicities amongst the several major *Spitzer* dust types is assured.

4.3. PNe nebular abundances versus *Spitzer* dust subtypes

Analysing the derived nebular gas abundances vs. the *Spitzer* dust subtypes is more difficult and uncertain due to the low number of objects in each dust subtype. Taking the results discussed in Section 4.1 into account, where we found that OC and DC PNe in the Galactic disc and bulge display very similar abundance patterns (Table 8), we decided to merge both galactic PNe samples with the intention of obtaining a higher statistical significance of any potential result. The results of our K-S and W statistical tests for the *Spitzer* dust subtypes DC (DC_{cr} vs. DC_{am+cr}), CC (CC_{ar} vs. CC_{al}), and OC (OC_{cr} vs. OC_{am} , OC_{cr}

⁹ Unfortunately, Karakas (2010) does not give the nucleosynthesis predictions for AGB models with PMZ for masses different than $3 M_{\odot}$.

¹⁰ OC_{cr} PNe are less frequent in the Galactic disc and have a negligible impact on the median abundances derived in OC disc PNe.

vs. OC_{am+cr} , and OC_{am} vs. OC_{am+cr}) in disc and bulge PNe are shown in Table 12. We still have somewhat low numbers (~ 10) of OC_{cr} and OC_{am+cr} PNe and an even lower number (~ 6) of CC_{ar} PNe, and the results for these *Spitzer* dust subtypes (especially for CC_{ar} objects) should be taken with caution. A higher number of sources (>10), however, is present among the two DC subtypes and the OC_{am} and CC_{al} PNe. Tables 13 and 14 list the median plasma parameters and abundances for all Galactic PNe (disc and bulge) for the OC subtypes and DC (and CC) subtypes, respectively.

Remarkably, O-rich PNe with crystalline silicate dust features (OC_{cr}) display median N and He abundances of $\log \epsilon(N)=8.01$ and $\log \epsilon(He)=11.06$, which are slightly higher than those in the OC_{am} and OC_{am+cr} subtypes with amorphous silicate dust features. OC_{am} and OC_{am+cr} PNe show very similar median N and He abundances; $\log \epsilon(N)=7.78$ and $\log \epsilon(He)=11.02$ are observed in OC_{am} PNe while these values are 7.75 and 11.03 in the OC_{am+cr} sources. The median N/O ratio in OC_{cr} PNe (-0.65) is also slightly higher than those in the OC_{am} (-0.80) and OC_{am+cr} (-0.88) objects. Unfortunately, our K-S and W statistical tests do not confirm the possible differences in the He/H, N/H and N/O between the different OC subtypes (Table 12). In addition, OC_{cr} PNe display a high (nearly solar) median Ar abundance ($\log \epsilon(Ar)=6.44$), which contrasts with the subsolar Ar abundances of $\log \epsilon(Ar)=6.03$ and 6.13 obtained in OC_{am} and OC_{am+cr} PNe, respectively.

This difference in the Ar/H abundance seems to be real and it is confirmed by the K-S and W statistical tests in Table 12. We note that two OC_{cr} PNe (PNG 007+03.2 and PNG 357.6+01.7, both in the bulge) display an abundance pattern (with high He, N, Ar, and N/O; see Table 3) almost identical to the one shown by the DC PNe. Their classification as OC_{cr} PNe is based on the lack of PAH-like dust features in the $\sim 5\text{--}10\ \mu\text{m}$ region. The S/N in the $\sim 5\text{--}10\ \mu\text{m}$ region of their *Spitzer* spectra is very low and both sources only display a very weak PAH-like emission feature at $11.3\ \mu\text{m}$. Thus, PNG 007+03.2 and PNG 357.6+01.7 should be truly DC PNe, where the weak PAH-like features have probably escaped detection from *Spitzer*. The rest of the OC_{cr} PNe dominate the median abundances mentioned above (see also Table 13). Thus, our chemical abundances confirm that OC_{cr} PNe are more metal-rich than the other OC subtypes with amorphous silicates (see also the next section). Furthermore, the O-rich PNe with amorphous (OC_{am} and OC_{am+cr}) and crystalline (OC_{cr}) silicate dust features are more numerous in the disc and bulge, respectively, dominating the observed distributions of chemical abundances (median values) in the major OC-type PNe and studied in the previous sections (see also Section 6).

With only crystalline silicate dust features (DC_{cr}), the DC PNe display a median abundance pattern (He, N, O, Ne, Ar, and S; see Table 14) almost identical (differences ≤ 0.15 dex) to those PNe also showing amorphous silicates (DC_{am+cr}). The K-S and W statistical tests (Table 12) indicate that there are no statistically significant differences between both DC subtypes. There is a tentative hint that DC_{cr} PNe could be slightly more metal-rich (i.e. higher Ar abundances) and more N-rich than their DC_{am+cr} counterparts, as suggested by their slightly higher Ar and N median abundances ($\log \epsilon(N)=8.39$ and $\log \epsilon(Ar)=6.56$). Indeed, we find relatively low statistical probabilities for these two elements (Table 12) but not low enough to consider these possible differences to be real. Thus, we conclude that, on average, both DC subtypes are chemically indistinguishable and that they probably evolve from the same AGB progenitors (see also Section 4.2).

Regarding the CC PNe, we note that there are few objects amongst the different CC dust subtypes (CC_{ar} , CC_{al} , and CC_{ar+al}). In particular, we only have data for eight CC_{ar} PNe and three CC_{ar+al} PNe (with the simultaneous presence of aromatic and aliphatic dust features). Curiously, two (PNG 006.1+08.3 and PNG 345.2-08.8) of these CC_{ar+al} sources are PNe where the complex fullerene (e.g. C_{60} and C_{70}) molecules have recently been found (e.g. García-Hernández et al. 2010, 2012). The third object (PNG 041.8+04.4) is an infrared spectroscopic twin of PNG 006.1+08.3 (PN M 1-20), but the fullerene features are not detected in its *Spitzer* spectrum. Thus, we do not list the three CC_{ar+al} objects mentioned above¹¹ in Table 14, and they have not been considered in our K-S and W statistical test displayed in Table 12.

More interesting is that C-rich PNe with aliphatic dust features (CC_{al}) display median N ($\log \epsilon(N)=7.66$) and He ($\log \epsilon(He)=11.03$) abundances lower than those in the CC_{ar} subtype with aromatic (PAH-like) dust features; $\log \epsilon(N)=8.20$ and $\log \epsilon(He)=11.12$ are observed in CC_{ar} PNe. The median N/O ratio of -0.71 in CC_{al} PNe is also considerably lower than in the CC_{ar} (-0.38) sources. Also, CC_{al} PNe show a median subsolar Ar abundance ($\log \epsilon(Ar)=5.97$), while CC_{ar} PNe show a nearly solar Ar content ($\log \epsilon(Ar)=6.44$). The median S abundances are $\log \epsilon(S)=6.71$ and 6.35 for the CC_{ar} and CC_{al} PNe, respectively. However, taking the metal-poor character of CC_{al} PNe into account, the S depletion (of ~ 0.4 dex) is similar in both types of CC PNe.

Our K-S and W tests give relatively low statistical probabilities ($\leq 8\%$) for all elements (He, N, O, Ar, and S) available in the CC_{ar} sources (Table 12). However, the number of CC_{ar} PNe is still too low, preventing us from reaching a firm statistical confirmation of these differences in the median chemical abundances for both subtypes of CC PNe. We believe that these differences (at least to some extent) may be real. Indeed, at least half (four) of the CC_{ar} objects (i.e. PNG 010.6+03.2, PNG 309.5-02.9, PNG 336.3-05.6, and PNG 355.7-03.0) show an abundance pattern (with high He, N, Ar, and N/O; see Table 3) identical to the one shown by the DC PNe. This is also evident in Figures 5 and 6, where it can be seen that several CC_{ar} PNe are located in the same regions as occupied by the DC PNe. Their classification as CC_{ar} relies on the apparent lack of clear crystalline silicate features in the $\sim 20\text{--}38\ \mu\text{m}$ spectral region. As pointed out by Stanghellini et al. (2012), some dust classifications may be uncertain. Indeed, the shape of the dust continuum emission seen in their *Spitzer* spectra is not very different to the one in DC PNe; e.g., PNG 010.6+03.2 even seems to show some tentative crystalline silicate features in its *Spitzer* spectrum (see Fig. 4 in Stanghellini et al. 2012). Thus, the last four sources should be true DC PNe where the weak crystalline silicate features were possibly not detected by *Spitzer*. By inspecting the *Spitzer* spectra of the remaining (four) CC_{ar} PNe, we also find some doubtful classifications. In two sources (PNG 297.4+03.7 and PNG 344.8+03.4), the aromatic (PAH-like) dust features are very weak, while the other two sources (PNG 014.3-05.5 and PNG 285.4+01.5) show somewhat unusual infrared spectra with the presence of a strong bump emission around $\sim 24\ \mu\text{m}$ (see fig. 4 in Stanghellini et al. 2012). In short, our chemical abundances confirm that CC_{al} PNe are metal-poor objects and that they dominate the median chemical abundances of the CC-type PNe in our PNe samples (Sections 4.1 and 4.2).

¹¹ The chemical composition of the three CC_{ar+al} in the sample is very similar to the bulk of CC_{al} PNe (Table 14).

4.4. *Spitzer* dust subtypes vs. AGB nucleosynthesis predictions

Comparison of the chemical abundances among the different *Spitzer* dust subtypes with the theoretical nucleosynthesis predictions (see also Section 4.1) turns out to be straightforward. This is because the median abundances in the major *Spitzer* CC and OC dust types are dominated by specific dust subtypes (the more numerous ones) while these values in DC PNe are representative of the two DC subtypes. Thus, the comparison done in Section 4.1 for the major *Spitzer* dust types holds here for the particular dust subtypes dominating the abundance distributions among the major dust classes.

In particular, DC PNe with both crystalline and amorphous silicate dust features (DC_{cr} and DC_{am+cr}) are high-metallicity related objects, and their median He abundances and N/O abundance ratios agree very well with the theoretical predictions for the solar metallicity ($z \sim 0.02$) $\sim 5 M_{\odot}$ AGB star shown in Table 11. This contrasts with Górný et al. (2010), who found unusual chemical compositions of the nebular gas in the few DC_{am+cr} PNe in the Galactic bulge they analysed and linked this fact to their dust subtype. We have shown here that when using larger and homogeneous PNe samples (i.e. the Stanghellini et al. 2012, sample), any possible difference in the chemical composition of both DC subtypes disappear. Still, a difference between bulge and disc DC PNe remains and there are a few DC bulge PNe (and a few OC_{cr} ones) with somewhat low O content and the highest N/O ratios that are not present in the disc sample. This O-N anticorrelation could indicate even higher progenitor masses and a stronger HBB (i.e. the activation of the O-N cycle) in these peculiar DC PNe in the bulge. As indicated by the derived nebular gas abundances, a few OC_{cr} PNe and some CC_{ar} PNe in our sample may be truly DC PNe where the PAH-like and the crystalline silicate features, respectively, may have escaped detection by *Spitzer* (see Section 4.3 for more details).

On the other hand, OC PNe with amorphous silicate dust features (OC_{am} and OC_{am+cr}) seem to evolve from the same low metallicity progenitors. Their median He abundances and N/O abundance ratios are consistent with predictions for a low metallicity ($z \sim 0.008$) $\sim 1 M_{\odot}$ AGB star (Table 11). More interesting is that the bulk of OC_{cr} PNe are of higher metallicity (nearly solar) than the other OC subtypes with amorphous silicates. Their median He and N/O of $\log \epsilon(\text{He}) = 11.06$ and -0.65 suggest solar metallicity ($z \sim 0.02$) $\sim 1-1.5 M_{\odot}$ AGB stars (see Table 11) as likely progenitors. The observed median Ne/O ratio of -0.63 is also higher than the model predictions. As discussed in Section 4.1, this disagreement may be solved when using AGB nucleosynthesis models with PMZ. Furthermore, the unusual chemical compositions (e.g. very low abundances of N) found by Górný et al. (2010) in a few OC_{am+cr} PNe in the Galactic bulge do not seem so pronounced and usual in the more homogeneous sample of Galactic disc PNe (see Fig. 6). The suggestion that they are rather peculiar and rare objects that may originate in binary systems (see Górný et al. 2010 for more details) has not been confirmed by photometric observations (Hajduk et al. 2014, in press; Hajduk, private communication).

Similar to the OC PNe, we find that the CC PNe with aliphatic dust features (CC_{al} and CC_{ar+al}, which are mostly located in the Galactic disc) probably evolve from low-metallicity and relatively low-mass progenitors. They completely dominate the chemical pattern observed in the major CC type, and the conclusions reached in Section 4.1 for the CC PNe hold here. Although the observed median He abundances and N/O abundance ratios in CC PNe with aliphatic dust are not completely repro-

duced by the theoretical predictions, they should evolve from low-metallicity ($z \sim 0.008$) and relatively low-mass ($1.9 \leq M < 3 M_{\odot}$) AGB stars. Finally, as mentioned above, a large number of the rather rare (and unusual) CC PNe with aromatic dust (CC_{ar}) show He abundances and N/O abundance ratios consistent with predictions for a solar metallicity ($z \sim 0.02$) $\sim 5 M_{\odot}$ AGB star.

5. Nebular properties and evolutionary status

In this section the physical properties of the PNe with different *Spitzer* dust types/subtypes and their evolutionary status are presented. We start with the electron temperatures (T_e) derived from the [O III] $\lambda 4363/5007$ and [N II] $\lambda 5755/6584$ ratios. Their median values for the different *Spitzer* dust types in the Galactic disc and bulge are presented in Tables 9 and 10, respectively. The results of our K-S and W statistical tests are presented in Table 7, and in Fig. 10 we present the relations $T_e(\text{O III})$ vs. $T_e(\text{N II})$ separately for PNe in the Galactic disc and bulge regions. It can be seen that, even though the two ratios can in principle provide an electron temperature of slightly different regions of the nebula (zones of ions of lower and higher ionization potentials), both are relatively well correlated in Fig. 10. Only in the case of OC PNe located in the Galactic bulge is the median $T_e(\text{N II})$ ~ 0.13 dex higher than $T_e(\text{O III})$, but this sample is obviously not uniform with a few clear outliers as seen in Fig. 10. Concerning the differences between the major dust types, DC PNe in the Galactic disc differ from OC and CC PNe by having lower $T_e(\text{O III})$ (the median values are 3.98 vs. identical 4.05 in OC and CC PNe). The DC bulge PNe, however, differ from OC PNe by having lower $T_e(\text{N II})$ temperatures (the median values are 3.94 and 4.14, respectively). The physical explanation of such behaviour could be that DCs in the disc are more oxygen abundant so that these atoms can cool the nebulae more efficiently.

The ionization level of the nebular gas can be evaluated with the $\text{O}^{++}/(\text{O}^{+} + \text{O}^{++})$ and $\text{He}^{++}/(\text{He}^{+} + \text{He}^{++})$ ionic ratios. In Tables 9 and 10 the median values of these parameters are given for PNe of different dust types in the Galactic disc and bulge separately. In Fig. 11 their histograms for dust subtypes are presented. It can be seen that in both regions of the Milky Way most of the groups analysed here (disregarding only the featureless F-type PNe that are expected to represent more advanced evolutionary stages) show a similar intermediate level of ionization. A median $\text{He}^{++}/(\text{He}^{+} + \text{He}^{++}) = 0$ is found for all of them, and the median $\text{O}^{++}/(\text{O}^{+} + \text{O}^{++})$ ranges from 0.83 in CC disc PNe to 0.92 for OC disc PNe. The exceptions are DC PNe in the Galactic bulge with a median $\text{O}^{++}/(\text{O}^{+} + \text{O}^{++}) = 0.55$. The results of our statistical tests¹² presented in Table 7 confirm that in the Galactic bulge there is indeed a statistically significant difference between DC and OC PNe. On the other hand, the difference between DC PNe in the Galactic disc vs. DC PNe in the bulge is not confirmed (Table 8), although the median $\text{O}^{++}/(\text{O}^{+} + \text{O}^{++})$ values (0.84 and 0.55, respectively) seem to suggest that it could be present.

The distinction between $\text{O}^{++}/(\text{O}^{+} + \text{O}^{++})$ in Galactic disc and bulge DC PNe is in fact a consequence of the difference between the nebular properties of the DC_{cr} and DC_{am+cr} subtypes. The former dominate the Galactic bulge DC sample, and at the same time, are found more frequently in a lower ionization state (see Tables 6 and 14). As can be seen in the top left-hand panel of Fig. 11, in reality the difference is, however, not that profound. Indeed, the median $\text{O}^{++}/(\text{O}^{+} + \text{O}^{++})$ value is lower for

¹² The Wilcoxon test is not reliable in the case of $\text{He}^{++}/(\text{He}^{+} + \text{He}^{++})$ because the derived ratios are mostly 0 and the distributions are flat cut on one side.

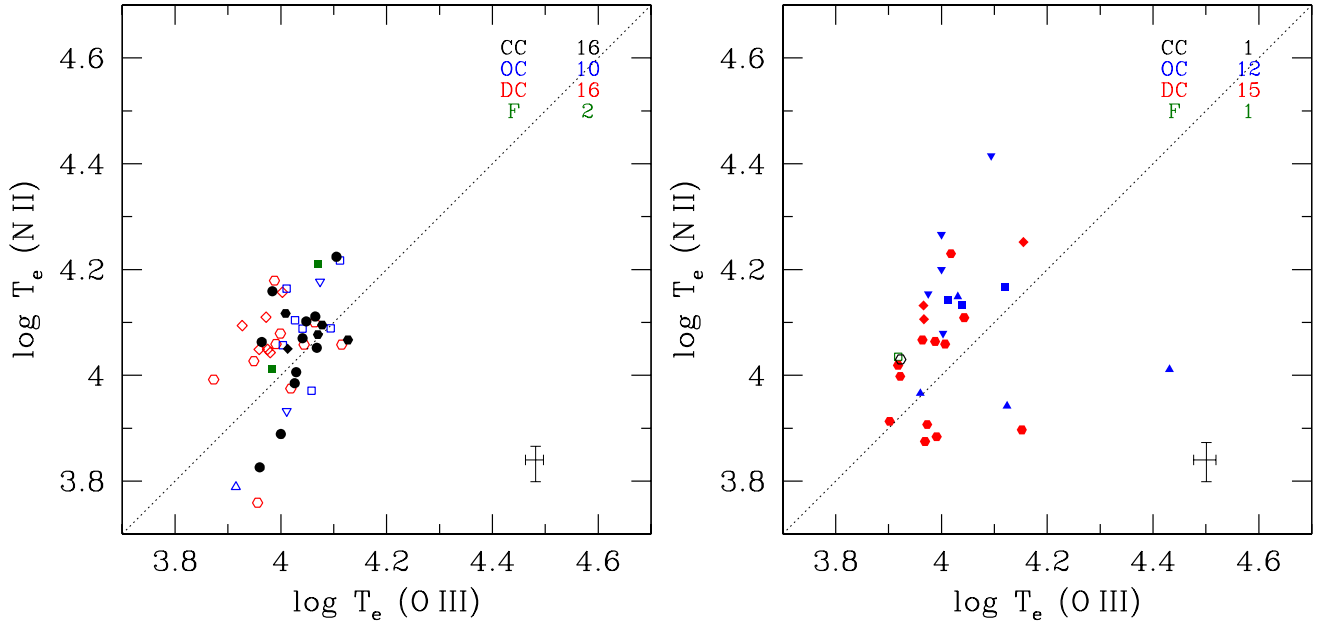


Fig. 10. Diagrams of nebular electron temperature T_e from the [O III] $\lambda 4363/5007$ vs. T_e from the [N II] $\lambda 5755/6584$ ratios for Galactic disc (left panel) and Galactic bulge PNe (right panel). The same meaning of symbols as in Figs. 5 and 6.

DC_{cr} than for DC_{am+cr} , but in both groups their members can be found in a whole range of ionization stages. What is intriguing is that proportionally more DC_{cr} show the presence of doubly ionized He^{++} ions than in the case of DC_{am+cr} (Fig. 11 top right). This issue could indicate that DC_{am+cr} evolve towards the DC_{cr} stage, but it contradicts the $O^{++}/(O^+ + O^{++})$ distribution. For the other dust subtypes, there are no clear differences in the ionization level either for OC or for CC PNe, as can be inferred from Fig. 11 and Table 14. This is confirmed by the statistical tests in Table 12.

The electron density (N_e) is a parameter that can provide information on the evolutionary status of the individual nebula. However, the distributions analysed for some PNe subsamples will also depend on the properties of the central stars. Older nebulae show lower electron densities, but if the nebular gas expands more rapidly, then the drop in the electron density is also rapid. Furthermore, the more massive central stars have a higher probability of detecting the surrounding nebulae when they are still relatively dense. With our own observations and literature spectra, we derived electron densities N_e from the [S II] $\lambda 6731/6717$ ratio. The median values of N_e for all *Spitzer* main dust types are given in Tables 9 and 10 for the Galactic disc and bulge PNe, respectively. The histograms of the corresponding distributions are presented in Fig. 12. Only DC and OC PNe are numerous enough in both Galactic regions to allow for statistically meaningful comparisons. The median N_e values and their distributions seem to be very similar for the DC PNe in the Galactic disc and bulge. In contrast, the N_e distribution for the OC PNe in the Galactic disc is flatter but has a higher median value than in the bulge, where it also has a more peaked shape. These differences are not strictly confirmed by the statistical tests, though (see Tables 7 and 8). In any case, we have to remember that the histograms in Fig. 12 are the superposition of the distributions of the various *Spitzer* dust subtypes within each main dust group (see below). We do not have enough data for the CC and F *Spitzer* dust types to analyse them in the Galactic bulge. In the Galactic disc, the major CC and F *Spitzer* dust types display the lowest median N_e in accordance with the assumption that they

represent later stages of nebular evolution. In the case of Galactic disc CC PNe, the median electron density is very similar to the DC PNe, but the N_e distribution clearly has a low-density tail, indicating that more evolutionarily advanced nebulae with C-rich dust features are still present in this group.

In the left-hand and centre panels of Fig. 13, we present the distributions of the derived N_e separately for DC_{cr} and DC_{am+cr} and for OC_{cr} , OC_{am} , and OC_{am+cr} , respectively, by using merged samples from the Galactic disc and bulge. It can be seen that the $\log N_e$ distributions for the DC_{cr} and DC_{am+cr} PNe clearly peak around their median values of 3.71 and 3.89, and the statistical significance of this difference is close to being confirmed by our statistical tests (probability 0.05 and 0.03 for K-S and W tests in Table 12). In the case of the OC dust subsamples, there are probably not enough objects to reach firm conclusions. However, the N_e distribution of OC_{am} PNe seems to be fairly flat. Concerning OC_{am+cr} PNe, they clearly seem to be denser (or younger) than the OC_{cr} and OC_{am} subsamples. Since OC_{am} dominate in the Galactic disc sample (Table 6), the general N_e distribution for disc OC PNe (Fig. 12) was flatter and shifted to higher values than for bulge OC PNe where OC_{cr} PNe compose half of that sample. The differences in spatial distribution (i.e. galactic latitude) and chemical abundances among the several OC subtypes mentioned in the previous sections rule out the possibility that OC_{am} and OC_{am+cr} sources could evolve into OC_{cr} ones as a result of silicates crystallization. On the other hand, evolution of OC_{am} objects into OC_{am+cr} ones or DC_{am+cr} into DC_{cr} would still be possible and consistent with the idea that the amorphous silicates are transformed/processed to crystalline silicates from the AGB to the PNe phase. In the right-hand panel of Fig. 13, the $\log N_e$ distributions for the several subtypes of PNe with carbon-rich dust features are also presented. Although the distributions seem to be rather broad, they indicate that the CC_{ar} sources generally are less dense (or older) than the CC_{al} ones. However, the much lower median metallicity displayed by the CC_{al} objects with respect to the CC_{ar} ones (with a nearly solar metal content) seem to discard any possible evolutionary link between both types of PNe.

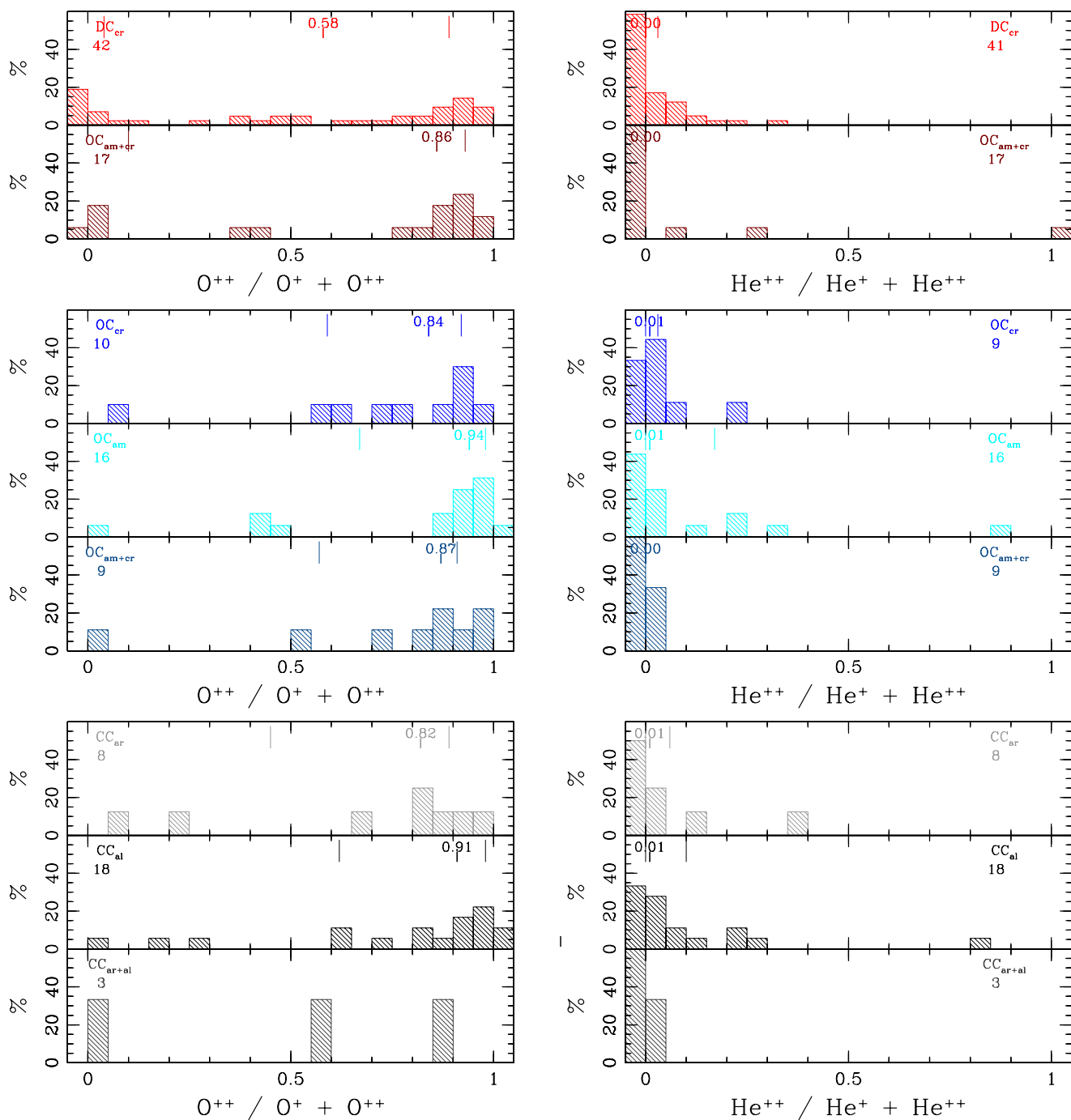


Fig. 11. The distribution of $O^{++}/(O^{+}+O^{++})$ (left panel) and $He^{++}/(He^{+}+He^{++})$ (right panel) for *Spitzer* dust subtypes in combined Galactic disc and bulge samples. From top to bottom: distributions for dust subtypes of DC, OC and CC PNe respectively.

We note that any difference in the N_e distributions and their corresponding median values can also be interpreted as due to individual subsamples originating in parent stellar populations of different masses. Another way to analyse possible evolutionary links between PNe with different *Spitzer* dust subtypes is to compare objects in diagrams that follow the evolution of the planetary nebula itself and the central star. Such diagram is plotted in Fig. 14 where we present the nebular $H\beta$ surface brightness $S_{H\beta}$ versus S_V - a similarly defined parameter based on the stellar flux in the visual V band and nebular parameter θ ; $S_V = F_V/(\pi\theta^2)$ (Górný & Tylenda 2000). Both parameters are independent of distance so we plot them in Fig. 14 for the Galactic

disc and bulge PNe of all *Spitzer* dust subtypes. Unfortunately, many objects from our samples could not be placed in Fig. 14 since the stellar flux in the optical is needed to compute one of the parameters, and it is generally available for central stars of PNe alone. The difficulty of measuring the central star V magnitude seems natural for F type PNe that are presumably older and their very hot central stars can therefore be faint in the optical.¹³ For the PNe with O-rich and mixed chemistry dust, the relative percentages of central stars with measured stellar optical flux are

¹³ All analysed PNe have small apparent diameters. This usually makes measurements of stellar flux difficult, but it should influence all subsamples to a comparable extent.

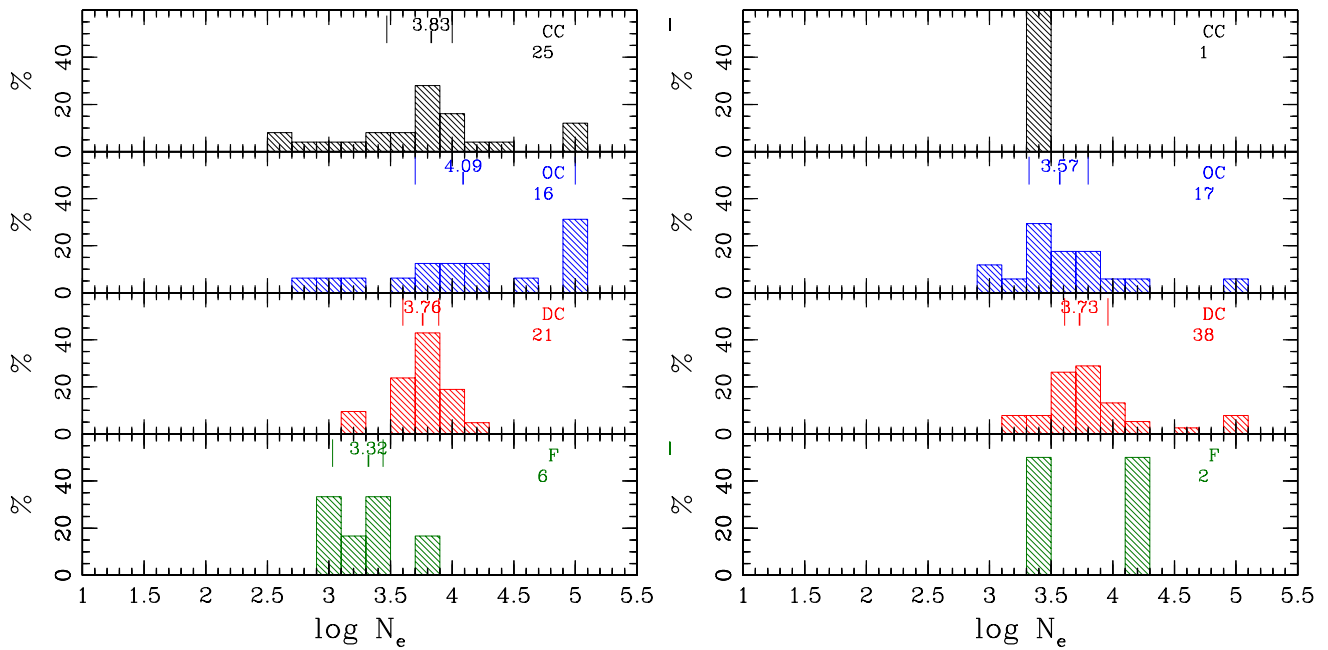


Fig. 12. Histograms of nebular electron density N_e derived from [S II] $\lambda 6731/6717$ ratio for Galactic disc PNe (left panel) and Galactic bulge PNe (right panel).

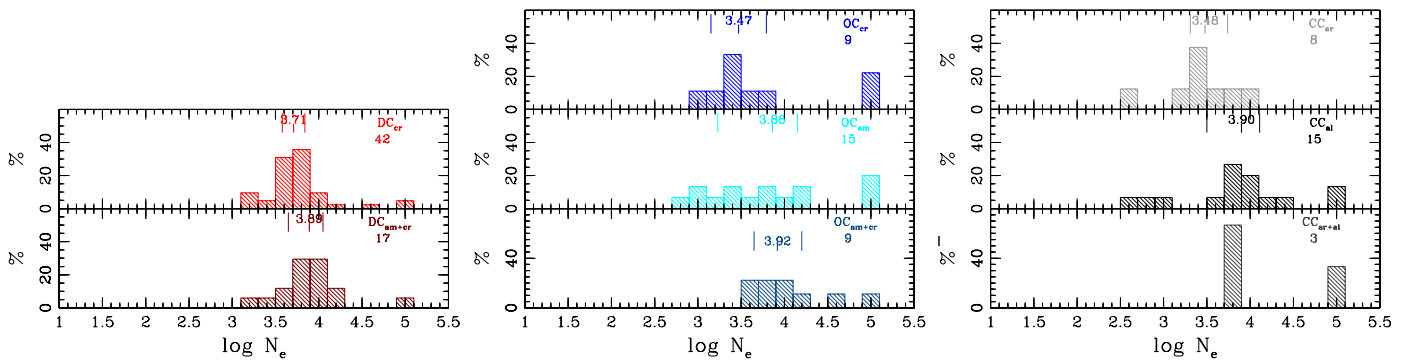


Fig. 13. Histograms of nebular electron density N_e derived from [S II] $\lambda 6731/6717$ ratio for combined samples of Galactic disc and bulge PNe. The left to right panels present distributions for dust subtypes of DC, OC, and CC PNe, respectively.

36% and 39%, respectively. Surprisingly, only seven (18%) PNe with C-rich dust have this data available. Most of them are found in the Galactic disc, and their smaller average distance (as compared to other groups consisting also of bulge objects) should make the measurements easier.

There are three theoretical tracks in Fig. 14 shown for comparison representing models with 0.56 , 0.60 , and $0.64 M_{\odot}$ central stars or progenitor masses of 1, 3, and $4 M_{\odot}$, respectively. They have been computed combining the evolution of a central star adopted from models by Blöcker (1995) with a simple model of spherical nebula with a total nebular gas mass of $0.20 M_{\odot}$, filling factor of 0.75 and an expansion velocity of 20 km s^{-1} . These tracks have been overplotted only for reference purposes, and their exact locations will change not only with variations in the nebular model parameters but also with the details of stellar evolution as the evolutionary timescale. The evolutionary timescale depends, for example, on the exact moment or thermal pulse phase when the central star left the AGB, but also on the mass loss rate from the central star during the AGB, post-AGB, and PNe phases (see Górný et al. (1994) for more details and Górný & Tylenda (2000) for some examples on how much track locations can be modified). Thus, the three simple theoret-

ical tracks displayed in Fig. 14 are probably not representative of the several types of PNe with *Spitzer* spectra. For example, the high-metallicity (solar/supra-solar) DC PNe are known to be non-spherical sources (Guzman-Ramirez et al. 2011), where a late thermal pulse could produce the observed mixed chemistry (Perea-Calderón et al. 2009). Also, several CC and OC dust subtypes (e.g. CC_{al} , OC_{amb} , and OC_{amb+cr}) display very low median metallicities that could significantly affect their evolutionary timescales (i.e. their mass loss rates). An exhaustive study of the space parameters affecting these theoretical tracks is beyond the scope of this paper, but one needs to keep these limitations in mind when comparing different PNe populations in Fig. 14. In any case, we have found useful the exploration of Fig. 14, and some interesting features have emerged.

Analysing the locations of DC PNe in Fig. 14 shows that they seem to occupy the largest space between the plotted 0.56 and $0.64 M_{\odot}$ tracks with roughly half of them above and below the $0.60 M_{\odot}$ model.¹⁴ This seems to be at variance with our conclu-

¹⁴ It can be added here that the six DC_{cr} PNe located closest to the plotted $0.64 M_{\odot}$ track in Fig. 14 all come from the Perea-Calderón et al. (2009) sample (M1-31, H1-50, M1-25, M1-40, M1-33, and Hb 4). This

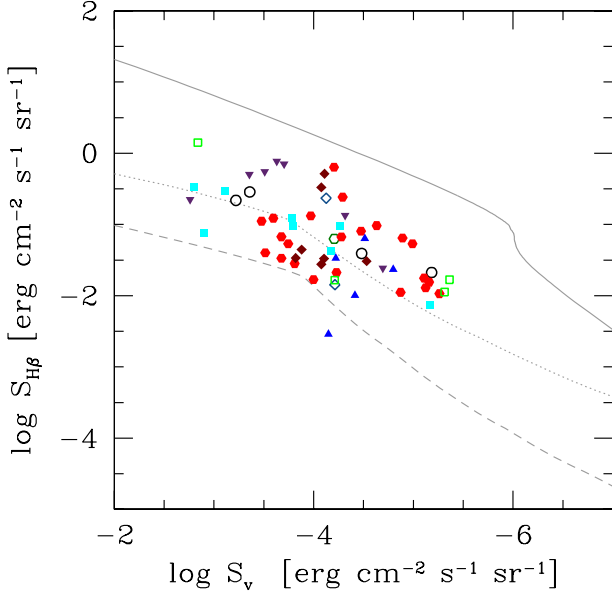


Fig. 14. Surface brightness $S_{H\beta}$ versus S_V for the different *Spitzer* dust subtypes of Galactic disc and bulge PNe combined. Three theoretical tracks, representing models with 0.56 (dashed line), 0.60 (dotted line), and 0.64 (solid line) M_{\odot} central stars are also shown for comparison (see text for more details). The same meaning of symbols as in Fig. 4 is used: CC_{ar^-} open hexagons; CC_{al^-} open circles; CC_{ar+al^-} open diamonds; OC_{cr^-} triangles; OC_{am^-} filled squares; OC_{am+cr^-} reversed triangles; DC_{cr^-} filled hexagons; DC_{am+cr^-} filled diamonds; F - open squares.

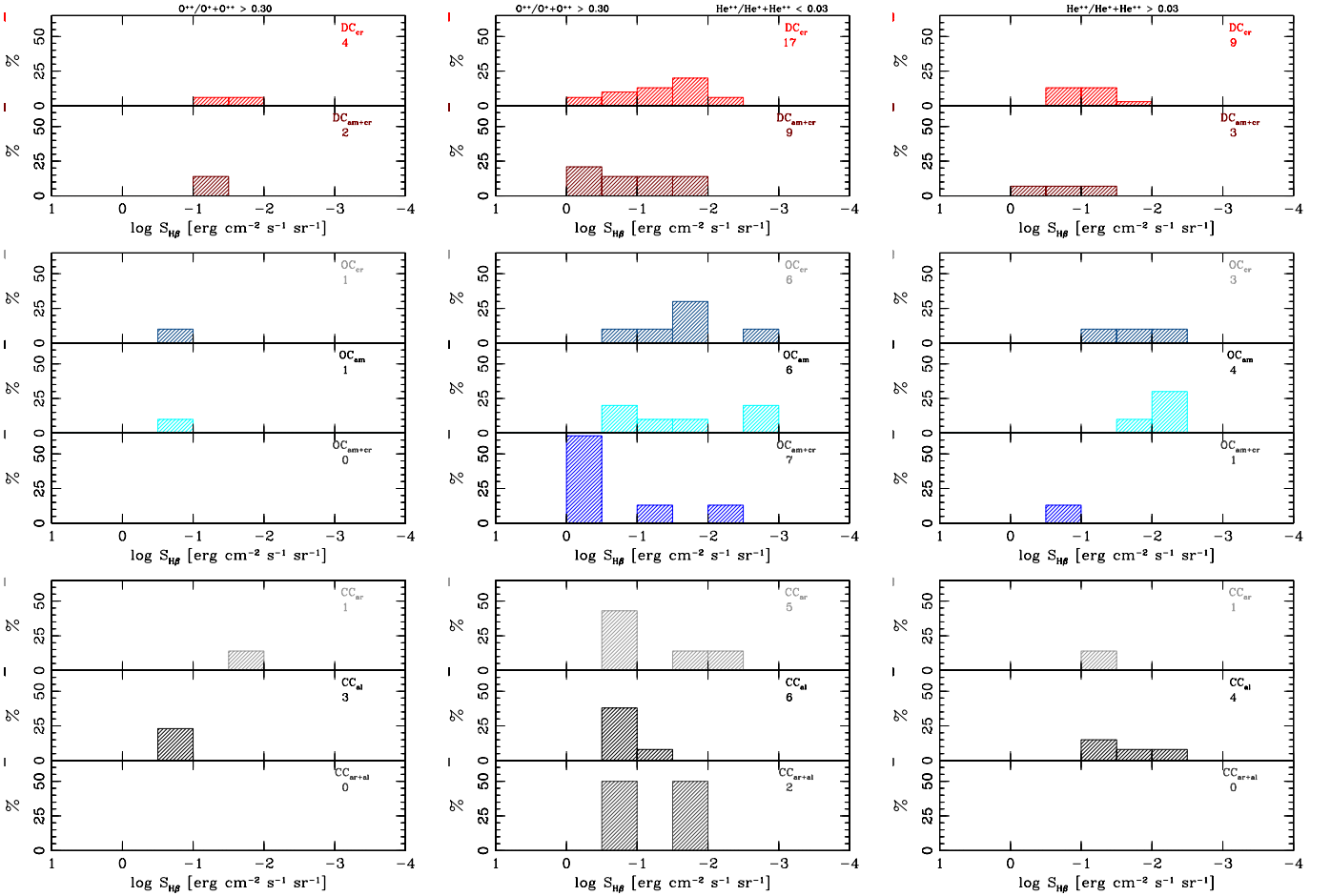


Fig. 15. The distribution of $S_{H\beta}$ surface brightness for *Spitzer* dust subtypes and different ionization classes. From top to bottom: distributions for dust subtypes of DC, OC, and CC PNe respectively. From left to right: distributions for low ionization ($O^{++}/(O^+ + O^{++}) < 0.3$); intermediate ionization ($O^{++}/(O^+ + O^{++}) > 0.3$, and $He^{++}/(He^+ + He^{++}) < 0.03$), and high ionization ($He^{++}/(He^+ + He^{++}) > 0.03$) are presented.

sions from Section 4 that the bulk of DC PNe probably represent the objects with the highest stellar masses among the PNe analysed in this work, as deduced from their enlarged N and He abundances. However, as underlined above, the theoretical tracks shown in Fig. 14 may not be appropriate for these non-spherical sources. Also, better agreement with higher mass central stars could be reached if the evolution is faster than in the Blöcker (1995) models or if the masses of the nebulae are higher than the assumed value of $0.2 M_{\odot}$. If the apparent dichotomy (with roughly half of the sources above and below the $0.60 M_{\odot}$ track) of DC PNe in Fig. 14 is real, then one may speculate that DC PNe could evolve through two different high-metallicity channels, such as from high-mass ($M \geq 3 M_{\odot}$) HBB stars and from less massive ($1 < M < 3 M_{\odot}$) stars with some extra mixing. We should add that among the DC_{cr} objects closest to the low-mass $0.56 M_{\odot}$ track in Fig. 14, there are three low-metallicity Galactic bulge PNe that are suspected of having undergone the O-N cycle out of four with available S_V surface brightness¹⁵ (see also comments in Sect. 4.1). Again, a detailed theoretical study of AGB evolution and nucleosynthesis at supra-solar metallicity would be desirable to get some insight into possible evolutionary channels for DC PNe. It is noteworthy that the DC_{cr} and DC_{am+cr} PNe occupy practically the same locations in Fig. 14, and it is hard to reconcile it with the idea of an evolutionary link or transition from DC_{am+cr} into DC_{cr}.

The situation of PNe with various forms of oxygen-rich dust in Fig. 14 is totally different. This group is composed of three dust subtypes (OC_{cr}, OC_{am}, and OC_{am+cr}), and all of them clearly occupy distinct locations in the plot. OC_{am+cr} are found among objects with largest $S_{H\beta}$ and S_V , whereas the opposite is true for OC_{cr}. Taking the different metallicity for both OC subtypes (see above) into account, this cannot be interpreted as an evolutionary sequence but rather suggests that both groups originate from different progenitor populations. However, the locations in Fig. 14 and dust properties do not exclude a possible evolutionary link from OC_{am} to OC_{am+cr} (see also below). Interestingly, the OC_{am} PNe span the whole range of S_V surface brightness because they are placed very close to the $0.6 M_{\odot}$ track. This suggests that OC_{am} PNe probably originates in progenitor stars in a narrow mass range. This is also the case for CC_{al} PNe (although the number of objects with available data is even smaller). For CC_{ar} and the scarcer CC_{ar+al} PNe, no statistically significant conclusions can be derived using Fig. 14. The situation of F type PNe with featureless *Spitzer* spectra is not much better, although the three low surface-brightness objects plotted in Fig. 14 confirm the natural assumption that F-type sources represent the later stages of nebular life. There could be, however, some special objects, as is probably the case for the high surface-brightness F-type outlier NGC 6833.

To analyse the evolutionary status of the different *Spitzer* dust subtypes by using larger samples, one can limit the discussion to the $S_{H\beta}$ distributions. This is because $S_{H\beta}$ is available for almost all PNe (except the smallest star-like objects with unmeasured diameters). To simultaneously preserve some information on the central stars, we decided to divide PNe into those of low ionization (defined approximately as having $O^{++}/(O^{+}+O^{++}) < 0.3$), intermediate ionization (if

sample is biased towards PNe with various types of emission-line central stars, but among the six objects mentioned there is diversity with two [WC], two wels, one unknown and one confirmed non-emission line central star PNe.

¹⁵ These objects are H 1-43, M 3-40, and M 4-6. In fact, the S_V for the last two are upper limits, as is also the case for the fourth, H 2-17, which is located close to $0.60 M_{\odot}$ track in Fig. 14.

$O^{++}/(O^{+}+O^{++}) > 0.3$ but $He^{++}/(He^{+}+He^{++}) < 0.03$), and high ionization PNe ($He^{++}/(He^{+}+He^{++}) > 0.03$). This should qualitatively divide PNe into groups with central stars below 35kK, between 35kK and 70kK, and above 70kK, respectively. The $S_{H\beta}$ distributions for the different *Spitzer* dust subtypes and ionization states are presented in Fig. 15. The theoretical predictions of $S_{H\beta}$ distributions for central stars of 0.56 , 0.60 , and $0.64 M_{\odot}$ (surrounded by the same nebula as are used to construct tracks presented in Fig. 14) can be found in Fig. 7 of Górný et al. (2010). For a qualitative comparison it is enough to realize that, owing to huge differences in the theoretical evolutionary timescales, it is reasonable to expect only PNe with 0.56 and $0.60 M_{\odot}$ central stars in the low and intermediate ionization groups and the latter will generally have higher $S_{H\beta}$ values. Only in the high ionization group should any PNe with $0.64 M_{\odot}$ central stars be expected. In this last high-ionization group, the PNe with $0.60 M_{\odot}$ stars should have their peak-of-discovery probability, whereas nebulae with $0.56 M_{\odot}$ stars should either be very faint or already too dispersed to be noticed (very low $S_{H\beta}$).

In the left-hand panel of Fig. 15 we present the $S_{H\beta}$ distributions for the DC, OC, and CC dust subtypes with the lowest ionization (or central star temperatures). Even though we are investigating small PNe with clear signs of the presence of dust that should therefore be expected to be at earlier evolutionary phases than the *general* Galactic PN population, we find very few low-ionization PNe in our samples. This can mean either that there are not many PNe with low-mass central stars among them or that the theoretical evolutionary timescales predicted by models of Blöcker (1995) are too slow compared to reality. The lack of OC PNe in the plots is particularly intriguing since, based on their chemical abundances (e.g. low N/O ratios, see Section 4), we expect them to come from the lowest mass AGB stars.

The middle panel of Fig. 15 shows the distributions of $S_{H\beta}$ for intermediate ionization PNe divided into the several *Spitzer* dust subtypes. Most of the objects we analysed fall into this category irrespective of their dust type. DC_{cr} and DC_{am+cr} both span a similar range in $S_{H\beta}$, suggesting also similar central star masses. The $S_{H\beta}$ of OC_{cr} and OC_{am} PNe also display a similar range among intermediate ionization PNe, but they are shifted (roughly by 0.5 dex) towards lower $S_{H\beta}$ values. This $S_{H\beta}$ shift would be consistent with the OC_{cr} and OC_{am} PNe being less massive than the DC PNe, as expected from our chemical abundances analysis (Section 4). This is not observed, however, for the OC_{am+cr} PNe, which display an apparent peak in their $S_{H\beta}$ distribution towards high values, indicating higher central stars masses (as could have already been deduced from their locations in Fig. 14). Concerning the objects with carbon-based dust among intermediate ionization PNe (bottom middle panel of Fig. 15), there are no clear signs of any significant difference in their central star masses.

The right-hand panel of Fig. 15 presents $S_{H\beta}$ for high ionization PNe in our samples. In general, there are two to three times fewer PNe in this ionization class than in the intermediate ionization group. This is the natural consequence of our PNe samples being dominated by compact (and relatively young) objects. By comparing the $S_{H\beta}$ distributions for high ionization PNe depending on the different dust types and subtypes, we reach similar conclusions to the intermediate ionization case. In particular, the OC PNe (at least the OC_{cr} and OC_{am} ones) are shifted towards lower $S_{H\beta}$ values with respect to the DC PNe. This again

suggests that DC PNe are more massive than the OC_{cr} and OC_{am} PNe.¹⁶

6. Discussion: A link between *Spitzer* dust properties, chemical abundances, and evolutionary status

This paper shows that the chemical abundances in our samples of Galactic PNe in the disc and bulge are intimately related to their *Spitzer* dust properties; i.e. the several *Spitzer* dust types/subtypes correspond to different populations of PNe (with different average progenitor masses and metallicities) in both Galactic environments.

The Galactic disc population of compact and presumably young PNe is dominated by low-metallicity OC and CC PNe, which are the descendants of very low-mass ($\sim 1-1.5 M_{\odot}$) and low-mass ($1.9 \leq M < 3 M_{\odot}$) AGB stars, respectively. These populations of OC and CC PNe in the disc are dominated by PNe with amorphous (OC_{am}) and aliphatic (CC_{al}) dust features, respectively; i.e. those PNe with unevolved/unprocessed dust (see below). DC and F PNe represent a significant fraction ($\sim 20\%$) of the Galactic disc PNe population. The DC PNe (both with amorphous and crystalline silicates) represent a younger population of high-metallicity sources evolving from relatively massive ($\sim 3-5 M_{\odot}$, depending on the theoretical modelling details) HBB AGB stars. High-metallicity and more massive (e.g. $\geq 6 M_{\odot}$) HBB PNe are (almost) completely lacking in our Galactic disc sample, probably because these sources evolve too fast (and are obscured by dust) to be detected in the optical. The disc F PNe are the most evolved objects and seem to be a mix of low- and high-metallicity PNe. The low-metallicity F PNe may be very low-mass and old PNe (with very low surface brightness) similar to those found in the Galactic halo.

Interestingly, the Galactic bulge population of PNe (most of them also compact and young) is dominated by a young population of high-metallicity DC PNe, with their progenitors being relatively massive ($\sim 3-5 M_{\odot}$) HBB AGB stars. The OC sources also represent a significant fraction ($\sim 30\%$) of the Galactic bulge PNe population, but CC (and F) PNe are very uncommon. The population of OC PNe in the bulge is dominated by those PNe with crystalline silicate dust features (OC_{cr}), which also have higher metallicity than PNe with amorphous silicate dust features (OC_{am} and OC_{am+cr}). Although the number of sources in each OC subtype is small, it seems that some OC_{cr} PNe are also massive, while the rest could be the result of the evolution of high-metallicity and very-low mass ($\sim 1-1.5 M_{\odot}$) AGB stars. The low-metallicity and very low-mass ($\sim 1-1.5 M_{\odot}$) OC PNe with amorphous silicates - which dominate in the Galactic disc - are more scarce towards the bulge. The lack of CC bulge PNe is not surprising if we consider that C-rich AGB stars are very rare in this Galactic environment (see e.g. Uttenhaler et al. 2007, and references therein). The high Ar abundances that we obtain for most bulge PNe indicate that high metallicity is an intrinsic property towards the bulge. Theoretical models predict that a high

metallicity can prevent the formation of C-rich AGB stars because a larger amount of C needs to be dredged up and the TDU is less efficient (e.g. Karakas et al. 2002; Marigo et al. 2013). Our results in bulge PNe are consistent with the recent findings in the bulge of M31 by Boyer et al. (2013), which also show a complete lack of C-rich AGB stars in this high-metallicity environment and suggests that there is a metallicity threshold above which O-rich AGB stars cannot be converted into C-rich ones.

Remarkably, our work shows that the double-dust chemistry (DC) phenomenon in PNe mainly takes place in high-metallicity and relatively high-mass ($\sim 3-5 M_{\odot}$) young PNe. It is worth mentioning here that García-Rojas et al. (2013) also confirm the relatively massive nature (e.g. high He and N) of DC PNe by obtaining precise chemical abundances in a small sample of PNe with [WC]-type central stars (although their sample is biased towards early [WC] types, see also below) from high resolution and high quality spectra. The dominance of such a young population of PNe in the Galactic bulge naturally explains the high detection rate of dual-dust chemistry found in this environment (Perea-Calderón et al. 2009). Although dual-dust chemistry is highly frequent in PNe with [WC]-type central stars, this phenomenon is also seen in weak emission-line stars (wels), as well as in other PNe with normal central stars (being neither [WC] nor wels) (Perea-Calderón et al. 2009). Unfortunately, for a majority of DC PNe there is no information about their central stars (e.g. [WC], wels, normal) but we find similar results to those of Perea-Calderón et al. (2009). The Perea-Calderón et al. sample of bulge PNe is heavily biased towards emission-line objects; twelve [WC] and VL PNe (all DC), seven wels (six DC and one OC), and 16 normal (nine DC, five OC, and one CC).¹⁷ In contrast, the Stanghellini et al. (2012) sample of compact (presumably young) PNe seems to be underpopulated in [WC] PNe: two [WC] PNe (both with DC), four wels (all of them with OC), and 44 normal (24 DC, nine OC, four CC, and seven F) are found in the bulge, while five [WC] and VL PNe (two DC and three CC), 14 wels (eight CC, four OC, one DC, and one F), and 79 normal (21 CC, 27 OC, 14 DC, and 17 F) are found in the disc. Thus, the last numbers suggest that the wels phenomenon is common to very different types of PNe (DC, CC, and OC). In addition, PNe in the Stanghellini et al. (2012) sample are very faint in the optical (i.e. fainter than average PNe), which could explain why there are so few [WC] objects in their sample; [WC] central stars can be associated primarily with brighter PNe (see Górný et al. 2009).

DC PNe with O-rich amorphous dust features seem to be more common in the Galactic disc than in the bulge, but it is not clear if this is just a selection effect. One expects the evolution of the O-rich dust features to proceed from amorphous silicates (in the AGB/post-AGB stage) to crystalline silicates (in the PN phase) (García-Lario & Perea-Calderón 2003; see also García-Hernández 2012 and references therein). Several models for the silicates crystallization have been proposed: i) low-temperature crystallization in circumbinary discs (e.g. Molster et al. 1999), and ii) high-temperature crystallization at the end of the AGB due to the strong mass loss (e.g. Waters et al. 1996). In the single-star evolutionary framework, the high-metallicity and high-progenitor masses of DC PNe would naturally explain an efficient crystallization of the silicates in their circumstellar envelopes as a consequence of the higher mass loss rates (and thus a higher amount of dust) experienced by these sources at the end of the previous AGB phase. In addition, DC

¹⁶ Our comparisons with theoretical tracks have to remain qualitative at this stage. For example, for every group of *Spitzer* dust type, about 1/4 of the analysed population have high-ionization PNe. Assuming the model predictions from Blöcker (1995) tracks and the model calculations presented in fig. 7 of Górný et al. (2010), which agree with the predicted probability for the $0.56 M_{\odot}$ model. At the same time it is discordant with very low $S_{H\beta}$ predictions from these calculations. Model fine-tuning is, however, beyond the scope of the present paper before new data on stellar V magnitudes are collected.

¹⁷ The smaller Gutenkunst et al. (2008) sample of bulge PNe also includes one [WC] PN and one wels (both with DC).

PNe with O-rich amorphous and crystalline silicates dust features (DC_{am+cr} and DC_{cr}) are, on average, chemically indistinguishable (i.e. they probably evolve from the same AGB progenitors). The higher median electron densities shown by the DC_{am+cr} PNe tentatively suggest that they may be the precursors of the DC_{cr} ones, in agreement with the expected AGB-PN evolution of the dust features in O-rich circumstellar shells. However, this is not confirmed by the $S_{H\beta}$ versus S_V diagram presented in Fig. 14, which otherwise seems to suggest that DC PNe could evolve through an additional high-metallicity channel, i.e. from less massive ($1 < M < 3 M_{\odot}$) AGB stars with some extra mixing. This should encourage theoretical modellers to explore AGB evolution and nucleosynthesis at supra-solar metallicity for a complete range of progenitors masses. Finally, at present we cannot completely discard the binary star scenario and the circumbinary discs as the responsible mechanism for the crystallization of silicates around DC PNe. This, however, seems to be less probable (see e.g. Perea-Calderón et al. 2009; Miszalski et al. 2009).

The simultaneous presence of PAHs and silicates in DC PNe is still unclear. Perea-Calderón et al. (2009) discuss several mechanisms to explain the double-dust chemistry phenomenon in the Galactic bulge, and their most plausible scenario is a final thermal pulse on the AGB (or just after), which may turn an O-rich outflow into a C-rich one (Waters et al. 1998b). The crystallization of amorphous silicates may be due to the enhanced mass loss, while the PAHs may form the newly released carbon-rich material. On the other hand, Guzmán-Ramírez et al. (2011) propose a chemical model where hydrocarbon chains can form within O-rich gas through gas-phase chemical reactions, and they conclude that the formation of PAHs in DC bulge PNe is best explained through hydrocarbon chemistry in an ultraviolet (UV)-irradiated, dense torus. Both proposals are based on the assumption that DC PNe in the bulge are low-mass objects. However, we have shown here that the chemical abundances observed in DC PNe (both in the bulge and disc) are consistent with their descendants being high-metallicity and relatively massive ($\sim 3-5 M_{\odot}$) AGB stars experiencing HBB (see also García-Rojas et al. 2013). For intermediate-mass HBB stars, the strong mass loss may deactivate the HBB (see e.g. García-Hernández et al. 2006a, and references therein) at the end of the AGB phase. The high temperature annealing may lead to the silicates crystallization, while carbon, again allowed to be dredged up to the stellar surface, may be used for the PAH formation. Indeed, recent exploratory synthetic evolution calculations of solar-metallicity HBB AGB stars with delayed superwinds (i.e. allowing for TPs near the tip of the AGB once HBB has ceased; see Karakas et al. 2012 for more details) predict that these stars could be converted to C-rich ones. We note that the chemical model presented by Guzmán-Ramírez et al. (2011) to explain PAH formation in an O-rich environment may be still applicable to intermediate-mass HBB stars.

García-Rojas et al. (2013) have very recently reported precise C/O nebular ratios in eight DC PNe with early [WC]-type central stars. Five DC PNe in their sample (four DC_{cr} and one DC_{am+cr}) have O-rich ($C/O < 1$) nebulae, but three of them (Cn 1-5, M 1-32, and NGC 2867, all DC_{cr}) have C-rich nebulae. Interestingly, the DC PNe with O-rich nebulae are those with the typical DC *Spitzer* spectrum, showing very weak PAH bands and crystalline/amorphous silicates, while the C-rich ones display very unusual *Spitzer* spectra with strong PAH bands (and a strong bump emission around $\sim 24 \mu\text{m}$) and very weak crystalline silicate features. Cn 1-5 is the most extreme case, displaying the lowest C/O nebular ratio of 1.29 and the highest He (11.21) and

N enrichments ($N/O=0.45$), which suggest a progenitor star that is even more massive than $5 M_{\odot}$. Further precise determinations of the C/O ratios (e.g. based on optical recombination lines as in García-Rojas et al. have recently been done from high-resolution and high-quality spectra) in a complete sample of DC PNe would be very useful for learning about the dominant mechanism for PAH formation (HBB deactivation and/or hydrocarbon chemistry within O-rich shells), as well as for a fine-tuning (e.g. the specific conditions for the C-star conversion) of the synthetic evolution calculations of high-metallicity HBB AGB stars with delayed superwinds.

The OC PNe with O-rich amorphous dust features are also more frequent in the Galactic disc than in the bulge. In particular, Stanghellini et al. (2012) have already pointed out that the OC_{cr} disc PNe show lower Galactic latitudes (b) than the OC_{am} disc PNe (see below; Fig. 4). This would be consistent with the OC_{cr} PNe being more massive (and/or more metal rich) than the OC_{am} ones. Here we have shown that OC_{cr} PNe (in the disc and bulge) are more metal rich and slightly more massive than OC PNe with amorphous dust features (OC_{am} and OC_{am+cr}). In the single star scenario, the metal-rich and probably more massive character of OC_{cr} PNe would again be consistent with a more efficient silicates crystallization as a consequence of the higher mass loss rates (and dust production) at the tip of the AGB. The metal-poor (and probably less massive) OC PNe with amorphous dust features would experience much lower mass loss rates (and thus smaller amount of dust) in the AGB phase. It is nevertheless not clear (i.e. not confirmed by our statistical tests) that OC_{am} and OC_{am+cr} could be evolutionarily linked (e.g. the OC_{am} PNe being the precursors of the OC_{am+cr} ones) or if they reflect slightly different progenitor masses and metallicities.

The CC PNe (being absent in the Galactic bulge, see above) with aliphatic dust features (CC_{al}) dominate the population of compact (and young) C-rich PNe in the Galactic disc. From the AGB to the PN stage, the evolution of C-rich dust proceeds from the amorphous state to aliphatic, and then to PAHs (e.g. García-Lario & Perea-Calderón 2003; García-Hernández 2012); the dust grains evolve from small clusters of molecules (e.g. PAH clusters) to ionized PAHs. Thus, the apparent lack of CC_{ar} disc PNe (i.e., with aromatic PAH-like features) is explained by the dominant evolutionary stage of the dust grains around the disc population of C-rich PNe. Our chemical analysis indicates that most CC_{al} PNe are the descendants of rather low-metallicity C-rich AGB stars. Low-metallicity environments favour the detection of unprocessed dust grains in PNe *Spitzer* spectra (see Stanghellini et al. 2007).

The transformation of aliphatic groups to aromatic ones (e.g. as a consequence of the UV radiation field of the central star Kwok et al. 2001) is not very efficient (and more slowly because of the low metallicity), and we detect the early aliphatic stages of the circumstellar carbonaceous grains or the precursors of the PAH-like molecules that are usually seen in more evolved PNe. The few higher metallicity CC_{al} PNe in our disc sample should be very young objects where there is not enough time for an efficient aliphatic to aromatic dust conversion. Furthermore, the CC_{ar} disc PNe are more evolved objects (i.e. with higher median electron density), although they are not evolutionarily linked to the CC_{al} ones. CC_{ar} PNe are higher metallicity (nearly solar) and rather peculiar PNe. At least half of them seem to be truly DC PNe where the weak crystalline silicates have escaped detection from *Spitzer*. Interestingly, the two CC_{ar+al} PNe with fullerenes also have low metallicity and electron densities lower than the bulk of CC_{al} objects, suggesting that they are evolutionarily linked (e.g. CC_{ar+al} PNe are slightly more evolved), as expected from

the C-rich dust evolution during the transition phase from AGB stars to PNe.

7. Summary and conclusions

We have combined new low-resolution ($R \sim 800$) optical spectra with recent data in order to construct representative samples of Galactic disc and bulge PNe (mostly compact and presumably young) with *Spitzer* spectra. Depending on the nature of the dust features - C-rich, O-rich, and both C- and O-rich dust features (or double chemistry) - seen in their *Spitzer* spectra, the Galactic disc and bulge PNe are classified into four major dust types (oxygen chemistry or OC, carbon chemistry or CC, double chemistry or DC, featureless or F) and subtypes (amorphous and crystalline, and aliphatic and aromatic) and their Galactic distributions are presented. Nebular gas abundances of He, N, O, Ne, S, Cl, and Ar, as well as plasma parameters, were derived in a homogeneous way by using the classical empirical method. We studied the median chemical abundances in the Galactic disc and bulge PNe depending on their *Spitzer* dust types and subtypes and compared them with the homogeneous dataset of AGB nucleosynthesis predictions by Karakas (2010). Also, we analysed the nebular properties among the several types and subtypes of PNe and discussed a possible link between the *Spitzer* dust properties, chemical abundances, and evolutionary status.

The main results of our work can be summarized as follows.

1. The several *Spitzer* dust types and subtypes of PNe (with the exception of F PNe) are distributed differently between the Galactic disc and bulge regions. In particular, DC PNe are less common in the Galactic disc than OC and CC PNe but clearly dominate the Galactic bulge region, which otherwise show an almost complete lack of CC PNe. Both OC and DC PNe with amorphous silicates (OC_{am} and DC_{am+cr}) are more uncommon in the Galactic bulge than in the disc, while the opposite is seen for OC and DC PNe with crystalline silicates (OC_{cr} and DC_{cr}). CC PNe with aliphatic features (CC_{al}) completely dominate in the Galactic disc. DC PNe in the Galactic disc are mainly located towards the Galactic centre with no significant difference between the DC_{am+cr} and DC_{cr} subtypes. OC PNe with amorphous silicates (OC_{am}) and featureless (F) PNe are located further away from the Galactic plane than the other types/subtypes of PNe.
2. The median abundance pattern (mainly N/H, He/H, Ar/H, and N/O) of DC PNe is statistically different from that of OC PNe in both Galactic environments with DC PNe and OC PNe in the Galactic disc and bulge sharing almost the same abundance pattern. CC disc PNe (lacking in the bulge region) display an abundance pattern that is quite similar to that of the OC disc PNe, with the exception of S, which is found to be significantly more depleted in the CC objects. Our dissection of the *Spitzer* dust subtypes vs. the nebular gas abundances shows that i) the DC subtypes (DC_{cr} and DC_{am+cr}) are indistinguishable, and they show an abundance pattern identical to the major DC type; ii) the OC subtypes with amorphous silicates (OC_{am} and OC_{am+cr}) are chemically very similar, dominating the abundance pattern observed in the major OC type, while the less numerous OC_{cr} PNe are more metal rich; iii) the CC subtypes with aliphatic dust features (CC_{al} and CC_{ar+al}) display similar abundances, dominating the chemical pattern observed in the major CC type, while CC_{ar} PNe, being more metal-rich, are also scarcer; iv) a few OC_{cr} and about half ($\sim 50\%$) of CC_{ar} PNe display nebular gas abundances that are almost identical to those seen in DC PNe, suggesting that they are related objects.
3. The several *Spitzer* dust types and subtypes correspond to different populations of PNe (with different average progenitor masses and metallicities) in both Galactic environments. We note that although the progenitor masses that we infer from comparisons with the AGB nucleosynthesis predictions may be rather uncertain, our finding of different average progenitor masses and metallicities among the several *Spitzer* dust types/subtypes is assured. In summary:
 - i) DC PNe both with amorphous and crystalline silicates (DC_{am+cr} and DC_{cr}) are high metallicity (solar/supra-solar) sources evolving from relatively massive $\sim 3\text{--}5 M_{\odot}$ AGB stars experiencing HBB. They show the highest median He abundances and N/O abundance ratios, which are consistent with solar metallicity ($z \sim 0.02$) $\sim 5 M_{\odot}$ HBB AGB stars. However, other possible evolutionary channels cannot be discarded now. In addition, it is still not clear that DC_{am+cr} PNe could evolve towards the DC_{cr} stage. Curiously, there are a few DC PNe in the bulge with some indications of the O-N cycle activation, which are not present in the disc.
 - ii) OC PNe with amorphous silicates (OC_{am}) are low-metallicity sources with median He abundances and N/O abundance ratios that agree well with predictions of low-metallicity ($z \sim 0.008$) and very low-mass ($\sim 1 M_{\odot}$) AGB stars. OC PNe with both amorphous and crystalline silicates (OC_{am+cr}) are chemically similar to the OC_{am} ones, but we have found tentative hints (i.e. in the $S_{H\beta}$ vs. S_V diagram and $S_{H\beta}$ distributions), suggesting that OC_{am+cr} PNe could be more massive than OC_{am} PNe. The bulk of OC PNe with only crystalline silicates (OC_{cr}) are higher metallicity (nearly solar) objects with their median He abundances and N/O abundance ratios consistent with solar metallicity ($z \sim 0.02$) $\sim 1\text{--}1.5 M_{\odot}$ AGB stars.
 - iii) CC PNe with aliphatic features (CC_{al} and CC_{ar+al}) (mostly located in the Galactic disc) are low-metallicity ($z \sim 0.008$) objects that probably evolve from relatively low-mass ($1.9 \leq M < 3 M_{\odot}$) AGB stars. The best fit to the observed abundances is given by the models for the low-metallicity ($z \sim 0.008$) $\sim 1.9 M_{\odot}$ AGB star.
4. In both Galactic regions (bulge and disc), most of the PNe dust classes analysed here show a similar intermediate level of ionization, probably reflecting that our PNe samples are dominated by relatively young PNe. The only exceptions are the featureless F-type PNe that represent more advanced evolutionary stages. There is an apparent dichotomy of DC PNe in the $S_{H\beta}$ vs. S_V diagram that could suggest an additional high-metallicity evolutionary channel for these objects; e.g. less massive ($1 < M < 3 M_{\odot}$) with some kind of extra mixing. Also, there is tentative evidence that OC_{am+cr} PNe could be slightly more massive than the OC_{am} ones. This evidence, however, comes from comparisons with simple theoretical tracks that may not be representative of the several types of PNe with *Spitzer* spectra. More interesting is that OC and CC with unevolved dust (OC_{am} and CC_{al} PNe, respectively) seem to originate in progenitor masses in a narrow mass range, in agreement with the nucleosynthesis predictions.

In short, our most remarkable result is that DC PNe, both with amorphous and crystalline silicates, display high-metallicity (solar/supra-solar) and the highest He abundances and N/O ratios, indicating that they likely evolve from relatively massive ($\sim 3\text{--}5 M_{\odot}$) HBB AGB stars; however, PNe with O-rich and C-rich unevolved dust (amorphous and aliphatic) evolve from subsolar metallicity ($z \sim 0.008$) and lower mass ($< 3 M_{\odot}$) AGB stars. Although we have obtained very interesting results

by studying more balanced samples of the Galactic disc and bulge PNe, more optical spectroscopic observations would be desirable. In particular, the available data for some *Spitzer* OC (OC_{cr} and OC_{am+cr}) and CC (CC_{ar} and CC_{ar+al}) dust subtypes are still very scarce, so more chemical abundances would be useful to discard or confirm any possible evolutionary link among the several *Spitzer* dust subtypes. More theoretical efforts (e.g. a detailed study of AGB evolution and nucleosynthesis at supra-solar metallicity) are also encouraged.

Acknowledgements. This work is based on observations made with the Telescopio Nazionale Galileo operated on the island of La Palma by the Centro Galileo Galilei of INAF (Istituto Nazionale di Astrofisica) at the Spanish Observatorio del Roque de Los Muchachos of the Instituto de Astrofísica de Canarias. We acknowledge A. I. Karakas for providing us with additional unpublished model predictions. We also acknowledge A. I. Karakas, M. Lugaro, and J. García-Rojas for very useful discussions as well as L. Stanghellini for sharing her *Spitzer* data on compact Galactic PNe with us. S.K.G. acknowledges support from grant N203 511838 of the Science and High Education Ministry of Poland. D.A.G.H. acknowledges support for this work provided by the Spanish Ministry of Economy and Competitiveness under grants AYA-2011-27754 and AYA-2011-29060.

References

- Acker, A., Marcout, J., Ochsenbein, F., et al. 1992, The Strasbourg-ESO Catalogue of Galactic Planetary Nebulae. Parts I, II.
- Aller, L. H. & Czyzak, S. J. 1979, *Ap&SS*, 62, 397
- Aller, L. H. & Keyes, C. D. 1987, *ApJS*, 65, 405
- Anders, E. & Grevesse, N. 1989, *Geochim. Cosmochim. Acta*, 53, 197
- Asplund, M., Grevesse, N., Sauval, A. J., & Scott, P. 2009, *ARA&A*, 47, 481
- Barker, T. 1978, *ApJ*, 219, 914
- Blöcker, T. 1995, *A&A*, 299, 755
- Boyer, M. L., Girardi, L., Marigo, P., et al. 2013, *ApJ*, 774, 83
- Cavichia, O., Costa, R. D. D., & Maciel, W. J. 2010, *Rev. Mexicana Astron. Astrofis.*, 46, 159
- Chiappini, C., Górny, S. K., Stasińska, G., & Barbuy, B. 2009, *A&A*, 494, 591
- Cuisinier, F., Acker, A., & Köppen, J. 1996, *A&A*, 307, 215
- Cuisinier, F., Maciel, W. J., Köppen, J., Acker, A., & Stenholm, B. 2000, *A&A*, 353, 543
- de Freitas Pacheco, J. A., Maciel, W. J., & Costa, R. D. D. 1992, *A&A*, 261, 579
- de Marco, O. 2009, *PASP*, 121, 316
- Escudero, A. V. & Costa, R. D. D. 2001, *A&A*, 380, 300
- Escudero, A. V., Costa, R. D. D., & Maciel, W. J. 2004, *A&A*, 414, 211
- Exter, K. M., Barlow, M. J., & Walton, N. A. 2004, *MNRAS*, 349, 1291
- García-Hernández, D. A., Abia, C., Machado, A., & García-Lario, P. 2006a, *A&A*, 452, 1049
- García-Hernández, D. A., García-Lario, P., Plez, B., et al. 2006b, *Science*, 314, 1751
- García-Hernández, D. A., García-Lario, P., Plez, B., et al. 2007a, *A&A*, 462, 711
- García-Hernández, D. A., Machado, A., García-Lario, P., et al. 2010, *ApJ*, 724, L39
- García-Hernández, D. A., Machado, A., Lambert, D. L., et al. 2009, *ApJ*, 705, L31
- García-Hernández, D. A., Perea-Calderón, J. V., Bobrowsky, M., & García-Lario, P. 2007b, *ApJ*, 666, L33
- García-Hernández, D. A., Villaver, E., García-Lario, P., et al. 2012, *ApJ*, 760, 107
- García-Hernández, D. A., Zamora, O., Yagüe, A., et al. 2013, *A&A*, 555, L3
- García-Lario, P. & Perea Calderón, J. V. 2003, in *ESA Special Publication*, Vol. 511, *Exploiting the ISO Data Archive. Infrared Astronomy in the Internet Age*, ed. C. Gry, S. Peschke, J. Matagne, P. Garcia-Lario, R. Lorente, & A. Salama, 97
- García-Rojas, J., Peña, M., Morisset, C., et al. 2013, *A&A*, 558, A122
- García-Rojas, J., Peña, M., & Peimbert, A. 2009, *A&A*, 496, 139
- Girard, P., Köppen, J., & Acker, A. 2007, *A&A*, 463, 265
- Górny, S. K. 2014, *A&A*, accepted
- Górny, S. K., Chiappini, C., Stasińska, G., & Cuisinier, F. 2009, *A&A*, 500, 1089
- Górny, S. K., Perea-Calderón, J. V., García-Hernández, D. A., García-Lario, P., & Szczerba, R. 2010, *A&A*, 516, A39
- Górny, S. K., Stasińska, G., Escudero, A. V., & Costa, R. D. D. 2004, *A&A*, 427, 231
- Górny, S. K. & Tylenda, R. 2000, *A&A*, 362, 1008
- Górny, S. K., Tylenda, R., & Szczerba, R. 1994, *A&A*, 284, 949
- Gutenkunst, S., Bernard-Salas, J., Pottasch, S. R., Sloan, G. C., & Houck, J. R. 2008, *ApJ*, 680, 1206
- Guzman-Ramirez, L., Zijlstra, A. A., Níchuimín, R., et al. 2011, *MNRAS*, 414, 1667
- Henry, R. B. C., Kwitter, K. B., Jaskot, A. E., et al. 2010, *ApJ*, 724, 748
- Henry, R. B. C., Speck, A., Karakas, A. I., Ferland, G. J., & Maguire, M. 2012, *ApJ*, 749, 61
- Herwig, F. 2000, *A&A*, 360, 952
- Herwig, F. 2005, *ARA&A*, 43, 435
- Iben, Jr., I. 1995, *Phys. Rep.*, 250, 2
- Izotov, Y. I., Stasińska, G., Meynet, G., Guseva, N. G., & Thuan, T. X. 2006, *A&A*, 448, 955
- Kamath, D., Karakas, A. I., & Wood, P. R. 2012, *ApJ*, 746, 20
- Karakas, A. I. 2010, *MNRAS*, 403, 1413
- Karakas, A. I., García-Hernández, D. A., & Lugaro, M. 2012, *ApJ*, 751, 8
- Karakas, A. I. & Lattanzio, J. C. 2003, *PASA*, 20, 393
- Karakas, A. I., Lattanzio, J. C., & Pols, O. R. 2002, *PASA*, 19, 515
- Karakas, A. I., van Raai, M. A., Lugaro, M., Sterling, N. C., & Dinerstein, H. L. 2009, *ApJ*, 690, 1130
- Kingsburgh, R. L. & Barlow, M. J. 1994, *MNRAS*, 271, 257
- Kwitter, K. B. & Henry, R. B. C. 2001, *ApJ*, 562, 804
- Kwok, S., Volk, K., & Bernath, P. 2001, *ApJ*, 554, L87
- Liu, X.-W., Barlow, M. J., Zhang, Y., Bastin, R. J., & Storey, P. J. 2006, *MNRAS*, 368, 1959
- Lugaro, M., Karakas, A. I., Stancliffe, R. J., & Rijs, C. 2012, *ApJ*, 747, 2
- Marigo, P., Bressan, A., Nanni, A., Girardi, L., & Pumo, M. L. 2013, *MNRAS*, 434, 488
- Mazzitelli, I., D'Antona, F., & Ventura, P. 1999, *A&A*, 348, 846
- Milingo, J. B., Kwitter, K. B., Henry, R. B. C., & Cohen, R. E. 2002, *ApJS*, 138, 279
- Miszalski, B., Acker, A., Moffat, A. F. J., Parker, Q. A., & Udalski, A. 2009, *A&A*, 496, 813
- Molster, F. J., Yamamura, I., Waters, L. B. F. M., et al. 1999, *Nature*, 401, 563
- Peña, M., Stasińska, G., & Medina, S. 2001, *A&A*, 367, 983
- Peimbert, M. 1967, *ApJ*, 150, 825
- Peimbert, M. 1978, in *IAU Symposium*, Vol. 76, *Planetary Nebulae*, ed. Y. Terzian, 215–223
- Perea-Calderón, J. V., García-Hernández, D. A., García-Lario, P., Szczerba, R., & Bobrowsky, M. 2009, *A&A*, 495, L5
- Pottasch, S. R. & Bernard-Salas, J. 2006, *A&A*, 457, 189
- Ratag, M. A., Pottasch, S. R., Dennefeld, M., & Menzies, J. 1997, *A&AS*, 126, 297
- Sackmann, I.-J. & Boothroyd, A. I. 1992, *ApJ*, 392, L71
- Seaton, M. J. 1979, *MNRAS*, 187, 73P
- Shaw, R. A., Lee, T.-H., Stanghellini, L., et al. 2010, *ApJ*, 717, 562
- Stanghellini, L., García-Hernández, D. A., García-Lario, P., et al. 2012, *ApJ*, 753, 172
- Stanghellini, L., García-Lario, P., García-Hernández, D. A., et al. 2007, *ApJ*, 671, 1669
- Stanghellini, L., Guerrero, M. A., Cunha, K., Machado, A., & Villaver, E. 2006, *ApJ*, 651, 898
- Stasińska, G., Richer, M. G., & McCall, M. L. 1998, *A&A*, 336, 667
- Stasińska, G., Tylenda, R., Acker, A., & Stenholm, B. 1991, *A&A*, 247, 173
- Tylenda, R., Acker, A., & Stenholm, B. 1993, *A&AS*, 102, 595
- Uttenthaler, S., Hron, J., Lebzelter, T., et al. 2007, *A&A*, 463, 251
- Vassiliadis, E. & Wood, P. R. 1993, *ApJ*, 413, 641
- Wang, W. & Liu, X.-W. 2007, *MNRAS*, 381, 669
- Waters, L. B. F. M., Beintema, D. A., Zijlstra, A. A., et al. 1998a, *A&A*, 331, L61
- Waters, L. B. F. M., Beintema, D. A., Zijlstra, A. A., et al. 1998b, *A&A*, 331, L61
- Waters, L. B. F. M., Molster, F. J., de Jong, T., et al. 1996, *A&A*, 315, L361
- Weidmann, W. A. & Gamen, R. 2011, *A&A*, 526, A6

Appendix A: New emission-line central stars

A considerable fraction of the Galactic PNe population has emission-line central stars of different types (Weidmann & Gamen 2011). We used our new TNG DOLORES observations to look for their presence in our sample. We found five objects (BI 2-1, He 2-440, IC 4846, K 3-56, and K 4-41) to be possible WELs-type objects (see Tylanda et al. 1993). Only one object (K 3-15) could tentatively be classified as a Wolf–Rayet type [WC 11] central star. Taking the very low-ionization state of this nebula into account we instead classified it as a VL-type object - a member of a class of emission-line stars recently introduced by Górný et al. (2009). The full optical spectrum of K 3-15 (low-ionization nebula) and also of K 3-56 (high-ionization nebula) have been presented in Fig. 1. In Fig. A.1 we present details of the spectra of all new emission-line central star candidates in our observed sample. In this plot the expected locations of the characteristic stellar emission lines are indicated with dotted lines, and if positively identified they are then marked with the name of the appropriate ion.

Appendix B: Spectra of the three suspected symbiotic stars

The full optical spectra of the three suspected symbiotic stars (CTSS 2, K 4-57, and Th 4-1) are displayed in Figure B.1. Their *Spitzer* IR spectra (with the unusual presence of hot dust emission) are very different from the other Galactic PNe studied here, and their optical spectra are suggestive of a possibly symbiotic classification. For example, the 2MASS colours of PN K 4-57 are consistent with a D-type symbiotic PN. A detailed analysis of this small group of symbiotic stars will be presented elsewhere.

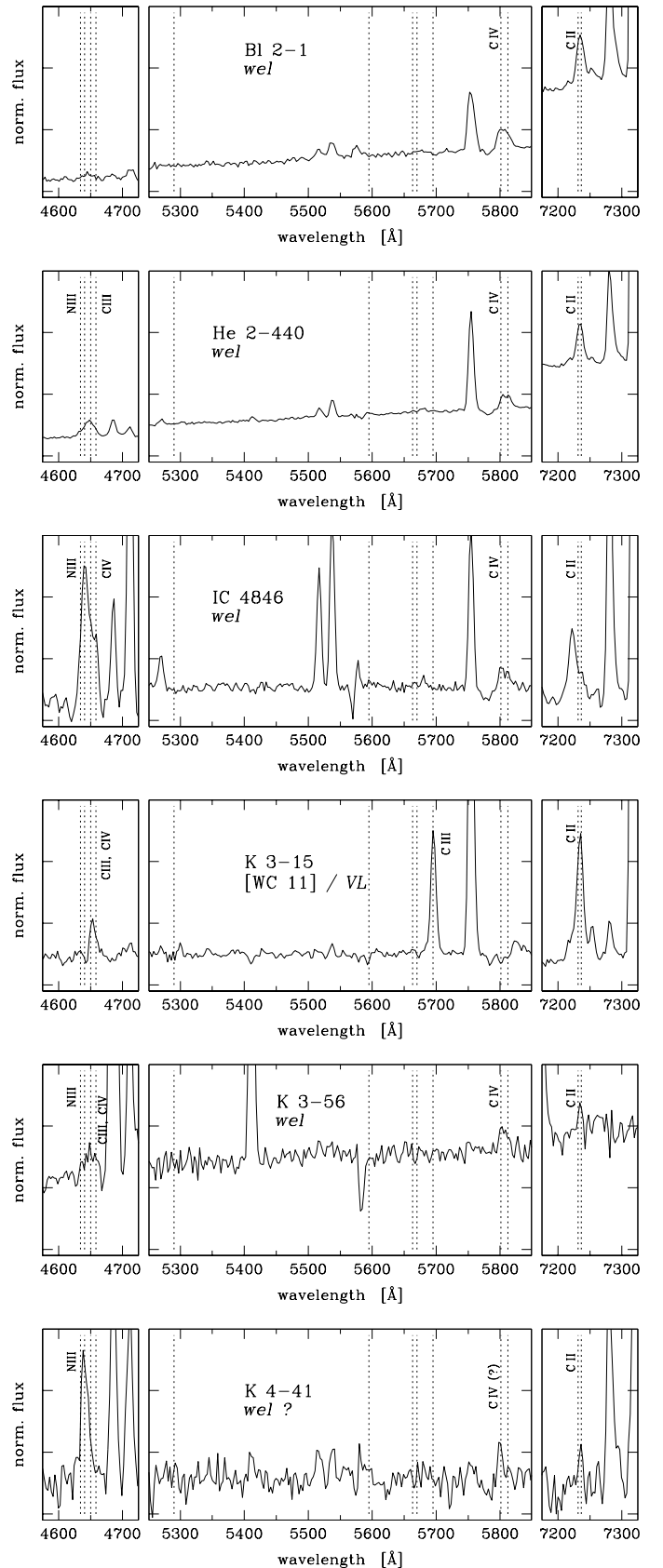


Fig. A.1. Spectra of the new PNe with emission-line central stars. Expected locations of characteristic features are indicated by dotted lines and labelled with the appropriate ion name if present in the spectra.

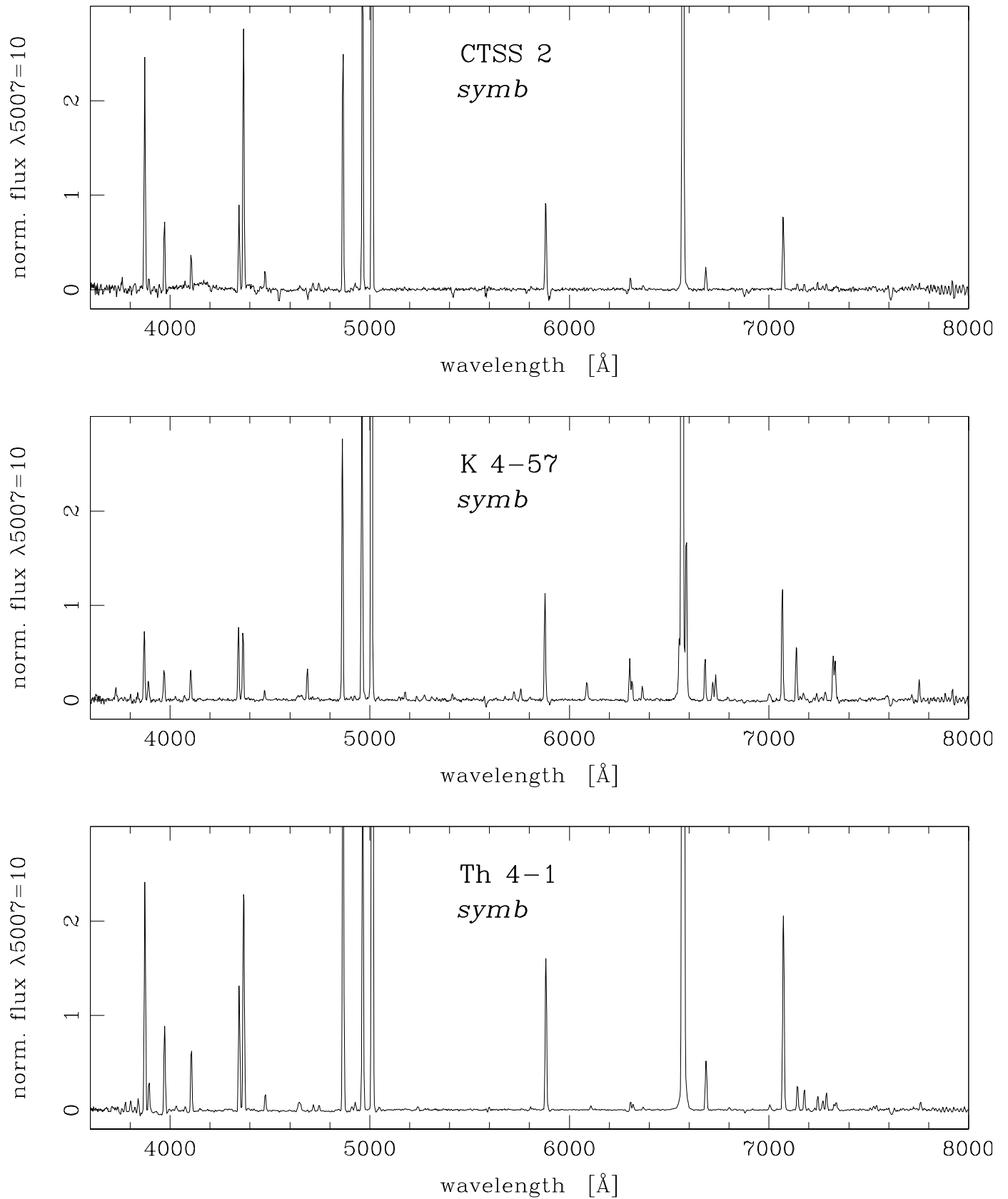


Fig. B.1. Spectra of the three suspected symbiotic stars.

Table 2. Observed line fluxes and dereddened intensities on the scale $H\beta=100$ of the main nebular lines. Meaning of the symbols: (:) - line error at 20%; (;) - line error at 40%; (p) - line present but not measurable; (?) - uncertain identification; (S) - saturated; (r) - recalculated using doublet pair; (b) - significantly blended with other line; (B) - blend or sum of two lines; (c) - additional reddening correction applied.

		107.4-02.6 K 3-87		097.6-02.4 M 2-50		095.2+00.7 B1 2- 1		079.9+06.4 K 3-56	
		F(λ)	I(λ)	F(λ)	I(λ)	F(λ)	I(λ)	F(λ)	I(λ)
3727	[O II]			12.34	22.72 c	9.38 :	48.44 :c		
3869	[Ne III]	21.88	46.79 c	66.30	113.19 c	17.34	72.67 c	18.79	46.30 c
4068	[S II]			0.33 ;	0.46 ;c				
4102	H I	14.36	26.23 c	17.37	26.07 c	8.60	25.80 c	13.59	26.29 c
4340	H I	29.40	47.30 c	35.21	47.09 c	22.67	52.03	30.44	47.38 c
4363	[O III]	7.18	11.11	10.99	14.67	2.89	6.44	7.27	11.71
4471	He I			3.59	4.50	3.15	5.75		
4686	He II	84.27	97.59	12.18	13.46	0.59 ;	0.78 ;	90.25	105.93
4711	[Ar IV]	7.18 :	8.17 :	4.94	4.72	1.07 :	:	7.51	8.61
4725	[Ne IV]							1.42 ;b	1.59 ;b
4740	[Ar IV]	4.79 :	5.32 :	3.49	3.75	0.76 :	0.97 :	6.09	6.83
4861	H I	100.00	100.00	100.00	100.00	100.00	100.00	100.00	100.00
4959	[O III]	209.23	193.41	427.13	408.92	380.56	327.03	181.74	168.30
5007	[O III]	626.15	558.00	1269.09	1190.65	1225.81	981.25	566.31	506.08
5200	[N I]			0.23 ;	0.17 ;	1.04 ;	0.62 ;		
5515	[Cl III]			0.72 :	0.54 :	0.93 ;	0.37 ;		
5537	[Cl III]			0.56 :	0.46 :	1.66 :	0.68 :		
5755	[N II]			0.47 ;	0.35 ;	6.35	1.84		
5876	He I	5.30 ;	2.58 ;	20.38 :	13.68 :	68.39	16.98	3.96 :	1.98 :
6300	[O I]			0.91 ;	0.53 ;	28.10 ;	4.49 ;		
6312	[S III]	3.76 ;	1.46 ;	2.79 b	1.65 b	b	b	2.19 ;	0.87 ;
6548	[N II]			4.61 b	2.54 b	65.69 ;	8.30 ;		
6563	H I	818.29	278.65	512.49	282.14	2312.76	288.45	794.27	277.47
6583	[N II]			27.25	14.89	576.90 :b	70.63 :b	4.96 b	1.73 b
6678	He I	3.25 ;	1.04 ;	6.75	3.64	35.60	4.03	3.55	1.16
6716	[S II]			3.70	1.96	7.22	0.79	1.36 ;	0.46 ;
6730	[S II]			5.50	2.91	27.93	3.03	1.36 ;	0.46 ;
7006	[Ar V]	3.93	1.11					6.68	1.97
7136	[Ar III]	11.97	3.27	22.47	10.94	179.46	14.52	12.77	3.59
7320	[O II]			1.89 :	1.64 :B	179.99 B	12.69 B		
7330	[O II]			1.61 :	1.64 :B	179.99 B	12.69 B		

Table 2. Continued.

		069.2+02.8 K 3-49		068.7+01.9 K 4-41		060.5+01.8 He 2-440		052.9+02.7 K 3-31	
		F(λ)	I(λ)	F(λ)	I(λ)	F(λ)	I(λ)	F(λ)	I(λ)
3727	[O II]	22.76	90.22 c	3.81 :	10.06 :c	17.10	72.94 c	5.26 ;	29.46 ;
3869	[Ne III]			35.35	81.69 c	5.20	18.38 c	27.11	121.65
4068	[S II]	2.20	5.42 c			1.29 :	3.53 :c		
4102	H I	10.88	25.59 c	14.03	25.74 c	9.87	25.68 c	7.10	22.41
4340	H I	26.75	46.45 c	30.62	46.65 c	22.88	46.08 c	21.05	50.25
4363	[O III]			3.59	5.63	1.00	1.96	5.74	13.13
4471	He I	p	p	4.79	6.78	3.39	5.72	3.11 :	5.91 :
4686	He II			4.08	4.76	1.83	2.26	1.52 :	1.99 :
4711	[Ar IV]			3.37	0.98	1.02		1.83 :	:
4725	[Ne IV]								
4740	[Ar IV]			2.77	3.11	?	?	2.63 :	3.17 :
4861	H I	100.00	100.00	100.00	100.00	100.00	100.00	100.00	100.00
4959	[O III]	5.68	5.18	375.12	342.22	164.24	144.49	574.88	490.54
5007	[O III]	18.09	15.72	1137.85	994.52	528.29	437.94	1850.95	1466.56
5200	[N I]	p	p			0.50 :	0.33 :	1.52 ;	0.91 ;
5515	[Cl III]			0.52 ;	0.29 ;	0.70	0.33	0.80 ;	0.32 ;
5537	[Cl III]			0.49 ;	0.29 ;	1.32	0.60	1.67 :	0.65 :
5755	[N II]	14.24	6.51	p	p	8.30	2.94	11.56	3.19
5876	He I	10.53	4.35	38.81	16.70	55.09	17.02	82.06	19.11
6300	[O I]	5.47	1.72			8.98	1.92	42.90 :	6.29 :
6312	[S III]	3.83	1.18	2.86 :	0.95 :	7.33 b	1.54 b	20.41 ;b	2.96 ;b
6548	[N II]	206.88	55.91			186.11	32.55	175.52	20.16
6563	H I	1093.01	292.87	1019.29	289.38	1681.72	290.82	2528.62	286.44
6583	[N II]	661.60	175.21	47.89 b	13.45 b	766.62	130.52	721.34	80.14
6678	He I	4.01 :	1.01 :	16.73	4.47	26.85	4.28	44.02	4.50
6716	[S II]	5.45	1.36	1.88 :	0.50 :	8.97	1.40	11.48	1.14
6730	[S II]	13.43	3.29	5.85 :	1.51 :	22.15	3.40	34.21	3.35
7006	[Ar V]	0.88 ;	0.19 ;			0.28 ;	0.04 ;	p	p
7136	[Ar III]	16.40	3.34	69.00	15.08	140.82	16.91	279.59	20.14
7320	[O II]	118.95	41.54 B	9.90 B	1.99 B	60.99 b	19.58 B	71.21 b	16.44 B
7330	[O II]	103.36	41.54 B	9.90 B	1.99 B	122.13 b	19.58 B	192.34 b	16.44 B

Table 2. Continued.

		051.0+02.8 WhMe 1		042.9-06.9 NGC 6807		041.8+04.4 K 3-15		038.7-03.3 M 1-69	
		F(λ)	I(λ)	F(λ)	I(λ)	F(λ)	I(λ)	F(λ)	I(λ)
3727	[O II]			17.16 :	27.77 :c	21.33	37.54 c	18.86	40.44 c
3869	[Ne III]	201.93 :b	938.15 :b	80.51	121.99 c			62.20	121.41 c
4068	[S II]			2.46	3.46 c	1.47 :	2.30 :c	2.15 ;	3.60 ;c
4102	H I			18.99	25.90 c	17.11	25.81 c	15.42	25.84 c
4340	H I			37.92	46.86 c	33.00	46.43	31.51	46.78 c
4363	[O III]			10.64	13.19	p	p	4.94	7.12
4471	He I	?	?	4.37	5.22	1.10 :	1.42 :	4.25	5.61
4686	He II	19.44 :	25.86 :	0.33 :	0.32 :			11.72	13.27
4711	[Ar IV]	17.67 :	22.68 :	1.47				3.14	2.75
4725	[Ne IV]								
4740	[Ar IV]	15.87 :	19.44 :	2.01	2.11			3.44	3.71
4861	H I	100.00 :b	100.00 :b	100.00	100.00	100.00	100.00	100.00	100.00
4959	[O III]	388.31	330.11	472.25	459.77	4.82	4.51	444.71	416.16
5007	[O III]	1241.27	978.23	S	1353.14 r	14.85	13.50	1341.19	1216.84
5200	[N I]			0.22 :	0.18 :			0.65 ;	0.57 ;
5515	[Cl III]			0.30 :	0.26 :			0.81 :	0.54 :
5537	[Cl III]			0.56 :	0.51 :	0.21 ;	0.14 ;	1.33 :	0.87 :
5755	[N II]	27.66 :	7.40 :	1.41	1.13	8.34	5.00	2.26	1.34
5876	He I	104.84 :	23.59 :	21.30	16.67	8.56	4.85	32.30 :	17.56 :
6300	[O I]	41.96 b	5.90 b	6.90 b	5.00 b	2.55	1.17	5.65 ;	2.56 ;
6312	[S III]	29.35	4.08	2.90 b	2.10 b	3.29	1.54	5.21 b	2.32 b
6548	[N II]	28.15	3.07	6.60 b	4.59 b	39.56 b	16.90 b	44.18 b	17.89 b
6563	H I	2658.51	286.43	412.31	285.88	678.23	287.90	713.82	287.24
6583	[N II]	112.45	11.88	31.76	21.98	190.27	80.17	178.92	71.41
6678	He I	42.41	4.11	5.77	3.95	2.84	1.14	11.26	4.36
6716	[S II]	9.05	0.85	1.50	1.02	0.76	0.32	10.49	3.99
6730	[S II]	14.05	1.31	3.48	2.37	2.42	0.96	20.60	7.80
7006	[Ar V]					0.32 :	0.11 :	0.29	0.10
7136	[Ar III]	117.95	8.00	17.34	11.12	5.65	2.02	71.48	23.81
7320	[O II]	38.39 :	6.04 :B	12.51	13.74 B	77.01	63.91 B	9.57 :	5.36 :B
7330	[O II]	64.85 :	6.04 :B	9.37	13.74 B	113.39	63.91 B	7.46 :	5.36 :B

Table 2. Continued.

		027.6-09.6 IC 4846		025.3-04.6 K 4- 8		011.1+07.0 Sa 2-237		008.6-02.6 MaC 1-11	
		F(λ)	I(λ)	F(λ)	I(λ)	F(λ)	I(λ)	F(λ)	I(λ)
3727	[O II]	21.09	31.17 c	16.06	28.43 c	291.41	688.31 c	5.20 :	20.69 :
3869	[Ne III]	61.13	85.88 c	66.69	109.32 c	105.38	220.58 c	18.53	61.98
4068	[S II]	1.08	1.44 c	1.54	2.21 c	21.24 :	37.12 :c		
4102	H I	20.02	25.88 c	17.93	25.93 c	15.26 :	25.99 :c	10.36 :	26.24 :
4340	H I	38.95	46.84 c	36.14	46.90 c	33.98 :	46.99 :c	24.39	49.07
4363	[O III]	6.12	7.31	7.79	10.15	7.19 :	10.47 :	3.85	7.64
4471	He I	4.47	5.18	4.16	5.16	4.54 :	6.03 :	3.28	5.55
4686	He II	0.42	0.43	0.81	0.88	45.82	52.21		
4711	[Ar IV]	1.65	0.86	1.89	1.22	2.61 ;	2.18 ;	1.97 :	1.62 :
4725	[Ne IV]								
4740	[Ar IV]	1.35	1.46	2.21	2.34	2.09 ;	2.30 ;	0.92 ;	1.05 ;
4861	H I	100.00	100.00	100.00	100.00	100.00	100.00	100.00	100.00
4959	[O III]	368.13	359.96	439.88	423.31	384.78	368.55	328.21	288.83
5007	[O III]	1081.33	1046.40	1306.76	1235.16	1140.33	1070.36	1048.84	869.54
5200	[N I]	0.18 :	0.19 :	0.28 :	0.27 :	40.72	35.49		
5515	[Cl III]	0.44	0.35	0.39	0.32	2.65 ;	2.02 ;	1.22 ;	0.57 ;
5537	[Cl III]	0.65	0.61	0.64	0.48	1.85 ;	1.46 ;	0.74 ;	0.32 ;
5755	[N II]	0.59	0.50	1.01	0.73	32.97	23.24	p	p
5876	He I	19.34	15.72	22.08	15.53	27.31	18.37	51.05	15.77
6300	[O I]	2.45 b	1.91 b	4.98	3.14	144.30	85.64	2.45 :	0.53 :
6312	[S III]	1.90 b	1.45 b	2.31	1.44	9.72 ;	5.74 ;	3.89 :	0.82 :
6548	[N II]	4.52 b	3.32 b	8.50 b	5.03 b	1112.58	617.79	25.27 :b	4.43 :b
6563	H I	389.12	286.25	483.24	285.14	512.94	283.71	1643.45	284.60
6583	[N II]	23.88	17.53	37.66	22.14	3450.20	1898.48	70.14 :b	11.95 :b
6678	He I	5.39	3.92	6.37	3.68	8.63	4.63	23.56	3.76
6716	[S II]	1.59	1.15	2.14	1.20	265.34	141.48	4.63	0.71
6730	[S II]	3.42	2.45	4.42	2.51	337.79	179.59	9.18	1.42
7006	[Ar V]								
7136	[Ar III]	14.82	10.21	19.20	10.15	91.29	44.65	58.17	7.00
7320	[O II]	3.94 b	6.09 B	6.30	7.30 B	14.06 b	17.21 B	12.41 b	3.53 B
7330	[O II]	5.14 b	6.09 B	8.00	7.30 B	22.49 b	17.21 B	20.63 b	3.53 B

Table 2. Continued.

		004.3-02.6		000.6-02.3		354.9+03.5	
		H 1-53		H 2-32		Th 3- 6	
		F(λ)	I(λ)	F(λ)	I(λ)	F(λ)	I(λ)
3727	[O II]	12.45 :	39.72 :	7.05	60.68 c	34.96 :	137.92 :c
3869	[Ne III]	23.16	64.28				
4068	[S II]						
4102	H I	10.63 :	23.12 :	6.23:	25.32 :c	9.49 ;	23.81 ;c
4340	H I	26.92	48.48	17.62	46.08 c	26.24 :	52.43 :
4363	[O III]						
4471	He I	4.43 :	6.82 :				
4686	He II						
4711	[Ar IV]						
4725	[Ne IV]						
4740	[Ar IV]						
4861	H I	100.00	100.00	100.00	100.00	100.00	100.00
4959	[O III]	231.51	207.86	0.77 ;	0.69 ;	77.78	68.53
5007	[O III]	714.43	609.99	5.74	4.62	238.97	198.41
5200	[N I]	2.23 ;	1.56 ;	1.59 :?	1.02 :?		
5515	[Cl III]	0.58 ;	0.32 ;	-	-		
5537	[Cl III]	1.32 ;	0.68 ;	1.68 ;	0.71 ;		
5755	[N II]	14.76	6.17	8.91 :	2.78 :	4.79 ;	1.71 ;
5876	He I	59.43	22.09	9.98 :	2.69 :	59.66	18.61
6300	[O I]	21.59 :	5.87 :	17.35	3.08	10.00 ;b	2.16 ;b
6312	[S III]	6.99 ;b	1.89 ;b	12.99	2.28	p	p
6548	[N II]	465.07	107.09	34.61 ;b	4.92 ;b	285.30	50.58
6563	H I	1316.47	300.26	2134.37	299.43	1747.26	306.34
6583	[N II]	1623.64	365.47	129.08 :	17.80 :	1472.48	254.20
6678	He I	25.64	5.45	4.15 :	0.54 :	33.16	5.36
6716	[S II]	14.85	3.08	7.64	0.94	44.44	6.99
6730	[S II]	40.49	8.37	11.20	1.38	137.52	21.45
7006	[Ar V]			2.16 :	0.22 :		
7136	[Ar III]	188.63	31.63	7.37	0.69	120.43	14.70
7320	[O II]	30.81	11.18 B	89.28	15.70 B	8.12 b	4.72 B
7330	[O II]	42.72	11.18 B	102.42	15.70 B	35.30 b	4.72 B

Table 3. Derived plasma diagnostics, elemental abundances and interstellar extinction. Columns give: (1) PNG number; (2) usual name; (3) disc or bulge Galactic location; (4) *Spitzer* spectra analysed in samples of Gutenkunst et al. (2008), Perea-Calderón et al. (2009), or Stanghellini et al. (2012); (5) dust classification; (6) references to data on optical lines used in the calculations; (7) electron density from [S II] (or assumed 2×10^3 if not computable); (8) and (9) electron temperature from [N II] and [O III]; (10) to (16) derived nebular abundance ratios; (17) logarithmic extinction at $H\beta$ (if not given, original data were already dereddened). For columns (7) to (17) there are three rows for each object: the first row gives the values of parameters computed from the nominal values of the observational data, whereas the second and third rows give the upper and lower limits of these parameters (see text for details).

PN G	name	loc.	sample	type	ref	N_e	$T_e(\text{N II})$	$T_e(\text{O III})$	He/H	N/H	O/H	Ne/H	S/H	Ar/H	Cl/H	C
184.0-02.1	M 1- 5	d	S	CC _{al}	Mi02	5.69E+03	12638	11177	1.06E-01	2.80E-05	1.21E-04	1.65E-05	1.32E-06	9.32E-07	3.33E-07	1.37E+00
						7.72E+03	13288	11542	1.12E-01	3.26E-05	1.42E-04	1.93E-05	1.57E-06	1.06E-06	4.91E-07	1.46E+00
						4.37E+03	11730	10683	9.95E-02	2.44E-05	1.10E-04	1.44E-05	1.16E-06	8.48E-07	2.47E-07	1.25E+00
205.8-26.7	MaC 2- 1	d	S	CC _{al}	Cu96	7.90E+03		11278	9.90E-02	2.13E-05	2.09E-04		1.09E-06	6.74E-07	2.20E-06	0.00E+00
						1.00E+05		11773	1.13E-01	9.96E-05	3.69E-04		2.66E-06	9.43E-07	2.99E-06	6.61E-02
						4.63E+02		9871	9.08E-02	2.85E-06	1.75E-04		2.97E-07	5.86E-07	-	-
235.3-03.9	M 1-12	d	S	CC _{al}	KB94,Cu96,He10	3.05E+04	9010		2.58E-02	5.76E-05	4.04E-04		2.73E-06	3.17E-07	8.76E-08	1.12E+00
						7.58E+04	11236		3.32E-02	2.18E-04	3.74E-03		1.86E-05	7.06E-07	1.68E-07	1.25E+00
						6.80E+03	7105		1.88E-02	2.18E-05	6.74E-05		5.14E-07	1.78E-07	5.01E-08	9.36E-01
263.0-05.5	PB 2	d	S	CC _{al}	Cu96	(2.00E+03)		13142	9.73E-02		2.04E-04		1.46E-06	8.04E-07		9.19E-01
								13783	1.11E-01		2.42E-04		2.14E-06	9.56E-07		1.16E+00
								12599	8.38E-02		1.68E-04		8.87E-07	6.44E-07		7.51E-01
264.4-12.7	He 2- 5	d	S	CC _{al}	FP92,Cu96	5.26E+03	10150	10684	8.57E-02	3.58E-05	2.39E-04	2.51E-05	9.33E-07	9.47E-07	5.30E-07	5.61E-01
						1.00E+05	13425	11912	9.58E-02	1.35E-04	5.31E-04	3.10E-05	5.69E-06	1.46E-06	2.14E-06	7.23E-01
						5.05E+02	4495	9456	7.66E-02	2.04E-05	1.63E-04	2.26E-05	5.71E-07	6.43E-07	-	3.81E-01
275.3-04.7	He 2- 21	d	S	CC _{al}	Mi02	1.21E+03	10114	12980	1.15E-01	4.23E-05	2.13E-04	3.98E-05	2.28E-06	8.78E-07	1.71E-06	3.75E-01
						2.40E+03	13172	13453	1.22E-01	5.17E-05	2.44E-04	4.62E-05	2.70E-06	9.64E-07	2.22E-06	4.62E-01
						7.74E+02	6709	12578	1.06E-01	3.90E-05	1.79E-04	3.52E-05	1.96E-06	7.82E-07	1.12E-06	2.67E-01
278.6-06.7	He 2- 26	d	S	CC _{al}	Cu96	4.31E+03	11273	11686	9.96E-02	9.94E-05	3.30E-04		3.04E-06	1.18E-06	7.78E-07	5.06E-01
						1.20E+04	13381	11996	1.08E-01	1.34E-04	4.23E-04		4.14E-06	1.40E-06	1.38E-06	6.05E-01
						1.89E+03	7896	11074	9.21E-02	7.46E-05	2.96E-04		2.10E-06	1.08E-06	3.93E-07	4.10E-01
285.4+01.5	Pe 1- 1	d	S	CC _{ar}	Gi07,Go14	1.02E+04	13079	10215	1.17E-01	1.12E-04	4.05E-04	8.67E-05	5.45E-06	2.64E-06	1.01E-06	1.94E+00
						1.94E+04	14010	10662	1.25E-01	1.37E-04	4.97E-04	1.01E-04	6.58E-06	2.96E-06	1.32E-06	2.17E+00
						6.08E+03	11390	9769	1.10E-01	9.39E-05	3.13E-04	7.45E-05	4.69E-06	2.31E-06	7.02E-07	1.72E+00
285.4+02.2	Pe 2- 7	d	S	F	KB94	1.71E+03		29697	1.14E-01	2.74E-05	3.05E-05	1.65E-05	1.10E-06	5.07E-07		-
						2.01E+03		31097	1.22E-01	2.99E-05	3.40E-05	1.85E-05	1.24E-06	5.54E-07		
						1.43E+03		28358	1.07E-01	2.39E-05	2.72E-05	1.47E-05	9.82E-07	4.52E-07		
286.0-06.5	He 2- 41	d	S	CC _{al}	Go14	6.74E+03	12917	11626	9.68E-02	4.53E-05	2.09E-04	4.53E-05	2.24E-06	9.05E-07	1.02E-06	4.67E-01
						1.33E+04	13591	11976	1.02E-01	5.12E-05	2.48E-04	5.37E-05	2.55E-06	1.03E-06	1.21E-06	5.57E-01
						3.99E+03	10618	11199	9.09E-02	3.73E-05	1.79E-04	4.15E-05	1.88E-06	8.02E-07	7.64E-07	3.59E-01
289.8+07.7	He 2- 63	d	S	F	Go14	9.86E+02		12459	9.87E-02	5.30E-05	2.66E-04	4.85E-05	2.61E-06	9.40E-07		1.27E-01
						1.93E+03		12885	1.03E-01	7.64E-05	3.11E-04	5.75E-05	3.62E-06	1.10E-06		2.17E-01
						4.38E+02		12078	9.16E-02	3.46E-05	2.31E-04	4.67E-05	1.70E-06	6.73E-07		1.63E-02
294.9-04.3	He 2- 68	d	S	CC _{al}	Go14	1.49E+04	9666	10614	7.57E-02	4.57E-05	2.27E-04	1.49E-05	1.94E-06	8.00E-07	1.31E-07	3.29E-01
						3.42E+04	10402	11330	8.06E-02	7.18E-05	6.44E-04	4.49E-05	3.72E-06	1.02E-06	2.25E-07	4.35E-01
						8.86E+03	8135	9485	7.01E-02	3.79E-05	1.68E-04	1.09E-05	1.56E-06	6.75E-07	8.94E-08	2.38E-01

Table 3. Continued

PN G	name	loc.	sample	type	ref	N_e	$T_e(\text{N II})$	$T_e(\text{O III})$	He/H	N/H	O/H	Ne/H	S/H	Ar/H	Cl/H	C
295.3-09.3	He 2- 62	d	S	OC_{am}	Go14	4.93E+03	16469	12945	1.03E-01	7.38E-05	1.41E-04	3.81E-05	3.18E-06	8.37E-07	1.00E-06	3.26E-01
						6.64E+03	17364	13389	1.11E-01	8.62E-05	1.64E-04	4.39E-05	3.75E-06	9.30E-07	1.30E-06	4.43E-01
						3.85E+03	15468	12481	9.64E-02	5.64E-05	1.22E-04	3.35E-05	2.57E-06	7.42E-07	6.44E-07	2.26E-01
296.3-03.0	He 2- 73	d	S	DC_{cr}	Go14	5.05E+03	12601	11580	1.22E-01	2.56E-04	4.15E-04	1.04E-04	8.50E-06	3.42E-06	1.39E-06	1.40E+00
						7.13E+03	13090	11942	1.28E-01	3.09E-04	4.74E-04	1.17E-04	9.78E-06	3.85E-06	1.75E-06	1.50E+00
						4.00E+03	11929	11241	1.16E-01	2.12E-04	3.59E-04	9.25E-05	7.16E-06	3.04E-06	1.02E-06	1.30E+00
297.4+03.7	He 2- 78	d	S	CC_{ar}	Go14	3.93E+03	7847		5.13E-02	7.43E-05	4.75E-04		5.63E-06	1.34E-06		8.94E-01
						5.17E+03	9025		5.44E-02	1.14E-04	1.23E-03		8.98E-06	2.05E-06		9.84E-01
						2.89E+03	6680		4.78E-02	5.39E-05	2.68E-04		4.26E-06	1.00E-06		8.03E-01
300.7-02.0	He 2- 86	d	S	DC_{am+cr}	Gi07,Go14	9.72E+03	11201	9100	1.37E-01	4.63E-04	4.50E-04	1.36E-04	1.62E-05	5.36E-06	4.78E-06	2.25E+00
						2.18E+04	11816	9542	1.45E-01	6.48E-04	6.38E-04	1.90E-04	2.35E-05	6.78E-06	8.47E-06	2.49E+00
						6.77E+03	10162	8481	1.27E-01	3.48E-04	3.58E-04	8.96E-05	1.29E-05	4.18E-06	2.18E-06	2.00E+00
307.5-04.9	My Cn 18	d	S	DC_{am+cr}	KB94,Cu96	1.33E+04	7712	8186	9.88E-02	1.91E-04	3.89E-04	1.70E-04	8.75E-06	2.74E-06	1.68E-06	9.52E-01
						1.00E+05	8430	9481	1.03E-01	1.10E-03	5.36E-03	5.68E-03	5.50E-05	6.93E-06	7.99E-06	1.19E+00
						5.99E+03	5440		9.18E-02	1.41E-04	1.79E-04	8.44E-05	5.02E-06	1.78E-06	9.46E-07	6.27E-01
309.0+00.8	He 2- 96	d	S	DC_{am+cr}	Go14	7.60E+03	12410	8444	1.35E-01	1.73E-04	6.05E-04	1.78E-04	1.91E-05	4.63E-06	1.18E-05	1.78E+00
						1.22E+04	13139	8564	1.43E-01	2.22E-04	7.86E-04	2.40E-04	2.55E-05	5.28E-06	1.85E-05	1.87E+00
						5.93E+03	11439	8068	1.27E-01	1.41E-04	5.71E-04	1.43E-04	1.68E-05	4.33E-06	7.46E-06	1.69E+00
309.5-02.9	MaC 1- 2	d	S	CC_{ar}	Go14	1.63E+03	11936	11754	1.32E-01	3.55E-04	3.94E-04	7.51E-05	4.10E-06	2.63E-06		1.27E+00
						1.96E+03	13156	13256	1.39E-01	6.42E-04	7.09E-04	1.53E-04	8.03E-06	4.03E-06		1.36E+00
						1.38E+03	10827	9507	1.23E-01	2.17E-04	2.76E-04	4.27E-05	1.97E-06	1.96E-06		1.18E+00
321.3+02.8	He 2-115	d	S	CC_{al}	Mi02,Go14	1.21E+04	11565	9205	1.14E-01	6.42E-05	3.89E-04	5.70E-05	5.33E-06	2.78E-06	2.63E-06	2.23E+00
						5.84E+04	12295	9665	1.20E-01	8.72E-05	9.82E-04	1.61E-04	8.32E-06	3.45E-06	4.98E-06	2.30E+00
						7.85E+03	9583	8596	1.05E-01	4.79E-05	3.30E-04	4.64E-05	3.56E-06	2.35E-06	8.56E-07	2.13E+00
324.2+02.5	He 2-125	d	S	DC_{am+cr}	Go14	3.83E+03	6158		2.80E-02	2.38E-04	5.37E-04		1.34E-05	9.45E-07		1.71E+00
						5.83E+03	6492		3.03E-02	3.24E-04	9.27E-04		2.09E-05	1.20E-06		1.81E+00
						3.13E+03	5763		2.63E-02	1.74E-04	2.89E-04		8.83E-06	7.39E-07		1.63E+00
324.8-01.1	He 2-133	d	S	DC_{am+cr}	Go14	7.82E+03	14361	10072	1.40E-01	4.88E-04	4.28E-04	1.65E-04	1.25E-05	3.39E-06	4.67E-06	3.59E+00
						1.32E+04	15328	11171	1.49E-01	7.56E-04	6.82E-04	2.89E-04	2.19E-05	4.63E-06	1.07E-05	3.67E+00
						5.42E+03	13180	8719	1.29E-01	3.14E-04	2.88E-04	1.02E-04	7.20E-06	2.57E-06	1.61E-06	3.51E+00
325.8-12.8	He 2-182	d	S	OC_{am}	Cu96	1.74E+04	12245	10997	1.02E-01	2.30E-05	2.24E-04		2.47E-06	8.47E-07	2.30E-07	1.92E-01
						1.00E+05	15538	11733	1.16E-01	5.77E-05	4.28E-04		4.51E-06	1.13E-06	8.20E-07	2.86E-01
						1.93E+03	7241	9784	9.83E-02	1.43E-05	1.89E-04		1.78E-06	6.95E-07	-	1.02E-01
327.1-01.8	He 2-140	d	S	DC_{cr}	Mi02,Go14	7.68E+03	8075		8.25E-02	1.32E-04	3.08E-04	2.28E-05	7.73E-06	2.46E-06	5.62E-07	1.99E+00
						1.22E+04	8579		8.87E-02	1.79E-04	5.66E-04	4.72E-05	1.34E-05	3.20E-06	7.17E-07	2.12E+00
						4.77E+03	7471		7.76E-02	1.03E-04	2.04E-04	1.42E-05	5.31E-06	1.98E-06	4.01E-07	1.90E+00
327.8-06.1	He 2-158	d	S	DC_{am+cr}	Mi02	1.93E+03	11207	9430	1.15E-01	9.26E-05	2.81E-04	6.32E-05	4.03E-06	1.56E-06	4.70E-07	4.43E-01
						2.36E+03	11544	9656	1.22E-01	1.07E-04	3.21E-04	7.49E-05	4.85E-06	1.75E-06	6.56E-07	5.30E-01
						1.65E+03	10744	9151	1.08E-01	7.80E-05	2.60E-04	5.71E-05	3.44E-06	1.42E-06	3.42E-07	3.45E-01
334.8-07.4	SaSt 2-12	d	S	OC_{cr}	FP92	(2.00E+03)		31797	5.58E-02	6.99E-06	4.53E-06					8.52E-01
								34650	5.99E-02	8.03E-06	5.23E-06					9.60E-01
								29816	5.04E-02	5.68E-06	3.88E-06					7.68E-01

Table 3. Continued

PN G	name	loc.	sample	type	ref	N_e	$T_e(N II)$	$T_e(O III)$	He/H	N/H	O/H	Ne/H	S/H	Ar/H	Cl/H	C	
336.3-05.6	He 2-186	d	S	CC_{ar}	Ca10	3.16E+03	11659	13385	1.33E-01	2.31E-04	3.87E-04	1.01E-04	4.89E-06	2.82E-06		-	
						3.74E+03	12060	13660	1.42E-01	2.53E-04	4.30E-04	1.13E-04	5.56E-06	3.10E-06			
						2.50E+03	11157	13001	1.26E-01	2.01E-04	3.56E-04	9.44E-05	4.32E-06	2.63E-06			
336.9+08.3	StWr 4-10	d	S	OC_{am}	Go14	(2.00E+03)										1.02E+00	
								13224	1.08E-01	1.94E-05	1.76E-04	4.96E-05	2.93E-06	1.04E-06			9.49E-01
								13224	1.08E-01	1.94E-05	1.76E-04	4.96E-05	2.93E-06	1.04E-06			1.02E+00
								11893	9.39E-02	1.21E-05	1.21E-04	3.67E-05	1.96E-06	6.62E-07			8.51E-01
340.9-04.6	Sa 1-5	d	S	F	Ca10	2.99E+03	16268	11756	1.17E-01	5.64E-05	2.51E-04	6.75E-05	3.49E-06	1.23E-06		-	
						3.66E+03	17992	12005	1.23E-01	6.39E-05	2.78E-04	7.35E-05	3.94E-06	1.32E-06			
						2.29E+03	14132	11506	1.06E-01	4.88E-05	2.20E-04	5.87E-05	3.15E-06	1.12E-06			
343.4+11.9	H 1- 1	d	S	OC_{am}	Cu96	1.00E+05		12526	8.78E-02	1.06E-04	3.52E-04		7.90E-06	6.60E-07	1.28E-06	3.97E-01	
						1.00E+05		12857	9.34E-02	1.52E-04	4.16E-04		1.42E-05	7.74E-07	2.30E-06	4.96E-01	
						1.00E+05		11984	8.32E-02	7.47E-05	3.02E-04		2.66E-06	5.88E-07	-	2.97E-01	
344.4+02.8	Vd 1-5	d	S	CC_{al}	Ca10	7.39E+02	16751	12737	1.16E-01	4.34E-05	2.85E-04	4.99E-05	2.18E-06	1.90E-06		-	
						1.21E+03	21859	13109	1.23E-01	5.04E-05	3.20E-04	5.56E-05	2.69E-06	2.07E-06			
						4.42E+02	11005	12417	1.08E-01	3.74E-05	2.50E-04	4.50E-05	1.93E-06	1.73E-06			
344.8+03.4	Vd 1-3	d	S	CC_{ar}	Ca10	4.15E+02	8330		9.75E-02	5.76E-05	3.22E-04		1.24E-05	1.80E-06		-	
						4.96E+02	8702		1.05E-01	6.57E-05	4.17E-04		1.40E-05	2.07E-06			
						3.26E+02	8052		9.06E-02	5.13E-05	2.72E-04		1.14E-05	1.60E-06			
345.2-08.8	Tc 1	d	P	CC_{ar+al}	KB94,Cu96	6.78E+03		9334	8.84E-02	3.15E-05	2.84E-04		8.90E-06	2.03E-06	1.33E-06	2.07E+00	
						6.43E+04		10565	1.13E-01	3.50E-05	6.19E-04		2.47E-05	3.64E-06	2.83E-06	2.41E+00	
						3.94E+03		7597	6.38E-02	2.77E-05	1.04E-04		3.31E-06	8.17E-07	1.52E-07	1.72E+00	
348.4-04.1	H 1-21	d	S	DC_{cr}	Cu96	4.67E+03	12008	9983	1.15E-01	4.33E-04	5.19E-04		1.04E-05	3.54E-06		1.71E+00	
						6.35E+03	12688	10463	1.21E-01	6.00E-04	6.74E-04		1.56E-05	4.55E-06		1.79E+00	
						3.55E+03	11081	9305	1.08E-01	3.17E-04	4.34E-04		8.39E-06	2.98E-06		1.63E+00	
348.8-09.0	He 2-306	d	S	F	Cu96	2.53E+03		7589			5.22E-04		5.94E-06	2.96E-06	3.46E-06	5.98E-01	
						1.00E+05		8725			1.38E-03		1.66E-05	5.10E-06	5.92E-06	8.42E-01	
						7.59E+01		4431			1.48E-04		1.01E-06	-	4.40E-01		
351.2+05.2	M 2- 5	d	G	DC_{cr}	Ra97	1.74E+03	5739	9034	9.08E-02	2.55E-04	4.92E-04		1.07E-05	7.16E-07		-	
						2.17E+03	6036	10677	9.57E-02	3.48E-04	7.93E-04		1.41E-05	1.61E-06			
						1.43E+03	5546	6778	8.36E-02	2.08E-04	3.58E-04		9.00E-06	4.54E-07			
351.9-01.9	Wray 16-286	b	S	DC_{am+cr}	Es01	5.44E+03	12751	9273	1.23E-01	1.86E-04	5.48E-04	1.71E-04	1.05E-05	2.77E-06		2.47E+00	
						8.33E+03	13146	9492	1.30E-01	2.39E-04	6.50E-04	1.91E-04	1.25E-05	3.03E-06		2.57E+00	
						4.07E+03	11832	8979	1.14E-01	1.48E-04	4.81E-04	1.55E-04	8.69E-06	2.43E-06		2.38E+00	
352.6+03.0	H 1- 8	b	S	DC_{cr}	Go04,Ca10	5.62E+03	7890	14176	1.02E-01	3.04E-04	4.16E-04	1.11E-04	6.41E-06	4.32E-06		2.23E+00	
						8.53E+03	8414	14572	1.52E-01	4.83E-04	5.76E-04	1.36E-04	1.11E-05	6.52E-06		2.46E+00	
						2.70E+03	7367	13689	5.20E-02	1.25E-04	2.57E-04	9.50E-05	1.72E-06	2.28E-06		1.76E+00	
354.2+04.3	M 2-10	b	S/G	DC_{cr}	Ra97,Mi02,Go09	1.41E+03	7089		1.24E-01	2.44E-04	4.43E-04	1.39E-04	7.72E-06	3.48E-06	7.22E-07	1.29E+00	
						1.82E+03	7481		1.41E-01	2.99E-04	7.00E-04	2.04E-04	1.04E-05	4.32E-06	1.24E-06	1.38E+00	
						1.15E+03	6678		9.46E-02	2.13E-04	2.73E-04	7.31E-05	5.91E-06	2.92E-06	4.18E-07	1.21E+00	
354.5+03.3	Th 3- 4	b	P	DC_{am+cr}	Go04	1.57E+04	16346		1.09E-01	1.28E-04	1.64E-04	3.38E-05	2.98E-06	1.57E-06		2.83E+00	
						3.13E+04	18100		1.23E-01	2.21E-04	2.76E-04	6.35E-05	5.23E-06	2.34E-06		2.92E+00	
						9.85E+03	10776		1.01E-01	9.96E-05	1.28E-04	2.41E-05	2.22E-06	1.27E-06		2.71E+00	

Table 3. Continued

PN G	name	loc.	sample	type	ref	N_e	$T_e(N II)$	$T_e(O III)$	He/H	N/H	O/H	Ne/H	S/H	Ar/H	Cl/H	C
354.9+03.5	Th 3- 6	b	S	DC _{cr}	t.w.	1.00E+05	4639		1.17E-01	2.25E-03	7.86E-02		1.39E-03	2.47E-05		2.34E+00
						1.00E+05	4990		1.23E-01	4.38E-03	2.82E-01		2.65E-03	4.37E-05		2.43E+00
						1.00E+05	4165		1.10E-01	1.55E-03	3.23E-02		9.91E-04	1.82E-05		2.22E+00
355.2-02.5	H 1-29	b	S	DC _{cr}	Cu00,Go04,Gi07	4.16E+03	11452	10172	1.21E-01	1.43E-04	4.16E-04	1.00E-04	6.30E-06	2.09E-06	1.72E-06	1.61E+00
						5.80E+03	12004	11614	1.29E-01	2.31E-04	5.14E-04	1.42E-04	8.96E-06	2.49E-06	3.12E-06	1.69E+00
						3.29E+03	10759	9391	1.14E-01	7.15E-05	2.72E-04	5.89E-05	2.97E-06	1.71E-06	3.62E-07	1.51E+00
355.6-02.7	H 1-32	b	P	OC _{am+cr}	Ra97,Cu00	5.78E+03	18469	9996	1.03E-01	3.80E-05	4.10E-04	9.62E-05	4.37E-06	1.66E-06	1.56E-06	1.63E+00
						1.33E+04	20786	10282	1.13E-01	5.21E-05	5.17E-04	1.15E-04	5.47E-06	1.93E-06	2.17E-06	1.71E+00
						3.44E+03	12777	9570	9.38E-02	2.39E-05	3.63E-04	9.03E-05	3.65E-06	1.51E-06	6.02E-07	1.52E+00
355.7-03.0	H 1-33	b	S	CC _{ar}	Cu00	2.57E+03	10714	8375	1.42E-01	4.57E-04	6.24E-04		1.63E-05	3.34E-06	3.75E-06	1.60E+00
						3.50E+03	11580	8959	1.50E-01	6.76E-04	9.14E-04		2.76E-05	4.77E-06	8.31E-06	1.69E+00
						1.96E+03	9984	7633	1.33E-01	3.21E-04	4.78E-04		1.08E-05	2.75E-06	1.67E-06	1.51E+00
355.7-03.5	H 1-35	b	P	OC _{am+cr}	WL07	1.83E+04	14253	9438	1.14E-01	2.84E-05	4.41E-04	5.80E-05	6.28E-06	1.93E-06	1.31E-06	1.33E+00
						1.00E+05	16171	9644	1.20E-01	5.03E-05	5.85E-04	7.66E-05	7.92E-06	2.16E-06	1.74E-06	1.43E+00
						9.56E+03	10438	9030	1.07E-01	2.48E-05	3.82E-04	5.25E-05	5.59E-06	1.79E-06	9.35E-07	1.24E+00
356.2-04.4	Cn 2-1	b	S	OC _{am+cr}	Cu00,Pe01,Mi02,Go04,WL07	4.31E+03	11986	10071	1.08E-01	2.01E-04	5.62E-04	1.26E-04	9.73E-06	2.37E-06	3.12E-06	9.24E-01
						8.64E+03	13096	10438	1.27E-01	3.78E-04	6.59E-04	1.48E-04	1.35E-05	2.83E-06	4.28E-06	1.02E+00
						3.08E+03	10298	9634	5.73E-02	1.40E-04	4.71E-04	8.49E-05	7.86E-06	2.00E-06	1.97E-06	7.95E-01
356.5-02.3	M 1-27	b	P	DC _{cr}	Cu00	5.06E+03	6737		8.91E-03	1.32E-04	3.81E-04		2.45E-05	2.54E-07		1.90E+00
						6.47E+03	7108		1.02E-02	1.96E-04	9.01E-04		3.60E-05	3.99E-07		1.99E+00
						3.52E+03	6021		7.39E-03	1.06E-04	2.47E-04		1.89E-05	1.98E-07		1.83E+00
356.9+04.4	M 3-38	b	P	DC _{am+cr}	Go04,Go09	4.14E+03	17856	14282	1.23E-01	3.16E-04	2.39E-04	6.37E-05	7.00E-06	2.75E-06	7.55E-07	2.06E+00
						5.22E+03	18704	14896	1.30E-01	3.95E-04	2.81E-04	7.13E-05	8.36E-06	3.03E-06	9.96E-07	2.17E+00
						3.06E+03	16727	13677	1.15E-01	2.38E-04	2.08E-04	5.75E-05	5.82E-06	2.49E-06	5.47E-07	1.98E+00
357.1-04.7	H 1-43	b	P	DC _{cr}	Go09	8.86E+03	6137		1.50E-02	2.05E-04	1.32E-04		2.49E-05	3.03E-07		1.07E+00
						1.75E+04	6849		1.84E-02	5.96E-04	1.14E-03		1.09E-04	9.46E-07		1.14E+00
						5.14E+03	4829		1.17E-02	1.22E-04	3.94E-05		1.35E-05	3.62E-08		1.01E+00
357.6+01.7	H 1-23	b	S	OC _{cr}	Ra97	2.96E+03	9250	9120	1.34E-01	3.25E-04	6.28E-04	2.02E-04	1.03E-05	4.21E-06		-
						3.76E+03	9833	9527	1.41E-01	3.89E-04	8.13E-04	2.68E-04	1.40E-05	5.09E-06		
						2.30E+03	8371	8546	1.24E-01	2.10E-04	5.32E-04	1.68E-04	6.93E-06	3.62E-06		
357.6+02.6	H 1-18	b	S	DC _{cr}	Ex04	1.00E+05	5881		9.21E-02	2.44E-03	7.62E-03		1.88E-04	2.28E-05		-
						1.00E+05	8737		9.89E-02	2.57E-03	8.56E-03		2.05E-04	2.35E-05		
						2.36E+04	5796		8.59E-02	9.66E-04	9.96E-04		2.61E-05	6.88E-06		
358.2+03.6	M 3-10	b	S	OC _{cr}	Cu00	6.55E+03	14103	10739	1.15E-01	1.00E-04	5.08E-04		5.80E-06	2.47E-06	1.04E-06	1.73E+00
						9.28E+03	15360	11109	1.22E-01	1.18E-04	5.58E-04		6.57E-06	2.72E-06	1.42E-06	1.85E+00
						5.11E+03	12453	10474	1.06E-01	8.93E-05	4.37E-04		5.05E-06	2.14E-06	7.36E-07	1.63E+00
358.2+04.2	M 3- 8	b	P	DC _{am+cr}	Cu00	5.41E+03	10105		1.35E-01	1.31E-04	2.38E-04		3.47E-06	2.53E-06		1.93E+00
						1.00E+05	12034		1.45E-01	5.73E-04	3.26E-03		4.25E-05	1.20E-05		1.98E+00
						2.66E+03	6818		1.19E-01	9.39E-05	1.03E-04		1.37E-06	1.46E-06		1.78E+00
358.5-04.2	H 1-46	b	S	OC _{am+cr}	Go09	3.75E+03	15848	9992	1.10E-01	5.98E-05	1.87E-04	3.19E-05	5.75E-06	1.28E-06	3.42E-07	1.38E+00
						5.28E+03	16829	10287	1.19E-01	7.44E-05	2.10E-04	3.43E-05	6.72E-06	1.41E-06	6.59E-07	1.48E+00
						3.06E+03	15077	9778	1.02E-01	5.13E-05	1.61E-04	2.56E-05	4.85E-06	1.17E-06	1.83E-07	1.27E+00

Table 3. Continued

PN G	name	loc.	sample	type	ref	N_e	$T_e(N II)$	$T_e(O III)$	He/H	N/H	O/H	Ne/H	S/H	Ar/H	Cl/H	C
358.6+01.8	M 4- 6	b	S	DC _{cr}	Ra97	4.45E+03	14396		1.07E-01	3.77E-05	7.92E-05	5.73E-05	1.36E-06	9.86E-07		-
						5.36E+03	14913		1.15E-01	4.25E-05	9.41E-05	6.86E-05	1.59E-06	1.11E-06		
						3.66E+03	13616		9.97E-02	3.38E-05	7.07E-05	5.09E-05	1.23E-06	9.11E-07		
358.7-05.2	H 1-50	b	P	DC _{cr}	WL07	4.87E+03	12847	11052	1.17E-01	1.93E-04	4.54E-04	1.31E-04	7.37E-06	2.35E-06	1.63E-06	6.84E-01
						5.80E+03	13386	11462	1.24E-01	2.23E-04	5.13E-04	1.43E-04	8.53E-06	2.61E-06	2.01E-06	7.58E-01
						3.62E+03	12191	10829	1.08E-01	1.52E-04	3.86E-04	1.08E-04	6.04E-06	2.06E-06	1.16E-06	5.86E-01
358.7+05.2	M 3-40	b	S	DC _{cr}	Ca10	6.79E+03	6856		2.10E-02	1.39E-04	1.60E-04		1.03E-05	7.47E-07		-
						1.23E+04	7093		2.26E-02	1.84E-04	2.30E-04		1.51E-05	9.28E-07		
						4.75E+03	6513		1.97E-02	1.17E-04	1.32E-04		8.32E-06	6.54E-07		
358.9+03.2	H 1-20	b	G	DC _{cr}	Cu00	3.73E+03	9899		1.43E-01	3.20E-04	4.05E-04		7.51E-06	3.98E-06	1.14E-06	2.31E+0
						5.24E+03	10585		1.50E-01	3.83E-04	5.11E-04		9.76E-06	4.61E-06	1.90E-06	2.42E+0
						3.11E+03	9253		1.30E-01	2.77E-04	3.28E-04		6.36E-06	3.45E-06	6.51E-07	2.21E+0
358.9+03.4	H 1-19	b	S	DC _{cr}	Cu00	1.29E+04	10165		1.40E-01	1.79E-04	1.82E-04		4.09E-06	3.57E-06		2.38E+00
						2.78E+04	10907		1.50E-01	2.61E-04	3.56E-04		7.89E-06	5.59E-06		2.47E+00
						8.00E+03	7198		1.32E-01	1.41E-04	1.35E-04		2.77E-06	2.89E-06		2.26E+00
358.9-03.7	H 1-44	b	S	DC _{cr}	Ex04	2.02E+03	6850		1.04E-01	2.98E-04	4.70E-04		1.45E-05	3.86E-06	4.47E-05	-
						2.53E+03	7025		1.14E-01	3.42E-04	5.91E-04		1.63E-05	4.31E-06	4.91E-05	
						1.67E+03	6682		9.56E-02	2.69E-04	3.94E-04		1.31E-05	3.50E-06	4.05E-05	
359.3-01.8	M 3-44	b	P	DC _{cr}	Go04	5.26E+03	6978		8.24E-03	1.22E-04	1.23E-04		2.32E-05	1.71E-07		3.43E+00
						7.23E+03	7234		9.15E-03	1.53E-04	1.90E-04		3.15E-05	2.09E-07		3.53E+00
						4.06E+03	6563		7.33E-03	1.03E-04	8.79E-05		1.90E-05	1.46E-07		3.32E+00
359.3+03.6	Al 2- E	b	S	F	Ra97	1.80E+04		16847	1.05E-01	1.73E-04	2.64E-04	6.37E-05	1.14E-05	8.68E-07		-
						3.30E+04		17520	1.12E-01	2.12E-04	3.21E-04	7.84E-05	1.63E-05	9.85E-07		
						1.04E+04		16087	9.83E-02	1.34E-04	2.26E-04	4.83E-05	8.76E-06	7.89E-07		
359.7-02.6	H 1-40	b	P	DC _{am+cr}	Ra97,Cu00	1.07E+04	13563	9249	1.10E-01	8.76E-05	3.37E-04	1.45E-04	5.04E-06	1.71E-06		2.52E+00
						5.28E+04	15591	9421	1.22E-01	1.85E-04	8.49E-04	1.61E-04	1.45E-05	3.24E-06		2.61E+00
						3.22E+03	9712	9061	1.01E-01	6.50E-05	1.56E-04	1.31E-04	3.01E-06	1.17E-06		2.40E+00
359.9-04.5	M 2-27	b	P	DC _{cr}	Ra97,Go04, Go09,WL07	5.14E+03	9948	8355	1.39E-01	6.69E-04	7.01E-04	2.33E-04	1.72E-05	5.57E-06	4.74E-06	1.60E+00
						7.51E+03	10504	8991	1.50E-01	8.75E-04	8.94E-04	3.14E-04	2.24E-05	6.34E-06	7.50E-06	1.68E+00
						3.88E+03	8799	7895	1.19E-01	3.68E-04	4.97E-04	1.67E-04	1.25E-05	4.55E-06	2.35E-06	1.50E+00
000.0-06.8	H 1-62	b	P	DC _{cr}	Ex04	4.93E+03	5826		1.06E-02	2.54E-04	6.69E-04		1.29E-05	4.07E-07		-
						6.74E+03	6075		1.13E-02	3.23E-04	1.11E-03		4.80E-05	5.41E-07		
						3.67E+03	5535		9.78E-03	2.18E-04	5.11E-04		1.09E-05	3.19E-07		
000.1+04.3	H 1-16	b	P	DC _{cr}	Cu00	5.89E+03	16999	10425	1.13E-01	5.83E-05	6.76E-04		6.08E-06	2.94E-06		2.50E+00
						1.23E+04	21830	11420	1.22E-01	8.31E-05	1.10E-03		1.06E-05	4.38E-06		2.59E+00
						3.20E+03	10517	9183	1.06E-01	4.56E-05	4.84E-04		4.44E-06	2.12E-06		2.41E+00
000.7+03.2	He 2-250	b	G	OC _{cr}	Ra97,Cu00	2.02E+03	8746	13295	1.58E-01	2.91E-04	4.24E-04	5.33E-05	1.12E-05	4.25E-06		2.12E+0
						2.39E+03	9577	14379	1.70E-01	4.05E-04	7.96E-04	8.17E-05	1.72E-05	6.53E-06		2.23E+0
						1.70E+03	7778	12171	1.45E-01	1.78E-04	2.48E-04	4.16E-05	8.39E-06	2.66E-06		2.03E+0
000.7+04.7	H 2-11	b	G	DC _{cr}	Go04,Es04	4.26E+04	7658	9801	1.52E-01	3.09E-04	5.93E-04		8.47E-06	4.13E-06		3.07E+0
						7.55E+04	9279	12275	1.64E-01	6.49E-04	1.55E-03		2.08E-05	7.75E-06		3.17E+0
						9.61E+03	6038	4769	1.40E-01	1.87E-04	1.77E-04		3.40E-06	3.07E-06		2.98E+0

Table 3. Continued

PN G	name	loc.	sample	type	ref	N_e	$T_e(\text{N II})$	$T_e(\text{O III})$	He/H	N/H	O/H	Ne/H	S/H	Ar/H	Cl/H	C
001.4+05.3	H 1-15	b	G	OC _{cr}	Cu00	9.02E+02	8982		1.18E-01	2.23E-05	2.64E-04		2.81E-06	2.24E-06		1.45E+0
						1.78E+03	12559		1.24E-01	4.01E-05	2.11E-03		1.22E-05	6.22E-06		1.54E+0
						4.63E+02			9.92E-02	1.33E-05	2.69E-05		3.48E-07	5.42E-07		1.36E+0
001.6–01.3	Bl Q	b	G	OC _{cr}	EXs1	2.71E+03	12521		9.62E-02	2.79E-04	1.84E-04		8.23E-06	1.97E-06		-
						3.23E+03	13069		1.03E-01	3.58E-04	2.06E-04		1.01E-05	2.15E-06		
						2.12E+03	12063		8.99E-02	2.39E-04	1.63E-04		7.26E-06	1.71E-06		
001.7–01.6	H 2-31	b	S	DC _{am+cr}	Ex04	3.02E+03	8842		1.67E-02	7.11E-05	9.74E-05		7.65E-06			-
						3.51E+03	10047		1.79E-02	1.18E-04	2.20E-04		1.25E-05			
						2.40E+03	7467		1.54E-02	5.14E-05	4.58E-05		5.76E-06			
001.7–04.6	H 1-56	b	S	OC _{cr}	Ra97,Go09	1.26E+03	10146	7902	1.23E-01	5.81E-05	5.79E-04	1.29E-04	5.13E-06	3.39E-06	2.00E-06	6.69E-01
						5.04E+04	13490	8234	1.33E-01	2.06E-04	8.38E-04	1.48E-04	1.63E-05	4.19E-06	1.12E-05	7.26E-01
						5.28E+02	3497	7414	1.15E-01	4.22E-05	4.71E-04	1.16E-04	1.84E-06	2.96E-06	9.96E-07	5.91E-01
002.0–13.4	IC 4776	d	P	DC _{am+cr}	Mi02	3.48E+03	15114	9731	1.08E-01	3.84E-05	4.97E-04	1.13E-04	6.85E-06	2.09E-06	1.90E-06	1.59E-01
						4.48E+03	16116	9880	1.15E-01	4.01E-05	5.91E-04	1.30E-04	7.68E-06	2.34E-06	2.24E-06	2.70E-01
						2.89E+03	13979	9445	1.02E-01	3.14E-05	4.53E-04	9.86E-05	5.89E-06	1.92E-06	1.47E-06	5.11E-02
002.2–02.7	M 2-23	b	P	OC _{am+cr}	Ra97,Go09,WL07	1.00E+04	26006	12419	1.08E-01	2.04E-05	2.08E-04	4.39E-05	2.57E-06	9.54E-07	6.78E-07	1.17E+00
						5.66E+04	30499	12871	1.16E-01	3.33E-05	2.61E-04	5.54E-05	5.03E-06	1.11E-06	1.07E-06	1.28E+00
						5.73E+03	16624	11752	1.01E-01	1.41E-05	1.80E-04	3.45E-05	1.31E-06	8.63E-07	3.58E-07	1.05E+00
002.2–09.4	Cn 1-5	b	P	DC _{cr}	Pe01,Gi07,WL07	3.47E+03	8076	9408	1.30E-01	2.77E-04	6.41E-04	2.42E-04	1.32E-05	5.31E-06	1.03E-06	3.84E-01
						4.51E+03	8752	10867	1.44E-01	4.23E-04	7.65E-04	2.93E-04	1.59E-05	6.60E-06	1.24E-06	5.57E-01
						2.84E+03	7400	8675	1.16E-01	1.31E-04	5.30E-04	2.01E-04	1.07E-05	4.14E-06	8.14E-07	2.08E-01
002.4–03.7	M 1-38	b	S	DC _{am+cr}	Ra97,Mi02,Go09	1.09E+04	6635		1.36E-02	1.86E-04	1.64E-03	2.09E-02	6.11E-05	4.11E-07		1.09E+00
						3.79E+04	7414		1.69E-02	9.08E-04	3.54E-02	6.29E-01	7.59E-04	8.68E-07		1.30E+00
						4.40E+03	5522		1.08E-02	8.91E-05	2.63E-04	3.95E-03	4.41E-06	2.64E-07		9.42E-01
002.6–03.4	M 1-37	b	S	DC _{cr}	Ra97,Cu00	6.17E+03	5703		1.19E-02	3.52E-04	4.74E-04		3.70E-05	3.20E-07		1.14E+00
						1.00E+04	6091		1.38E-02	5.90E-04	1.68E-03		7.69E-05	6.30E-07		1.20E+00
						4.48E+03	4987		1.04E-02	2.37E-04	1.80E-04		2.37E-05	1.94E-07		1.04E+00
002.8+01.7	H 2-20	b	G	DC _{cr}	Ra97	4.66E+03	5731		6.26E-02	4.04E-04	1.35E-03		2.89E-05	2.38E-06		-
						6.17E+03	5968		6.60E-02	4.86E-04	1.92E-03		3.68E-05	2.77E-06		
						3.49E+03	5441		5.87E-02	3.48E-04	1.05E-03		2.38E-05	2.01E-06		
002.9–03.9	H 2-39	b	S	OC _{am}	Go09	2.38E+03	14648	13197	1.05E-01	8.04E-05	2.58E-04	5.36E-05	2.53E-06	1.07E-06	1.81E-06	1.30E+00
						2.90E+03	18062	13717	1.10E-01	9.12E-05	3.03E-04	6.62E-05	2.91E-06	1.22E-06	2.46E-06	1.39E+00
						2.02E+03	11543	12774	1.00E-01	6.44E-05	2.18E-04	4.91E-05	1.91E-06	9.34E-07	1.12E-06	1.23E+00
003.0–02.6	KFL 4	b	S	CC _{al}	Go09	(2.00E+03)		11383	1.59E-01		3.20E-04	8.03E-05				1.25E+00
								12054	1.73E-01		4.40E-04	1.02E-04				1.46E+00
								10286	1.45E-01		2.57E-04	4.55E-05				9.51E-01
003.1+02.9	Hb 4	d	P	DC _{cr}	Pe01,Gi07	4.38E+03	11454	9806	1.29E-01	4.45E-04	5.00E-04	1.01E-04	1.40E-05	3.58E-06	2.91E-06	1.76E+00
						6.18E+03	11992	10001	1.38E-01	5.30E-04	5.75E-04	1.21E-04	1.65E-05	3.97E-06	3.97E-06	1.84E+00
						3.56E+03	10979	9559	1.19E-01	3.51E-04	4.45E-04	8.95E-05	1.20E-05	3.32E-06	1.99E-06	1.64E+00
003.1+03.4	H 2-17	b	S	DC _{cr}	Ra97	1.81E+03	8884		1.11E-02	5.02E-05	2.60E-05		6.42E-06			-
						2.16E+03	9549		1.21E-02	6.50E-05	3.92E-05		8.32E-06			
						1.54E+03	8179		1.02E-02	3.87E-05	1.76E-05		5.11E-06			

Table 3. Continued

PN G	name	loc.	sample	type	ref	N_e	$T_e(N II)$	$T_e(O III)$	He/H	N/H	O/H	Ne/H	S/H	Ar/H	Cl/H	C
003.2–04.4	KFL 12	b	S	OC_{am}	Go09	1.00E+05		8453	1.01E-01	1.11E-05	7.75E-04	1.78E-04	3.10E-06	1.94E-06		1.17E+00
						1.00E+05		9006	1.07E-01	1.36E-05	1.05E-03	2.63E-04	5.30E-06	2.42E-06		1.27E+00
						1.00E+05		7864	9.42E-02	8.37E-06	5.72E-04	1.32E-04	1.40E-06	1.57E-06		1.07E+00
003.6+03.1	M 2-14	b	P	DC_{cr}	Go04	9.38E+03	8184	7983	1.48E-01	2.45E-04	3.64E-04	6.05E-05	9.83E-06	6.06E-06	1.46E-06	1.55E+00
						1.65E+04	8622	8373	1.57E-01	3.75E-04	5.94E-04	1.04E-04	2.08E-05	8.66E-06	2.85E-06	1.64E+00
						6.30E+03	7234	7149	1.38E-01	2.07E-04	3.01E-04	4.46E-05	7.73E-06	5.12E-06	8.74E-07	1.43E+00
004.1–03.8	KFL 11	b	S	OC_{am}	Go09	9.42E+02	13580	10929	1.09E-01	5.50E-05	2.62E-04	5.93E-05	2.38E-06	1.27E-06	7.09E-07	1.32E+00
						7.31E+03	16229	11556	1.15E-01	6.90E-05	4.05E-04	9.52E-05	4.81E-06	1.68E-06	1.46E-06	1.48E+00
						2.88E+02	8051	9839	9.82E-02	4.55E-05	2.11E-04	4.66E-05	1.82E-06	1.06E-06	3.66E-07	1.14E+00
004.3–02.6	H 1-53	b	S	DC_{am+cr}	t.w.	1.00E+05	5705		1.45E-01	1.78E-03	7.95E-03	3.82E-03	1.11E-04	2.26E-05	5.92E-06	1.98E+00
						1.00E+05	5831		1.56E-01	2.06E-03	9.30E-03	5.33E-03	1.49E-04	2.57E-05	8.70E-06	2.07E+00
						1.00E+05	5586		1.36E-01	1.53E-03	6.67E-03	2.99E-03	8.07E-05	1.96E-05	3.52E-06	1.88E+00
005.5+02.7	H 1-34	b	S	DC_{cr}	Es04	2.54E+03	7501	9309	1.40E-02	9.59E-05	3.01E-04		8.89E-06	7.07E-07		1.89E+00
						3.24E+03	7780	11142	1.48E-02	1.37E-04	4.62E-04		2.33E-05	1.26E-06		1.98E+00
						2.08E+03	7183	7552	1.27E-02	7.37E-05	2.30E-04		4.20E-06	4.37E-07		1.77E+00
005.9–02.6	MaC 1-10	b	P	DC_{cr}	Go04	1.88E+03		25874	6.75E-02	1.31E-05	1.41E-05		1.08E-06	3.80E-07		2.23E+00
						2.23E+03		29762	7.32E-02	1.55E-05	1.77E-05		1.32E-06	4.49E-07		2.32E+00
						1.58E+03		22652	6.00E-02	1.08E-05	9.51E-06		7.72E-07	2.98E-07		2.14E+00
006.0+02.8	Th 4- 3	b	S	DC_{am+cr}	Go09	6.78E+03	8679		1.09E-02	5.27E-05	2.32E-04		8.77E-06	2.53E-07		1.71E+00
						1.00E+05	9698		1.51E-02	8.50E-04	2.48E-02		4.99E-04	1.60E-06		1.80E+00
						1.45E+03	5293		7.71E-03	3.46E-05	1.52E-04		4.25E-06	1.95E-07		1.52E+00
006.0–03.6	M 2-31	b	G	DC_{cr}	Ra97,Go04,Go09, WL07,Gi07	3.94E+03	11595	9736	1.16E-01	2.29E-04	4.59E-04	1.24E-04	1.08E-05	2.49E-06	2.59E-06	1.33E+0
						5.21E+03	12397	10092	1.24E-01	3.66E-04	5.34E-04	1.36E-04	1.44E-05	2.87E-06	3.51E-06	1.42E+0
						3.04E+03	9738	9410	9.40E-02	1.37E-04	3.86E-04	1.05E-04	6.02E-06	2.05E-06	1.62E-06	1.23E+0
006.1+08.3	M 1-20	d	P	CC_{ar+al}	Ra97,WL07	6.70E+03	11224	10308	1.04E-01	5.96E-05	3.62E-04	7.74E-05	2.84E-06	9.87E-07	7.42E-07	1.18E+00
						1.30E+04	11936	10572	1.13E-01	7.12E-05	4.32E-04	9.38E-05	3.50E-06	1.14E-06	9.94E-07	1.28E+00
						4.65E+03	9976	9950	9.83E-02	5.02E-05	3.15E-04	6.84E-05	2.19E-06	8.34E-07	4.75E-07	1.08E+00
006.3+04.4	H 2-18	b	S	OC_{am}	Ra97,Go09,Mi10	2.85E+03	13871	10278	1.13E-01	6.24E-05	4.82E-04	9.97E-05	4.55E-06	1.47E-06	2.21E-06	1.52E+00
						3.47E+03	16898	10928	1.20E-01	7.62E-05	5.64E-04	1.18E-04	5.63E-06	1.71E-06	3.28E-06	1.63E+00
						2.26E+03	10518	9673	1.05E-01	5.03E-05	3.67E-04	8.10E-05	3.18E-06	1.10E-06	1.42E-06	1.42E+00
006.4+02.0	M 1-31	b	P	DC_{cr}	Go04,Gi07,Go09	9.44E+03	10443	8288	1.44E-01	3.66E-04	5.02E-04	1.64E-04	1.40E-05	4.85E-06	3.30E-06	2.00E+00
						1.60E+04	11047	8937	1.54E-01	7.29E-04	8.05E-04	2.46E-04	2.80E-05	6.80E-06	8.05E-06	2.09E+00
						6.56E+03	9444	7639	1.35E-01	1.44E-04	2.36E-04	1.02E-04	4.42E-06	2.91E-06	5.81E-07	1.91E+00
006.5–03.1	H 1-61	b	P	DC_{cr}	Go04	4.91E+03	12108		1.26E-01	9.65E-05	1.13E-04		4.02E-06	3.03E-06		2.49E+00
						1.71E+04	13051		1.39E-01	1.49E-04	1.72E-04		6.51E-06	4.29E-06		2.59E+00
						2.07E+03	9204		1.19E-01	7.16E-05	9.20E-05		2.94E-06	2.49E-06		2.39E+00
006.8+04.1	M 3-15	b	P	DC_{cr}	Ra97,Pe01,KH01, Gi07,Go09	5.56E+03	11675	9206	1.26E-01	2.31E-04	5.29E-04	1.30E-04	1.24E-05	3.47E-06	4.27E-06	2.09E+00
						9.84E+03	14332	11437	1.41E-01	3.51E-04	1.05E-03	2.54E-04	2.24E-05	5.90E-06	1.22E-05	2.17E+00
						3.09E+03	9660	8126	1.14E-01	1.02E-04	1.99E-04	4.75E-05	4.17E-06	1.22E-06	9.68E-07	1.99E+00
007.2+01.8	Hb 6	d	P	DC_{cr}	Go04	3.42E+03	11422	11073	1.24E-01	2.98E-04	4.53E-04	1.47E-04	9.83E-06	3.72E-06	1.19E-06	2.10E+00
						4.37E+03	11848	11331	1.31E-01	3.89E-04	5.52E-04	1.66E-04	1.29E-05	4.36E-06	1.75E-06	2.21E+00
						2.91E+03	10937	10563	1.16E-01	2.61E-04	4.00E-04	1.25E-04	8.40E-06	3.40E-06	9.53E-07	2.03E+00

Table 3. Continued

PN G	name	loc.	sample	type	ref	N_e	$T_e(N II)$	$T_e(O III)$	He/H	N/H	O/H	Ne/H	S/H	Ar/H	Cl/H	C
008.1-04.7	M 2-39	b	S	OC _{cr}	WL07	4.94E+03	10267	26960	6.52E-02	6.08E-06	2.38E-05	6.19E-06	2.21E-07	2.06E-07	1.91E-08	1.09E+00
						6.42E+03	10478	30285	6.93E-02	6.94E-06	2.62E-05	6.67E-06	2.49E-07	2.31E-07	2.22E-08	1.17E+00
						4.09E+03	9909	25945	5.87E-02	4.85E-06	1.96E-05	4.99E-06	1.80E-07	1.79E-07	1.40E-08	9.58E-01
008.2-04.8	M 2-42	b	S	F	WL07	2.15E+03	10836	8280	1.13E-01	2.14E-04	6.12E-04	1.65E-04	1.37E-05	2.18E-06	5.45E-06	9.57E-01
						2.59E+03	11246	8704	1.19E-01	2.57E-04	6.70E-04	1.58E-04	1.52E-05	2.28E-06	6.14E-06	1.04E+00
						1.83E+03	10420	8219	1.05E-01	1.58E-04	4.72E-04	1.24E-04	9.97E-06	1.85E-06	3.30E-06	8.59E-01
008.2+06.8	He 2-260	d	P	OC _{am+cr}	Es04,Ha13	4.00E+04	10493		1.18E-02	5.66E-05	1.16E-03		8.33E-06	2.33E-07		7.30E-01
						1.00E+05	13336		1.37E-02	1.42E-04	3.33E-03		2.24E-05	3.78E-07		8.23E-01
						5.25E+03	6983		9.19E-03	1.03E-05	5.06E-05		9.30E-07	1.26E-07		6.11E-01
008.3-01.1	M 1-40	d	P	DC _{cr}	Go04	5.53E+03	11417	13039	1.32E-01	3.27E-04	3.15E-04	8.42E-05	1.05E-05	5.04E-06	4.73E-07	2.60E+00
						7.26E+03	11909	13345	1.39E-01	4.05E-04	3.63E-04	9.43E-05	1.30E-05	5.70E-06	6.24E-07	2.70E+00
						4.27E+03	10944	12535	1.25E-01	2.94E-04	2.79E-04	7.40E-05	9.43E-06	4.65E-06	3.86E-07	2.51E+00
008.6-02.6	MaC 1-11	b	S	OC _{am}	t.w.	7.32E+03		10924	1.04E-01	3.87E-05	2.46E-04	5.04E-05	2.53E-06	7.78E-07	1.42E-06	2.35E+00
						1.08E+04		11334	1.12E-01	4.78E-05	2.85E-04	5.81E-05	3.05E-06	8.86E-07	2.26E-06	2.44E+00
						5.28E+03		10491	9.83E-02	2.95E-05	2.07E-04	4.22E-05	1.90E-06	7.13E-07	7.88E-07	2.23E+00
009.3+04.1	Th 4- 6	d	S	OC _{am+cr}	Go09	8.38E+03		10053	1.15E-01	1.00E-04	3.68E-04		5.32E-06	9.76E-07		1.35E+00
						1.00E+05		10352	1.23E-01	3.27E-04	6.10E-04		1.06E-05	1.30E-06		1.41E+00
						2.89E+03		8978	1.06E-01	6.27E-05	3.46E-04		3.65E-06	8.88E-07		1.29E+00
010.6+03.2	Th 4-10	d	S	CC _{ar}	Cu96,Go09	2.92E+03	8402	8562	1.30E-01	2.43E-04	3.71E-04		9.98E-06	3.00E-06	2.37E-06	1.33E+00
						6.38E+03	9953	10191	1.39E-01	5.14E-04	1.33E-03		2.25E-05	5.32E-06	8.19E-06	1.40E+00
						1.90E+03	6363	6367	1.16E-01	9.34E-05	1.88E-04		4.54E-06	1.73E-06	3.67E-07	1.25E+00
011.1+07.0	Sa 2-237	d	S	OC _{am}	t.w.	1.10E+03	9350	11423	1.77E-01	8.04E-04	6.55E-04	3.80E-04	1.76E-05	4.52E-06	2.90E-07	7.95E-01
						1.30E+03	9632	12118	1.85E-01	1.03E-03	8.24E-04	5.60E-04	2.58E-05	5.73E-06	5.29E-07	8.84E-01
						9.49E+02	9073	10329	1.67E-01	6.85E-04	6.02E-04	2.80E-04	1.48E-05	3.96E-06	2.06E-07	6.81E-01
011.3-09.4	H 2-48	d	S	OC _{am}	Es04	7.50E+03	14596	10262	5.63E-02	1.88E-05	8.24E-05		2.60E-06	4.84E-07	7.41E-07	9.64E-01
						1.36E+04	15461	10648	5.97E-02	2.36E-05	1.05E-04		3.50E-06	5.57E-07	1.05E-06	1.05E+00
						5.59E+03	13430	9591	5.16E-02	1.72E-05	7.02E-05		2.21E-06	4.22E-07	3.99E-07	8.86E-01
011.9+04.2	M 1-32	d	P	DC _{cr}	Pe01,Gi07	7.07E+03	9445	10457	1.31E-01	1.94E-04	3.34E-04	2.02E-05	7.50E-06	3.82E-06	2.36E-07	1.33E+00
						9.90E+03	9861	11251	1.42E-01	2.20E-04	4.09E-04	2.94E-05	8.75E-06	4.51E-06	3.26E-07	1.44E+00
						5.18E+03	8909	9663	1.20E-01	1.68E-04	2.99E-04	1.09E-05	6.25E-06	3.14E-06	2.01E-07	1.25E+00
012.5-09.8	M 1-62	d	S	CC _{al}	Cu96	4.68E+02		12023	1.09E-01	6.67E-06	2.65E-04		1.74E-07	7.17E-07		6.49E-01
						1.00E+05		12325	1.17E-01	6.33E-05	4.39E-04		3.79E-06	8.67E-07		7.60E-01
						3.00E+01		10668	9.28E-02	4.47E-06	2.31E-04		1.08E-07	6.11E-07		5.77E-01
012.6-02.7	M 1-45	d	S	DC _{cr}	Cu96,Ra97	1.04E+04	6480		1.14E-02	2.02E-04	3.84E-04		3.60E-05			1.88E+00
						3.76E+04	7404		1.33E-02	6.81E-04	4.81E-03		3.04E-04			1.99E+00
						5.53E+03	5254		9.31E-03	8.40E-05	8.80E-05		1.38E-05			1.80E+00
014.3-05.5	V-V 3-6	d	S	CC _{ar}	Cu96	7.77E+03	12436	11981	9.22E-02	5.65E-05	2.67E-04		1.95E-06	7.35E-07	4.91E-07	1.12E+00
						1.00E+05	14900	12202	1.05E-01	1.89E-04	4.29E-04		4.91E-06	1.05E-06	1.12E-06	1.21E+00
						1.42E+03	6597	10655	8.70E-02	3.18E-05	2.53E-04		1.56E-06	7.32E-07	2.99E-07	1.02E+00
018.6-02.2	M 3-54	d	S	F	Es04	1.19E+03		10813	1.25E-01	1.13E-05	4.09E-04	1.06E-04	2.71E-06	2.17E-06		1.47E+00
						2.67E+03		11065	1.29E-01	1.52E-05	4.62E-04	1.15E-04	3.25E-06	2.38E-06		1.58E+00
						6.91E+02		10442	1.18E-01	9.33E-06	3.56E-04	8.90E-05	2.22E-06	1.90E-06		1.35E+00

Table 3. Continued

PN G	name	loc.	sample	type	ref	N_e	$T_e(N II)$	$T_e(O III)$	He/H	N/H	O/H	Ne/H	S/H	Ar/H	Cl/H	C
019.2-02.2	M 4-10	d	S	OC _{am+cr}	Cu96	5.05E+03	15022	11853	1.06E-01	6.01E-05	3.77E-04		3.73E-06	1.27E-06		2.06E+00
						2.67E+04	20565	13057	1.15E-01	1.13E-04	6.06E-04		7.20E-06	1.74E-06		2.15E+00
						2.30E+03	7694	10481	9.74E-02	4.32E-05	2.68E-04		2.45E-06	1.06E-06		1.96E+00
019.4-05.3	M 1-61	d	S	DC _{am+cr}	Gi07,WL07	1.12E+04	12880	9368	1.08E-01	1.02E-04	4.68E-04	1.18E-04	5.50E-06	2.40E-06	1.16E-06	1.64E+00
						2.05E+04	13632	9588	1.14E-01	1.17E-04	5.84E-04	1.43E-04	7.19E-06	2.75E-06	1.62E-06	1.74E+00
						7.29E+03	11327	9000	1.01E-01	8.89E-05	4.04E-04	9.20E-05	3.81E-06	2.21E-06	7.03E-07	1.54E+00
019.7+03.2	M 3-25	d	S	DC _{am+cr}	Cu96,Go04	1.13E+04	11051	9544	7.01E-02	1.64E-04	5.50E-04		1.01E-05	5.31E-06	1.05E-06	2.08E+00
						6.34E+04	11880	10499	1.37E-01	2.52E-04	1.02E-03		2.21E-05	8.62E-06	2.18E-06	2.28E+00
						6.24E+03	9282	8256	3.21E-03	1.31E-04	3.75E-04		6.70E-06	3.89E-06	5.69E-07	1.86E+00
019.7-04.5	M 1-60	d	P	DC _{cr}	Gi07	5.37E+03	10646	8886	1.37E-01	5.98E-04	5.96E-04	1.66E-04	1.75E-05	5.71E-06		1.51E+00
						7.49E+03	11080	9158	1.46E-01	6.86E-04	6.60E-04	1.84E-04	1.93E-05	6.17E-06		1.60E+00
						4.06E+03	10173	8765	1.30E-01	4.69E-04	5.03E-04	1.52E-04	1.41E-05	5.24E-06		1.39E+00
020.9-01.1	M 1-51	d	P	DC _{cr}	Gi07,He10	5.78E+03	9807	7465	1.55E-01	3.73E-04	6.47E-04	1.36E-04	2.41E-05	6.49E-06	2.99E-06	3.42E+00
						7.96E+03	10060	7795	1.65E-01	5.54E-04	8.89E-04	1.69E-04	3.94E-05	9.06E-06	5.27E-06	3.50E+00
						4.29E+03	9290	7167	1.44E-01	1.91E-04	4.04E-04	1.11E-04	8.83E-06	3.92E-06	7.06E-07	3.33E+00
023.8-01.7	K 3-11	d	S	DC _{cr}	Ca10	7.23E+03	8028		1.04E-02	8.38E-05	2.16E-04	2.48E-02	2.84E-06	1.89E-07		-
						1.21E+04	8383		1.12E-02	1.06E-04	3.34E-04	4.08E-02	4.13E-06	2.39E-07		
						5.49E+03	7640		9.60E-03	7.27E-05	1.83E-04	2.05E-02	2.21E-06	1.47E-07		
025.3-04.6	K 4- 8	d	S	OC _{am}	t.w.	1.14E+04	12694	10636	1.02E-01	6.10E-05	3.91E-04	1.01E-04	4.57E-06	1.27E-06	9.91E-07	7.08E-01
						1.87E+04	13673	10911	1.10E-01	6.64E-05	4.84E-04	1.19E-04	5.41E-06	1.40E-06	1.25E-06	7.95E-01
						7.65E+03	11341	10214	9.53E-02	5.27E-05	3.35E-04	8.98E-05	4.10E-06	1.18E-06	7.16E-07	6.11E-01
027.6-09.6	IC 4846	d	S	OC _{am}	t.w.	1.33E+04	11415	10082	1.04E-01	4.84E-05	4.00E-04	9.87E-05	5.41E-06	1.36E-06	1.37E-06	4.12E-01
						6.02E+04	12705	10281	1.12E-01	6.30E-05	5.39E-04	1.30E-04	7.31E-06	1.62E-06	1.68E-06	4.90E-01
						8.17E+03	7257	9585	9.89E-02	4.03E-05	3.62E-04	9.00E-05	4.79E-06	1.27E-06	9.55E-07	3.20E-01
032.9-02.8	K 3-19	d	S	CC _{al}	Cu96	8.09E+03	11738	10984	9.34E-02	1.78E-04	3.79E-04		2.95E-06	1.23E-06	9.94E-07	2.28E+00
						1.00E+05	13749	12267	1.00E-01	5.84E-04	6.24E-04		6.29E-06	1.62E-06	2.14E-06	2.39E+00
						2.31E+03	6679	9660	8.66E-02	1.06E-04	2.54E-04		1.60E-06	9.67E-07		2.20E+00
038.7-03.3	M 1-69	d	S	F	t.w.	6.38E+03	10291	9629	1.30E-01	2.68E-04	5.59E-04	1.75E-04	1.22E-05	3.54E-06	2.18E-06	1.22E+00
						1.03E+04	10669	9875	1.59E-01	3.44E-04	6.77E-04	1.94E-04	1.51E-05	4.02E-06	3.07E-06	1.33E+00
						4.61E+03	9748	9306	1.09E-01	2.04E-04	4.90E-04	1.55E-04	1.01E-05	3.22E-06	1.44E-06	1.15E+00
041.8+04.4	K 3-15	d	S	CC _{ar+al}	t.w.	1.00E+05	9340		3.18E-02	4.15E-05	3.54E-04		4.57E-06	3.22E-07	2.31E-07	1.15E+00
						1.00E+05	9723		3.36E-02	4.84E-05	4.40E-04		5.35E-06	3.63E-07	3.05E-07	1.23E+00
						1.00E+05	9003		2.93E-02	3.43E-05	2.69E-04		3.82E-06	2.65E-07	1.07E-07	1.05E+00
042.9-06.9	NGC 6807	d	S	OC _{am+cr}	t.w.	1.00E+05	8559	10265	1.07E-01	6.62E-05	5.77E-04	1.37E-04	7.32E-06	1.41E-06	6.96E-07	4.92E-01
						1.00E+05	15270	11011	1.12E-01	6.32E-05	6.68E-04	1.56E-04	7.72E-06	1.51E-06	1.03E-06	5.52E-01
						1.59E+04	8422	10014	1.01E-01	4.16E-05	4.02E-04	9.81E-05	5.19E-06	1.20E-06	5.27E-07	4.18E-01
052.9+02.7	K 3-31	d	S	CC _{al}	t.w.	1.00E+05	7745	9994	1.25E-01	1.56E-04	9.75E-04	2.17E-04	9.96E-06	2.73E-06	5.62E-07	2.92E+00
						1.00E+05	7965	10338	1.34E-01	1.81E-04	1.14E-03	3.18E-04	1.29E-05	3.02E-06	7.67E-07	3.01E+00
						1.00E+05	7528	9771	1.15E-01	1.29E-04	8.51E-04	1.91E-04	7.25E-06	2.41E-06	3.23E-07	2.82E+00
055.5-00.5	M 1-71	d	S	CC _{al}	Gi07	9.00E+03	14430	9631	1.32E-01	1.21E-04	5.92E-04	1.30E-04	3.18E-06	3.17E-06	9.83E-07	2.18E+00
						1.90E+04	15568	9893	1.39E-01	1.39E-04	7.21E-04	1.54E-04	3.77E-06	3.55E-06	1.19E-06	2.29E+00
						6.56E+03	12430	9256	1.21E-01	9.55E-05	5.03E-04	1.13E-04	2.65E-06	2.89E-06	7.05E-07	2.08E+00

Table 3. Continued.

PN G	name	loc.	sample	type	ref	N_e	$T_e(\text{N II})$	$T_e(\text{O III})$	He/H	N/H	O/H	Ne/H	S/H	Ar/H	Cl/H	C
060.5+01.8	He 2-440	d	S	OC _{cr}	t.w.	1.00E+05	6153	8218	1.16E-01	2.55E-04	4.47E-03	5.81E-04	1.58E-05	3.74E-06	7.09E-07	2.36E+00
						1.00E+05	6585	8614	1.21E-01	2.86E-04	5.21E-03	6.73E-04	1.73E-05	4.21E-06	9.48E-07	2.46E+00
						1.00E+05	6032	7979	1.09E-01	1.88E-04	2.67E-03	3.01E-04	1.20E-05	3.20E-06	5.49E-07	2.27E+00
068.7+01.9	K 4-41	d	S	OC _{cr}	t.w.	1.00E+05		8743	1.15E-01	1.01E-04	7.34E-04	1.78E-04	7.50E-06	3.05E-06	1.33E-06	1.69E+00
						1.00E+05		8968	1.22E-01	1.30E-04	8.33E-04	1.84E-04	9.34E-06	3.39E-06	1.95E-06	1.77E+00
						1.00E+05		8500	1.07E-01	7.94E-05	6.12E-04	1.45E-04	6.03E-06	2.72E-06	9.87E-07	1.59E+00
069.2+02.8	K 3-49	d	S	OC _{am}	t.w.	1.00E+05	7548		2.92E-02	1.79E-04	1.71E-03		1.35E-05	9.42E-07		1.77E+00
						1.00E+05	7878		3.07E-02	1.98E-04	1.82E-03		1.51E-05	1.03E-06		1.88E+00
						6.31E+04	7337		2.65E-02	9.50E-05	5.04E-04		7.18E-06	7.02E-07		1.70E+00
079.9+06.4	K 3-56	d	S	OC _{am}	t.w.	5.20E+02		16315	1.08E-01		1.69E-04	3.67E-05		8.00E-07		1.41E+00
						2.52E+03		16789	1.14E-01		2.35E-04	4.70E-05		9.06E-07		1.50E+00
						3.00E+01		15169	1.00E-01		1.42E-04	3.16E-05		7.30E-07		1.33E+00
095.2+00.7	K 3-62	d	S	CC _{al}	t.w.	1.00E+05	6697	9112	1.13E-01	1.18E-04	2.05E-03	4.34E-04	2.95E-05	2.46E-06	1.93E-06	2.80E+00
						1.00E+05	7141	9207	1.21E-01	1.76E-04	3.17E-03	5.71E-04	3.87E-05	2.80E-06	2.67E-06	2.90E+00
						1.00E+05	6099	8759	1.05E-01	9.12E-05	1.50E-03	2.72E-04	2.44E-05	2.26E-06	1.50E-06	2.70E+00
097.6-02.4	M 2-50	d	S	OC _{am}	t.w.	1.95E+03	12286	12406	1.07E-01	8.36E-05	2.39E-04	6.11E-05	4.25E-06	1.21E-06	1.55E-06	8.02E-01
						2.33E+03	14366	12953	1.23E-01	9.79E-05	2.76E-04	7.05E-05	4.83E-06	1.33E-06	1.92E-06	8.70E-01
						1.61E+03	9728	12019	8.32E-02	6.90E-05	2.04E-04	5.38E-05	3.63E-06	1.08E-06	1.19E-06	7.11E-01
107.4-02.6	K 3-87	d	S	CC _{al}	t.w.	(2.00E+03)		15147	1.02E-01		1.96E-04	4.03E-05		6.93E-07		1.45E+00
								15785	1.12E-01		3.02E-04	6.35E-05		8.09E-07		1.56E+00
								14754	9.18E-02		1.56E-04	3.37E-05		5.63E-07		1.34E+00

References. (FP92) de Freitas Pacheco et al. (1992); (KB94) Kingsburgh & Barlow (1994); (Cu96) Cuisinier et al. (1996); (Ra97) Ratag et al. (1997); (Cu00) Cuisinier et al. (2000); (Es01) Escudero & Costa (2001); (KH01) Kwitter & Henry (2001); (Pe01) Peña et al. (2001); (Mi02) Milingo et al. (2002); (Es04) Escudero et al. (2004); (Ex04) Exter et al. (2004); (Go04) Górný et al. (2004); (Gi07) Girard et al. (2007); (WL07) Wang & Liu (2007); (Go09) Górný et al. (2009); (Ca10) Cavichia et al. (2010); (He10) Henry et al. (2010); (Go14) Górný (2014); (t.w.) this work.